Spring 2021

Mathematical Analysis of a Model of Blood Flow Through a Channel with Flexible Walls

Madeline Mayes Edwards
University of New Hampshire, Durham

MATHEMATICAL ANALYSIS OF A MODEL OF BLOOD FLOW THROUGH A CHANNEL WITH FLEXIBLE WALLS

BY

Madeline M. Edwards

BA, Mathematics, Elon University, 2015

DISSERTATION

Submitted to the University of New Hampshire

in Partial Fulfillment of

the Requirements for the Degree of

Doctor of Philosophy

in

Integrated Applied Mathematics

May, 2021

This dissertation has been examined and approved in partial fulfillment of the requirements for the degree of Doctor of Philosophy in Integrated Applied Mathematics by:

Marianna Shubov, Dissertation Director
Professor of Mathematics
Integrated Applied Mathematics
Department of Mathematics and Statistics

Mark Lyon
Associate Professor of Mathematics
Integrated Applied Mathematics
Department of Mathematics and Statistics

John Gibson
Associate Professor of Mathematics
Integrated Applied Mathematics
Department of Mathematics and Statistics

Rita Hibschweiler
Professor of Mathematics
Department of Mathematics and Statistics

Donald Hadwin
Professor of Mathematics
Department of Mathematics and Statistics

On April 9, 2021

Original approval signatures are on file with the University of New Hampshire Graduate School.

DEDICATION

To John

ACKNOWLEDGEMENTS

I would like to acknowledge those who supported me through my academic accomplishments. I would like to express immense gratitude and thanks to my advisor, Dr. Marianna Shubov, for her continuous guidance, encouragement, and expertise. I would also like to thank my committee for their individual comments and advice throughout the proposal, drafts, and submission of my final thesis. Additionally, I would like to thank the faculty and staff within the Integrated Applied Mathematics program, the Mathematics and Statistics Department, and the University of New Hampshire community who supported, educated, and encouraged me throughout the duration of my doctoral program.

Lastly, I would like to thank my parents for working endlessly to provide me with a childhood of security and encouragement. Thank you for supporting me with love and understanding.

TABLE OF CONTENTS

LIST OF FIGURES

ABSTRACT

MATHEMATICAL ANALYSIS OF A MODEL OF BLOOD FLOW THROUGH A CHANNEL WITH FLEXIBLE WALLS

by

Madeline M. Edwards

University of New Hampshire, May, 2021

The present research is devoted to the problem of stability of the fluid flow moving in a channel with flexible walls and interacting with the walls. The walls of the vessel conveying fluid are subject to traveling waves. Experimental data shows that the energy of the flowing fluid can be transferred and consumed by the structure (the walls), which induces "traveling wave flutter." The problem of stability of fluid-structure interaction splits into two parts: (i) stability of fluid flow in the channel with harmonically moving walls and (ii) stability of solid structure participating in the energy exchange with the flow. Stability of fluid flow is the main focus of the research. It is shown that using the mass conservation and the incompressibility condition one can obtain the initial boundary value problem for the *stream function*. The boundary conditions reflect the facts that (i) for the axisymmetrical flow, there is no movement in the vertical direction along the axis of symmetry, and (ii) there is no relative movement between the near-boundary flow and the structure ("no-slip" condition). The closed form solution is derived and is represented in the form of an infinite functional series.

INTRODUCTION

The present research is devoted to the mathematical analysis of the model describing incompressible fluid flow through a relatively long channel with flexible walls. The model has its origin in a specific biological setting of blood moving through blood vessels. Our choice of a model is motivated by the fact that the walls of the channel conveying fluid are subject to traveling waves, which means that we are dealing with complicated fluid-structure interaction. Experimental analysis of such a system shows that under some conditions, the energy of the fluid flow can be transferred and then consumed by the structure (the walls), which initiate "traveling wave flutter" [5]. Flutter is a specific type of instability that may occur as the result of energy transfer in fluid-structure interactions. Flutter is known to occur in many different areas of applied sciences such as marine and aerospace propulsion, outer skin panels of aircrafts, missiles, and aerospace vehicles, shell structures in jet pumps, heat exchanges and storage tanks.

The problem of stability of our model splits into two parts: the first one is related to the stability of the fluid flow in the channel, whose walls undergo axisymmetric harmonic movement, and the second part is related to the stability of the channel wall structure, which is participating in the energy exchange with the flow. The present dissertation deals with the first part of the problem, i.e. we provide a closed form solution of the problem of *stability of the fluid flow* in the channel with harmonically moving walls.

The main achievement of this research is the derivation of the explicit formulas for the flow velocities, which allows us to answer the question on the flow stability. We expect that the results obtained for two-dimensional configuration will be relevant to the flutter of partially collapsed tubes in a three-dimensional setting.

All fluid-conveying vessels in a human body are highly elastic and substantially deformable in their response to the pressure and viscous stress that the fluid exerts on them. In propagation of the *pulse wave* through the arterial system under normal conditions, the arteries are subject to *positive* transmural (internal minus external) pressure, which keeps them inflated and stiff during the pulse cycle. However, in the situation when fluid-conveying vessels are under the *negative* (compressive) transmural pressure, the vessels often buckle and collapse. Buckled vessels are very flexible and small changes in fluid pressure induce large changes in their cross-sectional areas, which in turn induces such phenomena as *flow limitation* and large amplitude self-excited oscillations.

Self-excited oscillations of collapsible airways in lungs are responsible for respiratory wheezes during forced expiration, for speech production during flow-induced vibrations of the vocal chords, and for snoring sounds during deformation of the soft palate and pharyngeal wall [2,6–13]. Medical observations show that human snoring is due to the soft palate vibrations induced by the inspiratory flow; in some cases the soft palate becomes aeroelastically unstable and, when it bumps against the pharingeal walls, it closes the upper airways causing large changes of pressure in inspiratory airflow and producing its characteristic noise [7, 10, 11]. A remarkable characteristic of snoring is that it occurs while the inspiratory flow rate is still increasing [5] where as wheezing [9] starts after the volume flow rate becomes limited.

Thin-walled circular *shell structures* containing or immersed in flowing fluid may be found in many engineering and biomechanical systems [14–17]. Numerous studies on the aeroelasticity of cylindrical shells reflect the enormous interest on the effect of high-speed flow on the outer-skin panels of aircraft, missiles, and aerospace vehicles.

Before we present the main findings of the research, we briefly discuss the main directions and scientific approaches in the area of fluid-structure interactions involving biological and engineering systems.

In general, the stability of fluid flow near a flexible surface is of interest in diverse applications such as marine and aerospace propulsion, biotechnology, and polymer processing applications. The flow of a fluid through a tube with flexible walls is observed in biological systems in the transport

of blood and other biological fluids, as well as biotechnology applications which involve flows past polymer matrices and membranes [18–23]. Practically all fluid-conveying vessels in the human body have two important characteristics: they are highly elastic and substantially deformable in response to the pressure and viscous stress that the fluid exerts on them. Experimental studies show that the interaction between internal flow and large deformations of the collapsible tube wall can cause large-amplitude self-excited oscillations.

Physiological examples of collapsible tubes are numerous. Flow-induced collapse of blood vessels plays an important role in the auto-regulation of blood supply to internal organs. In the cardiovascular system, spontaneous collapse can occur in veins above the heart and outside the skull, due to hydrostatic reduction of blood pressure. Coronary blood vessels collapse during systole; active compression of veins in the lower limbs is used as a therapy to prevent deep-vein thrombosis. Both veins and arteries also collapse when an inflatable cuff is placed around the upper arm to measure blood pressure.

Air flow in the lung is strongly affected by the elasticity of the airways. During forced expiration, contraction of the expiratory muscles increases the pleural pressure that drives the air out of the peripheral airways. Self-excited oscillations of collapsible airways are responsible for a number of respiratory noises. Flutter instabilities have been proposed as the origin of respiratory wheezes during forced expiration; speech production involved controlled flow-induced vibrations of the vocal chords; snoring sounds have their origins in flow-induced deformation of the soft palate and pharyngeal wall [2, 6–13].

An extensive amount of research is devoted to snoring. Even though modeling of the upper airways is extremely complicated, there are a number of quite interesting and informative studies in biomedical literature related to the loss of stability of mechanical oscillator interacting with a continuous flow. Medical observations show that human snoring is due to the soft palate vibrations induced by the inspiratory flow. It can be understood as follows: in some cases the soft palate becomes aeroelastically unstable and when it bumps against the pharyngeal walls, it closes the upper airways causing large changes of pressure in inspiratory airflow and producing its characteristic

noise [7, 10, 11].

In addition to snoring, flow-structure interaction can lead to such phenomena as flow limitation (when airway deformation limits the rate at which air can be forcibly expelled from the lungs) and noise-generating instabilities, such as wheezing in lung airways and Korotkoff sound generation in the compressed brachial artery [24–28]. One remarkable characteristic of snoring is that it occurs while the inspiratory flow rate is still increasing [5] where as other phenomena, such as wheezing [9] start after the volume flow rate becomes limited.

An additional area of study within fluid-structure interaction is modeling a structure as a thin-walled circular cylindrical shell. Technically such models are more complicated [14–17]. Thin-walled circular cylindrical shell structures containing or immersed in flowing fluid may be found in many engineering and biomechanical systems. Most of the studies on the aeroelasticity of cylindrical shells are for compressible and particularly supersonic flows, reflecting the enormous interest on the effect of high-speed flow on the outer-skin panels of aircraft, missiles, and aerospace vehicles. However, there are many other applications in which shells are subjected to incompressible or subsonic flows: thin cylindrical shells used as thermal shields in nuclear reactors and heat shields in aircraft engines; shell structures in jet pumps, heat exchangers and storage tanks; thin-walled piping for aerospace vehicles; and in the construction of shell-type Coriolis mass-flow meters.

Now we briefly discuss some previous research findings, where either new interesting results are presented or new techniques are developed.

In paper [29], Case considers the stability problem for inviscid incompressible fluid flowing between infinite parallel plates. The solution of the corresponding initial value problem is represented in the form of a normal mode decomposition. The asymptotic behavior of the solution, when time tends to infinity, for the case of the Couette flow is presented. Case [29, 30] shows that the continuum modes decay, as time $t \to \infty$, as a power of t.

Shivamoggi [31] notes that whereas a well-behaved initial perturbation generates a solution that decays according to a power law [1, 3], the special singular perturbation, taken in the form of

concentrated vorticity, generates a solution that decays exponentially as $t \to \infty$.

Carpenter and Garrad [1] present a consistent account of flow-induced surface instabilities of compliant surfaces and development of traveling wave flutter. The class of instabilities, investigated by the authors, could be modeled theoretically by a thin elastic plate (with or without applied longitudinal tension) supported on a spring elastic foundation, with or without a viscous fluid substrate, and with material damping being taken into account (see Fig. 0.1). The authors show that under a potential main flow, the instabilities can grow both in space and time. The shear flow in the boundary layer gives rise to a fluctuating pressure, which leads to the energy transfer from the main stream to the compliant surface. This mechanism is responsible for traveling wave flutter. An important question raised by the authors [1] is: *"Why, then, is the flow over compliant surfaces susceptible to so many types of instabilities? – The simple answer is that the dynamic system in question consists of two coupled wave-bearing media – the flowing fluid and the solid flexible wall."* The authors address the complexity of the problem by analyzing the model of potential flow over a flexible plate or tensioned membrane supported on a continuous springy elastic foundation (Fig. 0.1).

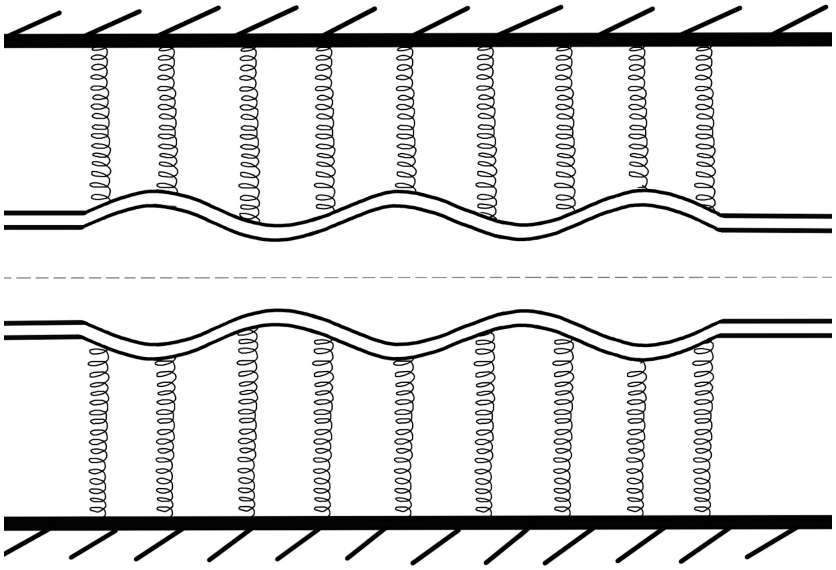

Figure 0.1: A schematic illustration of the theoretical model of our channel walls for a compliant surface inspired by the work of [1].

Kumaran [23] investigates the stability problem for the fluid flowing through flexible tubes, an application of this research are blood vessels in biological systems. As mentioned by the author of [23], it is usually assumed that the flow characteristics are the same as those of the flow through a *rigid tube*. However, the experiments of Krinder and Silberberg [32], done for the same ranges of the Reynolds numbers as in [23], suggest that the stability characteristics of the flexible channel flow could be very different from those of the flow in a tube with rigid walls. In particular, an anomalous drag force is observed when the fluid velocity is increased beyond a critical value, which depends on the fluid viscosity, the wall elasticity, and the dimensions of the tube and wall. The nature of the instability is also different: in a flexible tube, there is a gradual increase in the drag force as the Reynolds number is increased; in contrast to the sharp, almost discontinuous, jump in the drag force in a rigid tube at the critical Reynolds number. The collapse of a flexible tube due to the difference between the external and internal pressures has been extensively studied both experimentally [18–20] and theoretically [21, 22]. Kumaran [23] performs a linear analysis to determine the stability of a *viscous* flow in a tube with viscoelastic walls and to examine the mechanism that causes unstable oscillations *in the wall*. Perturbations in the form of Fourier modes (the normal mode analysis) are imposed on the base flow, and the temporal growth rate is determined as a function of the wavenumber, fluid velocity, and the wall and fluid properties.

In his paper [33], Kumaran derives the results on hydrodynamic stability for inviscid flow through a flexible tube, which are similar to the classical results of Drazin and Reid [34]. The results on both axisymmetric and non-axisymmetric perturbation in flow in cylindrical geometries are presented. Perturbations of the form $\exp[ik(x - ct) + in\phi]$ are imposed on a steady axisymmetric mean flow $V(r)$, and the stability of the mean velocity profiles and bounds for the phase velocity of the unstable modes are determined. (Here r, ϕ, and x are the radial, polar, and axial directions, and k and c are the wavenumber and phase velocity.) The flexible wall is represented by a standard constitutive equation, which contains inertial, elastic, and dissipative terms. Kumaran [33] derives the explicit results in two limiting cases: axisymmetric flows ($n = 0$) and highly non-axisymmetric flows ($n \gg k$). In particular, axisymmetric perturbations are always

stable for $(V'' - r^{-1}V')V \geq 0$ and could be unstable for $(V'' - r^{-1}V') < 0$; highly non-axisymmetric perturbations are always stable for $(V'' + r^{-1}V')V \geq 0$ and could be unstable for $(V'' + r^{-1}V')V < 0$. For the practically important case of the Poiseuille flow, the analysis shows that axisymmetric perturbations are always stable, while highly non-axisymmetric perturbations could be unstable.

Heil and Jensen [2] review research dealing with theoretical investigation of the behavior of collapsible tubes and applications of the results to several biological phenomena. The authors mention that most of the results are obtained for one- and two-dimensional models, which being relatively simple, involve a number of *ad hoc* assumptions whose validity needs to be assessed critically. The computational and asymptotic analyses of flows in two-dimensional collapsible channels provide deep insight into complex fluid-structure interactions. An asymptotic analysis is most appropriate approach to analyze flows in slightly deformed channels, whereas the stability of flows in strongly collapsed channels has to be determined using a numerical approach. Heil and Jensen indicate that their investigations of steady finite-Reynolds-number flows in three-dimensional collapsible tubes have already revealed many features which cannot be predicted by the lower-dimensional models. Asymptotic analyses of flows in slightly buckled elastic tubes provides useful insight into the flow separation and the development of flow instabilities. The authors have demonstrated that the combined use of theoretical, computational, and experimental techniques provides significant advances in areas that at first seemed intractable.

One of the most important equipment used in a laboratory to reproduce the physiologically observed phenomena is the *Starling resistor* (see Fig. 0.2).

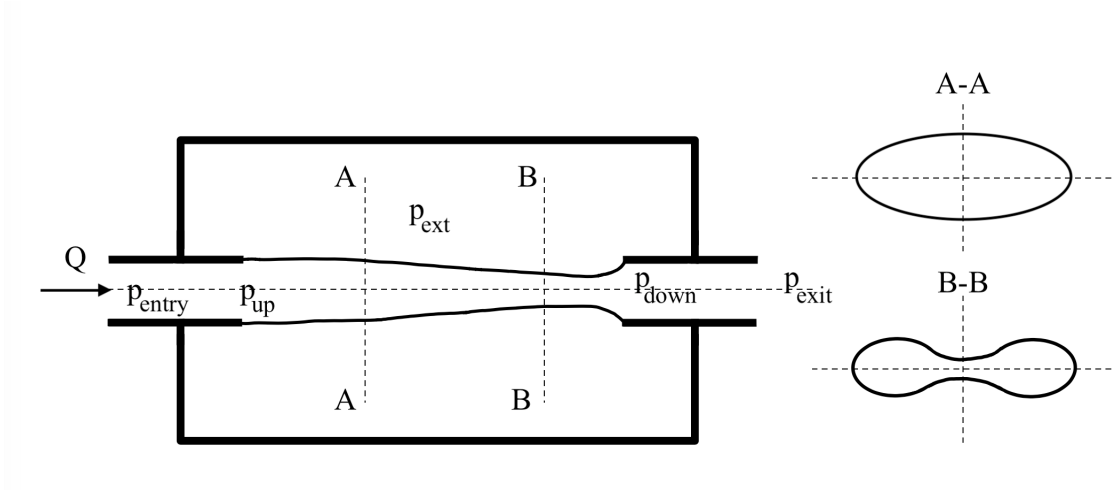

Figure 0.2: Left: sketch of the typical experimental setup which forms the basis of most theoretical models. Right: tube cross sections at A-A and B-B [2].

Inside a pressure chamber, a thin-walled elastic tube is mounted on two rigid tubes. Fluid (air or water) is driven through the tube, either by applying a controlled pressure drop ($p_{entry} - p_{exit}$) between the ends of the rigid tubes or by controlling the flow rate Q. The external pressure, p_{ext}, can be controlled independently. If p_{ext} exceeds the fluid pressure by a sufficiently large amount, the tube buckles non-axisymmetrically. Flow-structure interactions lead to nonlinear relations between pressure-drop and flow-rate, depending on which pressure differences are held fixed as the flow increases. The authors show that at sufficiently large Reynolds numbers, the system readily produces self-excited oscillations, multiple modes of oscillations (with a distinct frequency range), and rich and complex nonlinear dynamics.

Whittaker, et al. [13] develop a theoretical model describing self-excited oscillations in a three-dimensional elastic-walled tube. The mathematical model is given in the form of a system of ordinary differential equations and boundary conditions, governing the oscillatory component of the pressure as a function of the axial coordinate. Solutions provide information on the normal modes and associated frequencies. Consideration of the system's energy budget predicts that these modes grow exponentially. The leading-order oscillations are governed by a balance between axial fluid inertia and the elastic forces in the wall, and decouple from the steady flow.

The authors prove that the mode shapes and frequencies are independent of the imposed steady flux, but the flux is crucial in determining the growth rate. The fundamental (lowest frequency) mode always has the largest (most positive) growth rate, and therefore is the most unstable.

Substantial current research is devoted to modeling and explaining human snoring. Auregan and Depollier [7] ask the following questions: *"Why does one snore? What are the conditions for snoring?"* In order to find a biomechanical model providing answers to those questions, the authors have taken into account that the size of the vibrating structure is of the order of the perturbation wavelength (small aspect ratio). In this case, the simplest way to take the boundary conditions into account is a modal expansion in combination with Galerkin's method. The authors justify that the modal expansion makes the study easier, and the simplest modeling is associated with a two-mode flutter.

Liu, et al. [10] investigate the snoring mechanism from a biomechanical point of view through a Finite Element dynamic analysis of the *entire human head*. The authors suggest that the snoring sources and sinks, which may be used as snoring control or snoring treatment locations, can be identified by using the Structural Intensity Methodology. One of the main objectives of Liu, et al. [10] is to predict the snoring noise intensity level using the vibro-acoustic concept.

The mechanism of snoring is vibration of anatomical structures in the pharyngeal airway. Flutter of the soft palate accounts for the harsh aspect of the snoring sound. Natural or drug-induced sleep is required for its appearance. Snoring carries information related to the site and degree of obstruction of the upper airway. These considerations have inspired researchers, Pevernagie, et al. [11], to scrutinize the acoustic characteristics of snoring events. Similarly to speech, snoring is produced in the vocal tract. Existing techniques for speech analysis have been applied to evaluate snoring sounds. It appears that the pitch of the snoring sound is in the low-frequency range (< 500 Hz) and corresponds to a fundamental frequency with associated harmonics. The pitch of snoring is determined by vibration of the soft palate, while nonpalatal snoring is more 'noise-like', and has scattered energy content in the higher spectral sub-bands (> 500 Hz).

According to Wang, et al. [11], the coupled dynamics of airflow, soft-palate vibrations and

motion of the airway walls (the pharynx) in humans underpin snoring and the more serious condition of sleep apnea (the total closure of the airway). Endoscopic observations suggest that snoring noises originate from oscillations of the soft palate that separates oral and nasal inlets, while airway collapse occurs in the oropharynx near the tip, or just downstream of the soft palate. The dynamics of a cantilevered flexible plate in channel flow as a model for the mechanics of snoring has received a large amount of attention. Such studies focus upon the stability characteristics of the flexible plate, showing that beyond a critical flow speed (or Reynolds number), the plate succumbs to flutter instability. In their study, the authors of [6] describe an efficient experimental setup: the pharynx modeled as a flexible tube in which a cantilevered flexible, soft-palate is mounted. Each flexible component of the system has its own dynamics and these are coupled through the fluid flow.

Medical research has recently discovered that breathing may become compromised during sleep. As soon as one falls sleep, there is a physiologic relaxation of all postural muscles, including those surrounding and supporting the upper airway. With less muscle tone during sleep, the upper airway of some individuals may collapse and cause significant flow limitation or complete cessation of airflow (sleep apnea). The upper airway patency during sleep is determined by the balance between collapsing and dilating forces. Inspiration creates a negative airway pressure, which increases the tendency of the upper airway to collapse. Starling's resistor theory predicts that flow can increase with increasing driving pressure only up to a *critical value* for the transmural pressure (the pressure difference between the inside and outside of the upper airway). At higher driving pressures a partial collapse occurs and there is no further increase in flow despite greater respiratory effort. The critical value for the transmural pressure and thus the capability of the upper airway to resist the collapse depends strongly on the stiffness of the pharyngeal soft tissues and on the operation of the dilating muscles of the upper airway. Aittokallio, et al. [6] propose a mathematical model, which consists of a system of partial differential equations with supplementary boundary conditions, in which the operation of the lungs (both the inspiratory and the expiratory phase) is included. The model can partially explain

the normal behavior of the upper airway as well as the partial collapse and snoring.

In their study, Beck, et al. [8] discuss the acoustic properties of snoring sounds in the time and frequency domains. The authors of [8] identify two distinctly different patterns: the 'simple-waveform' and the 'complex-waveform.' The complex-waveform snore is characterized by repetitive, equally-spaced, train of sound structures, starting with a large deflection followed by a decaying amplitude wave. In the frequency domain, it is characterized by multiple, equally-spaced peaks of power (comb-like spectrum). Simple-waveform snores have a quasi-sinusoidal waveform, with a range of variants, and almost no secondary internal oscillations. Their power spectrum contains only 1 – 3 peaks, of which the first is the most prominent. The complex-waveform snores result from collision of the airway walls and represent actual brief airway closure. Simple-waveform snores are of higher frequency and probably result from oscillation around a neutral position without actual closure of the lumen.

Grotberg and Gavriely [9] present mathematical analysis of the model of the flow through a flexible channel. They are interested in flow-induced flutter oscillations that pertain to the production of wheezing breath sounds. The model predicts the critical fluid speed that initiates flutter of the wall. The mathematical results are separated into linear theory (small oscillations) and nonlinear theory (larger oscillations). Linear theory determines the onset of flutter, whereas nonlinear theory determines the relationship between the fluid speed and both the wave amplitudes and frequencies. The linear theory predictions correlate well with data taken at the onset of flutter and flow limitation during experiments of airflow in thick-walled collapsible tubes. The nonlinear theory predictions correlate well with data taken as these flows are forced to higher velocities while keeping the flow rate constant.

Païdoussis and Li [35] present a comprehensive study of different types of pipes conveying fluid, such as straight and curved pipes, cantilevered and supported pipes. The undeformed pipe is straight, thick-walled, and slender enough to be described as a beam, with no intermediate supports; the fluid is incompressible, and the motions small enough to be analyzed by linear theory. The study of pipes conveying fluid was initiated and carried out by Ashley and Haviland [36] in an attempt

to explain the vibrations observed in the Trans-Arabain Pipeline. Païdoussis and Li [35] provide a detailed analysis of two models: the first one is related to the dynamics of supported pipes and the second is related to the cantilevered pipes. The authors obtain the equation describing the dynamics of a pipe supported at both ends

$$EI\,\frac{\partial^4 w}{\partial x^4} + MU^2\,\frac{\partial^2 w}{\partial x^2} + 2MU\,\frac{\partial^2 w}{\partial x \partial t} + (M+m)\,\frac{\partial^2 w}{\partial t^2} = 0, \tag{0.0.1}$$

where EI – flexural rigidity of the pipe, M – the mass of the fluid per unit length, U – a steady flow velocity, m – the mass of the pipe per unit length, and w – the lateral deflection of the pipe. The fluid forces are modeled in terms of a plug flow model. The various terms in the equation may be identified as the flexural restoring force, a *centrifugal* term, a Coriolis term, and the inertia term. By comparing (0.0.1) to the equation of motion of a beam subjected to a compressive load, P,

$$EI\frac{\partial^4 w}{\partial x^4} + P\frac{\partial^2 w}{\partial x^2} + m\frac{\partial^2 w}{\partial t^2} = 0, \tag{0.0.2}$$

it becomes clear that the centrifugal force acts in the same manner as a compressive load. Thus, for sufficiently large U, the destabilizing centrifugal force may overcome the restoring flexural force, resulting in divergence, known as buckling, or as a *pitchfork bifurcation* [34]. For a pipe with supported ends, divergence is the expected form of instability. However due to the Coriolis term, the system could also be subject to post-divergence coupled-mode flutter by coalescence of two modes in the complex-frequency plane, which is predicted by linear theory.

The authors of [35] consider straight cantilevered pipes as their second case of study. A cantilevered pipe conveying fluid is a nonconservative system, which for sufficiently high flow velocity, loses stability by flutter of the single-degree-of-freedom type, i.e. via a *Hopf bifurcation*. The authors explain such behavior by analyzing the work done on the pipe over a cycle of oscillations. In this case, the work is nonzero and can be represented in the form

$$\Delta W = -MU \int_0^T \left[\left(\frac{\partial w}{\partial t} \right)^2 + U \left(\frac{\partial w}{\partial x} \right) \left(\frac{\partial w}{\partial t} \right) \right]_{x=L} dt \tag{0.0.3}$$

for a pipe fixed at the end $x = 0$ and free at the end $x = L$. For small $U > 0$, it can be seen from equation (0.0.3) that $\Delta W < 0$, and free motions of the pipe are damped. This damping effect is due to the Coriolis forces, which, in this case do the work. If, however, U is sufficiently large, while over most of the cycle $(\partial w/\partial x)_{x=L}$ and $(\partial w/\partial t)_{x=L}$ have opposite signs, then $\Delta W > 0$; i.e. the pipe will gain energy from the flow, and free motions will be amplified.

Amabili, et al. [37] discuss the nonlinear dynamics and stability of circular cylindrical shells containing fluid flow. Linear potential flow theory is applied to describe the fluid-structure interaction, where the amplitude of shell displacement remains small enough to make use of linear fluid mechanics. The nonlinearities due to large amplitude shell motions are taken into account by using Donnell's nonlinear shallow shell theory. The authors consider two different sets of boundary conditions for the fluid flow beyond the shell extremities, corresponding to (i) infinite baffles (rigid extensions of the shell) and (ii) connection with a flexible wall of infinite extent in the longitudinal direction, permitting the solution of the corresponding mathematical model by separation of variables. Numerical results show that the system loses stability by divergence.

The authors of [38], Païdoussis, Semler, and Wadham-Gagnon, present an extended review of the literature on the stability problem of the aspirating pipes. Collecting together multiple points of view of different authors, they conclude "In spite of the fact that so many researchers tried to resolve the problem, this deceptively simple looking question is still open." To support their theoretical analysis presented in [38], the authors design and conduct an experiment, involving two nominally identical vertical, cantilevered, flexible pipes, submerged in a water tank; at the free end, each pipe is fitted with a 90° elbow. One pipe discharges water at the free end, while the other aspirated. When the flow is turned on, the discharging pipe bent backward in the plane of the elbow as a result of the centrifugal force at the elbow. However after a starting transient, the aspirating pipe remained vertical and undeformed. This observation supports the theoretical conclusion stating *the stability* of aspirating pipes at least at low flow-rates.

In his paper [39], Païdoussis considers two different cases of the pipe dynamics. As the first

case, the author studies the discharging pipe described by equation (0.0.4),

$$EI\frac{\partial^4 w}{\partial x^4} + MU^2\frac{\partial^2 w}{\partial x^2} + 2MU\frac{\partial^2 w}{\partial x \partial t} + (M+m)\frac{\partial^2 w}{\partial t^2} = 0. \tag{0.0.4}$$

The first term in equation (0.0.4) is the flexural restoring force. Upon recalling that $\partial^2 w/\partial x^2 \sim 1/R$ where R is the local radius of curvature, it is obvious that the second term in equation (0.0.4) is associated with centrifugal forces as the fluid flows in curved portions of the pipe. The third term in equation (0.0.4) is associated with the Coriolis acceleration, and the last term represents inertial effects. For sufficiently small $U>0$, the dynamics are dominated by the Coriolis force, $2MU(\partial^2 w/\partial x \partial t)$, and the system is subjected to flow-induced damping. For sufficiently large U, the centrifugal force, $MU^2(\partial^2 w/\partial x^2)$, overcomes the Coriolis damping effect, and the system loses stability by single-mode flutter via a Hopf bifurcation. It is shown that the work $\Delta W \neq 0$ done by the fluid on the pipe during one period is given by equation (0.0.5),

$$\frac{\partial}{\partial t}[T + p_e A_e - p_i A_i - \rho_i (A_i U_i) U_i] = 0, \tag{0.0.5}$$

in which $(\partial w/\partial t)_L$ and $(\partial w/\partial x)_L$ are, respectively, the lateral velocity and slope of the free end. For small $U > 0$, the first term dominates, and the work done is negative, which means that the pipe loses energy to the flowing fluid, and free pipe motions are damped. For high enough U, however, the second term dominates, which means that the work done may be positive, and energy flows from the fluid (a source of *unbounded energy*) to the pipe, resulting in amplified oscillations.

As the second case, the author considers the situation with $U < 0$, i.e., consider the aspirating system, presuming that equation (0.0.4) still holds true, with $(-U)$ instead of U. In this case, equation (0.0.5) yields exactly the *opposite* conclusions: (i) in the course of free motions, the pipe absorbs energy from the fluid for sufficiently small $|U|$ and is, therefore, subjected to flutter; (ii) for higher $|U|$, the pipe loses energy to the fluid, and hence it is stabilized and its motions are damped. Consequently, the startling conclusion is reached that the system is unstable for quite small $|U|$. This is precisely the linear analysis result of the system obtained by Païdoussis and

Luu [16]. Several attempts to verify experimentally these findings failed: the pipe remained inert as the flow velocity was increased, up to the point where it collapsed as a shell in the second circumferential mode (i.e. it became flattened). Païdoussis formulates a paradox: a theory predicts that the aspirating pipe loses stability at quite small flow velocity, but experiments show the system to remain stable at least to the maximum attainable flow prior to pipe collapse. *Reversing the flow direction in the experiments does not invert the stability behavior of the pipe*.

For a long time, it was believed that subsonic/incompressible flows were associated with loss of stability in the form of mild (small amplitude) divergence, in contrast to the flutter observed with supersonic flows. Païdoussis and Denise [15] provide the first linear analytical model for clamped-clamped shells (i.e. shells with both ends clamped) and clamped-free shells conveying inviscid fluid, along with experimental results. Karagiozis, et al. [14] consider the analytical model which is based on Flügge's shell equations and potential flow theory. The equations are solved using a traveling wave solution. The experimental results for clamped-clamped shells show that at sufficiently high flow velocity the system develops flutter, with shell amplitudes much larger than the shell thickness. In contrast, the theoretical model predicts that the system loses stability by divergence, and then at higher flow velocity by coupled-mode flutter. The predicted coupled-mode flutter originates *directly* from a divergent state, i.e. without restabilization in-between. The interval between divergence and flutter is small, especially if the fluid conveyed is air. Hence, in the Païdoussis and Denise experiments [15], it is reasoned that flutter was entrained by the divergence, and that was the reason why divergence by itself was not observed.

Additionally, Païdoussis and Denise investigate in [15] the nonlinear dynamics and stability of clamped-clamped cylindrical shells subjected to axial fluid flow. The authors use a nonlinear theoretical model, which employs the Donnell nonlinear shallow shell equations to describe the geometrically nonlinear structure. The clamped beam eigenfunctions are used to describe the axial shell deformation, automatically satisfying the boundary conditions and the circumferential continuity condition. The fluid is assumed to be incompressible and inviscid, and the fluid-structure interaction is described by linear potential flow theory. The partial differential

equation of motion is discretized using the Galerkin method and the final set of ordinary differential equations are integrated numerically. A theoretical model for shells with simply supported ends is presented as well. The theoretical and experimental results indicate the loss of stability by divergence with a subcritical nonlinear behavior.

The author of [17] reviews numerous studies conducted by different researchers over a decade and concludes that in spite of enormous efforts, there are three groups of open problems. They are (i) post-divergence flutter of shells subjected to axial flow; (ii) stability of fluid-conveying shells with different upstream and downstream end support conditions; and (iii) stability of aspirating cantilevered pipes, such as those used in ocean mining.

In many applications, including the lung airways, the length of the flexible tube is shorter than the entrance length of the flow. The primary objective in the study by Larose and Grotberg [3] is to explore the fluid-elastic (flutter) instability with a *developing flow*. The authors choose a planar channel model to avoid additional issues involving the non-planar three-dimensional geometry of a collapsed tube or lung airway. (See Fig. 0.3 for schematic representation of the experimental part of reference [3].) The authors consider the full linear stability problem for a *developing profile* in a compliant channel. They introduce the model and present analytical (long wave) and numerical approximations for the solutions. Comparison of theoretical results indicate good agreement with representative experiments.

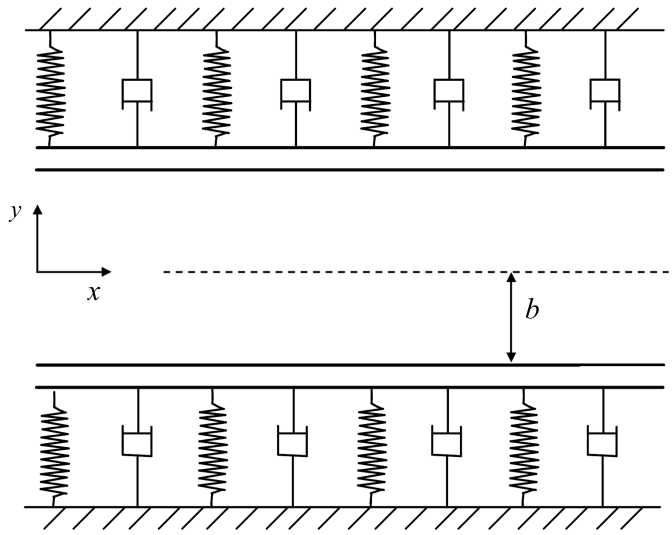

Figure 0.3: Flexible walled channel model [3].

In a series of works [40–42] Bach, et al. investigate and compare systematically the influence of various parameters on the stability behavior of the flexible channel walls conveying fluid. The fluid is assumed to be inviscid and irrotational where both compressible and incompressible cases are considered. The steady flow is bounded by a planar channel with a thin, flexible wall. The wall is modeled as a continuum on a viscoelastic foundation, which exhibits bending and extensional stiffness. The influence of the various characteristics on the complex eigenvalues relating to the stability of the steady state is discussed.

Armitstead, et al. [4] present the experimental and theoretical results of behavior on a collapsible tube. The main tool in experimental study is the Starling resistor (see Fig. 0.2). Armitstead, et al. propose mathematical models of collapsible-tube behavior that can be classified into two groups: (i) time-dependent (or lumped-parameter) models and (ii) time-space parameter dependent models. In lumped-parameter models, the flow is characterized by a number of time-varying, spatially invariant parameters (e.g., cross-sectional area at the point of collapse), and in more complex models, the selected parameters are considered to vary both temporally and over spatial dimensions. The former models can be represented mathematically in the form of a system of ordinary differential equations, while the latter models require the set of partial differential equations in order to account for both

spatial and temporal variations. In both cases, the equations are nonlinear due to the associated fluid-mechanical interactions. The authors of [4] analyze the system of three coupled ordinary differential equations and present their theoretical results on the bifurcation diagram (see Fig. 0.4). This diagram shows the topological changes in the model solutions as the control parameter, the external pressure, is varied.

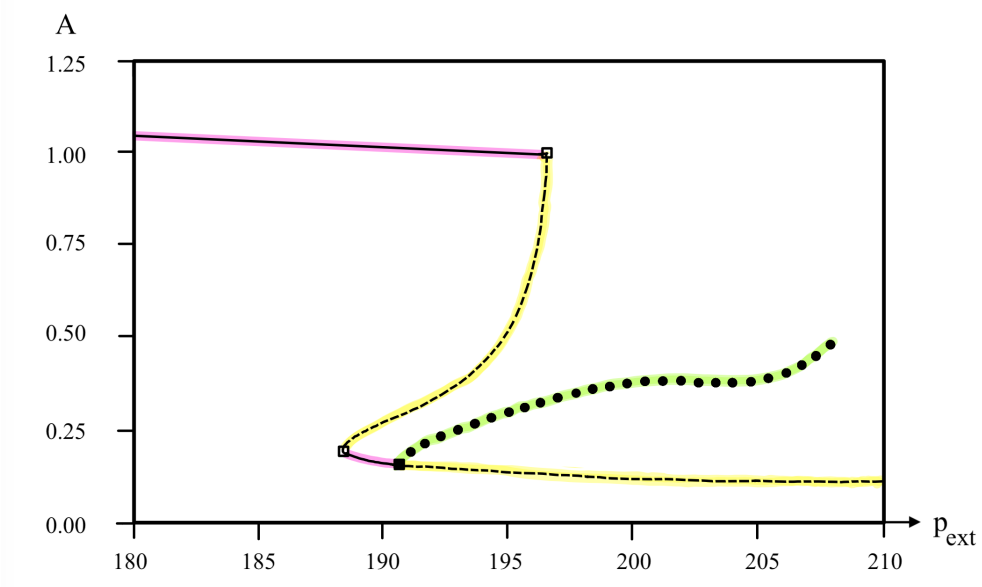

Figure 0.4: A bifurcation diagram in (p_{ext}, A) space for $p_{up} = 295$ [4].

Fig. 0.4 shows a bifurcation diagram with chamber pressure p_{ext} as the control parameter. The ordinate is A, the non-dimensional area at the most collapsed part of the tube, or in the case of unsteady behavior, the maximum of $A(t)$. *Stable steady* solutions are indicated by full lines; *unstable steady* solutions are indicated by dashed lines; *unstable unsteady* solutions are shown by blackened circles. Three bifurcations points are indicated on Fig. 0.4. A pair of folds or saddle-node bifurcations (marked by open squares) are associated with the hysteretic collapse of the tube as p_{ext} is increased. The filled square at $p_{ext} \approx 191$ denotes a Hopf bifurcation, which means that a *repellor* is thus created and limit cycles subsequently develop.

Jensen and Heil [26] derive high-Reynolds-number asymptotics and perform numerical simulations to describe two-dimensional, unsteady, pressure-driven flow in a finite-length

channel, one wall of which contains a section of membrane under longitudinal tension. Based on the results of their asymptotic analysis, the authors predict stability boundaries for small-amplitude, high-frequency, self-excited oscillations. It is shown that oscillations can grow by extracting kinetic energy from the mean Poiseuille flow faster than it is lost to viscous dissipation. Direct numerical simulations, based on a fully coupled finite-element discretization of the equations of large-displacement elasticity and the Navier-Stokes equations, support the predicted stability boundaries.

Ellis, et al. [25] suggest a mechanical model to simulate the palate and upper airway interaction. It comprises a round tube divided into two channels by a rigid partition equivalent to the hard palate, and a short length of flexible material analogous to the soft palate (see Fig. 1 of [25]). When air is sucked through the tube by a pump above a critical speed, the flexible membrane vibrates and a sound similar to snoring is produced. The vibrating membrane enables transfer of energy from flow to sound, which is an inevitable by-product of unsteady flow. Both the absolute wind speed and the difference in speed across the soft palate are important in the generation of sound. The shorter the membrane is the less likely it is to flutter. A very limp palate will flutter at a lower wind speed than a more rigid one. Palatal flutter is the dominant mechanical cause of snoring. The results of the authors' experimental work predict that either shortening or stiffening the soft palate would relieve snoring.

Huang and Williams [27] emphasize that snoring and obstructive apnea only occur during sleep, which means that effective *neuromuscular* functioning of the upper airway during sleep is vital for the maintenance of unimpeded breathing. Clinical studies in humans demonstrate that upper airway neural receptors sense the negative pressure generated by inspiration and 'trigger' (with a certain delay) reflex muscle activation to sustain the airway that might otherwise collapse. Based on these findings, Huang and Williams propose a model in which the mechanics are coupled to the neuromuscular physiology through the generation of reflex wall stiffening proportional to the retarded fluid pressure.

Huang [5] studies the collapse and subsequent self-excited oscillation of compliant tubes

conveying fluids. The author considers a two-dimensional, inviscid, shear flow in a flexible channel of infinite length subject to linear, traveling varicose waves. A boundary value problem is investigated for the pressure perturbation induced in shear flow through channels, whose walls undergo symmetric wave motions. One of the main results obtained by the author is the reversal of the collapsing tendency of compliant fluid passages proven for the flow having a moderate velocity gradient near the wall. The reversal of the Bernoulli effect can be seen as the channel-wall amplification of Miles's [43] water wave generation mechanism. Huang [5] also observes that the fluid pressure always has a component in phase with the wave slope causing wave drag and energy transfer from the flow to the perturbation waves. This energy transfer is suggested as a mechanism for traveling wave flutter. The corresponding eigenvalue problem is considered and the critical flow velocity and the wave speed for flutter onset are given for simply supported compliant channels.

Huang [44] presents a linear analysis of a coupled system describing the Poiseuille flow and a tensioned membrane of finite length using an eigenvalue approach. In particular, the author shows the following results. (i) Flutter and divergence may occur at similar flow velocities, and may coexist. Flutter and divergence exchange dominance when the wall properties change. Membrane inertia and membrane length are pro-flutter, while structural damping suppresses divergent oscillations. (ii) Conditions at the upstream and downstream ends of the channel crucially affect the structural stability. The author analyzes two problems, which Huang calls the 'blowing flow' case and the 'suction flow' case. In the blowing flow case, the upstream part has a fixed volume flow rate while the downstream one has a fixed pressure. In the suction flow case, the upstream part has a fixed pressure while the downstream one has a fixed volume flow rate. (iii) Lastly, the elastic waves over a finite membrane have a standing wave pattern, which can be decomposed into upstream traveling wave and downstream traveling wave. The component of the downstream traveling wave is responsible for energy transfer from the fluid to the wall.

Now we are in a position to outline briefly the content of the present dissertation. Chapter 1 is devoted to the derivation of the mathematical model describing pressure perturbation in the

horizontal channel. In the present work, we assume that the channel (the artery) is a horizontal tube with the following properties of the walls reflecting physical origin of the model.

(1) The model is symmetric with respect to the centre-line of the tubular channel. Due to this symmetry we obtain that the problem can be represented as a two-dimensional model with the horizontal axis being the x - coordinate axis and the vertical axis being the y - coordinate axis (see Fig. 1.1). Also based on the model's geometry, we can consider only half of the channel, whose upper boundary coincides with the center-line and the lower boundary coincides with the lower part of the flexible channel wall.

(2) There exists a large positive number, $R \gg 1$, such that within a symmetric interval $(-R, R)$ the wall is flexible and the lower boundary moves "almost harmonically" with the amplitude that changes according to the law

$$g(x,t) = C_0\, e^{i\omega(x-ct)}, \quad \omega > 0, \quad x \in [-R, R], \tag{0.0.6}$$

where ω is the wave number, c is the speed of the wave crest propagation (see [5], [23], [33]), and $g(x,t)$ denotes the transverse displacement of the channel wall at location x, at time t, and C_0 is a small, positive constant.

(3) We also assume that (i) here exists a positive number, $r : \ r \ll R$, such that outside the interval $[-R-r,\ R+r]$, the wall is rigid, i.e. the vertical displacement on $\mathbb{R}\backslash[-R-r,\ R+r]$ is reduced to zero, and (ii) there exists a smooth function $g_0(x)$ that governs the transition of displacement $g(x,t)$ from formula (0.0.6) to zero, i.e. we set

$$g(x,t) = g_0(x)e^{i\omega(x-ct)} \tag{0.0.7}$$

with $\text{supp}\{g_0(x)\} \in [-R-r, R+r]$ and $g_0(x) = g_0(0)$ for $x \in [-R, R]$ (see Fig. 0.5 below).

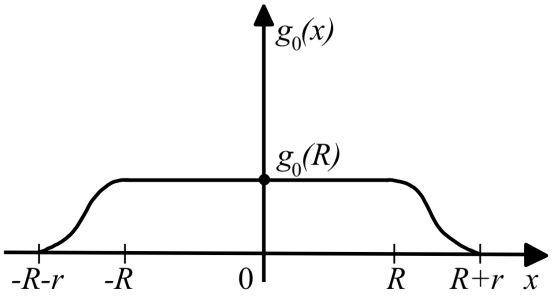

Figure 0.5: The amplitude profile function, $g(x,t)$.

For more precise description of the amplitude profile function, see Assumption 1.2.

In Section 1.1 we formulate the linearized version of the Naiver-Stokes equations using the mass conservation law and incompressibility condition. In Section 1.2 we derive the boundary conditions for the model which reflect an assumption chosen about the axial symmetry of the unperturbed problem with respect to the centerline of the channel. We consider quite general behavior of the boundary of the channel and derive the equation that relates the vertical component of the flow velocity and the velocity of the points of a solid boundary of the channel (see equation (1.2.3)). We emphasize here that we do not impose strong restrictions on the function describing the elevation of the lower boundary, which means that equation (1.2.3) can be used to analyze non-harmonic movement of the channel boundary.

In Section 1.2, we present the initial boundary value problem, IBVP: (1.2.10) – (1.2.13) for the stream function $\psi(x,y,t)$, in which an "almost harmonic" behavior of the wall is taken into account.

In Chapter 2, we provide a modification of the IBVP given by (1.2.10) – (1.2.13) and reduce it to a more tractable form. First, we apply the Fourier transformation to the equation and the boundary and initial conditions. As the result, we obtain an equation in which the partial derivatives, with respect to the x-variable, are replaced with polynomials with respect to the Fourier transform parameter, k (see equation (2.0.8)). Second, to the new equation we apply the Laplace transformation with respect to the time variable, t. The second integral transformation allows us to take into account the explicit expression for the unperturbed flow velocity profile,

$U(y)$. By applying the double integral transformations to the stream function, we reduce IBVP (1.2.10) – (1.2.13) to the new formulation (2.0.11) – (2.0.14). The main equation (2.0.11) is an ordinary differential equation with respect to the variable y (the width of the channel) parametrically depending on the complex parameter k (the result of the Fourier transformation). This equation has time-dependent right-hand side and non-homogeneous boundary conditions. We conclude this section with introducing and explicitly solving the boundary problem (2.1.6) – (2.1.8) for the corresponding stationary solution (2.1.9). Taking into account the stationary solution allows us to specify the set of functions that we use as the initial data for the IBVP (2.1.2) – (2.1.5) and reduce this problem to a new one having homogeneous boundary conditions (2.1.13) – (2.1.15).

The Section 2.2 is devoted to the construction of the inverse operator to the second order differential operator with the Dirichlet boundary conditions. The inverse operator is an integral operator, whose kernel is the Green's function. We derive an explicit formula for the Green's function (2.2.6) and present a closed-form expression for the Fourier transform of the stream function denoted by $\widetilde{\psi}(k, y, t)$ (see formula (2.2.8)). To examine the behavior of the stream function as a function of x, we have to evaluate the inverse Fourier transform of (2.2.8).

In the conclusion of the Introduction, we briefly explain the technical difficulties one has to overcome to yield these results, which are further discussed in Chapters 3 – 5. To this end, we describe some explicit formulae. As follows from (2.2.8), the Fourier transform of the stream function denoted by $\widetilde{\psi}(k, y, t)$, is represented as a sum of three terms. The inverse Fourier transform, which is the stream function ψ itself, also contains three terms denoted by I_1, I_2, and I_3. To demonstrate our technical results we consider the first term I_1, whose detailed analysis is given in Chapter 3, and outline the analytical tools needed to investigate the structure of I_1. Using Fourier and Laplace transforms we obtain the following formula for I_1 (see (3.0.2)):

$$I_1 = -\frac{c\omega}{\pi} e^{-i\omega ct} \int_R^{R+r} d\xi \; g_0'(\xi) \int_{-\infty}^{\infty} dk \; e^{ikx} \; \frac{\sinh(k(1-y))}{\sinh(k)} \; \frac{\sin(\xi(k-\omega))}{k-\omega}, \tag{0.0.8}$$

where R and r are introduced in (0.0.6) and (0.0.7) in the description of amplitude function. Formula (0.0.8) is not convenient for the analysis of the qualitative behavior of I_1 as a function of x and y. For this reason, we investigate the improper integral from (0.0.8) further and evaluate it using techniques of complex analysis. To carry out the integration in (0.0.8) with respect to k, we split $\sin(\xi(k-\omega))$ into two exponential functions and prove that each of the two resulting integrals, which we denote by $\mathcal{I}$ and $\widetilde{\mathcal{I}}$ respectively, converges in the sense of the *principal value*. Each integral, $\mathcal{I}$ and $\widetilde{\mathcal{I}}$, can be approximated by sequences of integrals $\mathcal{I}_n$ and $\widetilde{\mathcal{I}}_n$, $n \to \infty$, i.e. $I_1 = \lim_{n\to\infty}(\mathcal{I}_n + \widetilde{\mathcal{I}}_n)$. If we fix n, then the domain of integration for $\mathcal{I}_n$ (as well as $\widetilde{\mathcal{I}}_n$) is given by $(-\infty, \omega-\varepsilon_n) \cup (\omega+\varepsilon_n, \infty)$, with $\{\varepsilon_n\}_{n=1}^{\infty}$ being a sequence of positive numbers converging to zero. For each n, the domain consists of two disjoint subdomains. In turn, $\mathcal{I}_n$ can be represented as a limit of a sequence of integrals $\mathcal{I}_n^S$, where each $\mathcal{I}_n^S$ is defined on the domain $(-S, \omega-\varepsilon_n) \cup (\omega+\varepsilon_n, S)$, i.e. $\mathcal{I}_n = \lim_{S\to\infty} \mathcal{I}_n^S$. For a given pair (n, S) we consider a closed contour on the complex k-plane, obtained by connecting two segments $(-S, \omega-\varepsilon_n)$ and $(\omega+\varepsilon_n, S)$ by two semi-circles (see Fig. 0.6 below): $C_S(0)$ and $C_{\varepsilon_n}(\omega)$, where $C_S(0)$ is is a semi-circle centered at the origin of radius S and $C_{\varepsilon_n}(\omega)$ is a semi-circle centered at $x = \omega$ of radius ε_n.

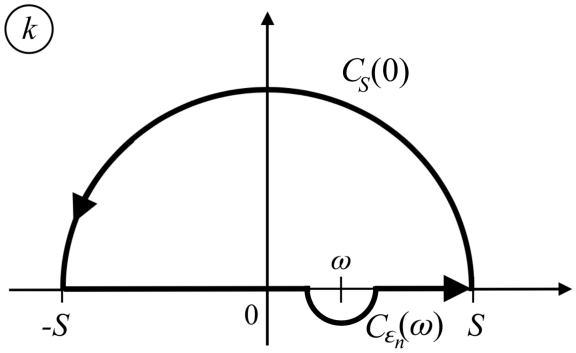

Figure 0.6: Closed semi-circle contour in the complex k-plane.

We show that the integral along $C_S(0)$ tends to zero as $S \to \infty$ and the integral along $C_{\varepsilon_n}(\omega)$ tends to zero as $\varepsilon_n \to 0$. Thus, we show that the integral $\mathcal{I}_n$ can be obtained as a limit of a sequence of the closed contour integrals. Similar steps can be carried out for evaluation of the integral $\widetilde{\mathcal{I}}_n$

by closing the contour of its integration in the lower half-plane. In turn, closed contour integrals can be evaluated by using the Residue theorem. As the result, we obtain that the term I_1 can be represented in the following form of an infinite series with respect to the residues:

$$I_1 = \frac{\omega c}{\pi}\, e^{-i\omega ct}\Bigg\{ e^{i\omega x}\, \frac{\sinh(\omega(1-y))}{2i\, \sinh(\omega)} + i\sum_{m=0}^{\infty} e^{\pi m x}\, \sin(\pi m y)\Bigg(\int_R^{R+r} d\xi\, g_0'(\xi)\, e^{-\pi m \xi}\, \frac{im\, \cos(\omega\xi) - \omega\, \sin(\omega\xi)}{m^2+\omega^2}\Bigg)\Bigg\}.$$

We notice that for $|x| < R$ and $\xi > x$, the series converges at an exponential rate. Thus to analyze the behavior of I_1 as a function of x, y, t, one can keep a finite number of terms in the sum and obtain the required accuracy.

The remaining Chapters 4 and 5 are devoted to a detailed derivation of the formulas for the terms I_2 and I_3. We carry out the evaluation of the improper integrals entering I_2 and I_3 and represent them as infinite series making use of the Residue theorem. Collecting together the results of Chapters 3 – 5, we obtain that the stream function $\psi(x, y, t) = I_1 + I_2 + I_3$ can be represented in the form of an infinite series with an exponential rate of convergence (see Theorems 3.6, 4.3, and 5.2 below). A summary of the results and technical tools is provided in Chapter 6.

CHAPTER 1

STATEMENT OF THE PROBLEM

We consider a two-dimensional, inviscid, incompressible shear flow through a long channel with elastic walls. The two channel walls undergo varicose heaving motions of small constant amplitudes in the form of a wave traveling in the direction of the flow. We assume that the unperturbed flow is moving in the horizontal direction along the x-axis (see Fig. 1.1). Using dimensionless variables, we set the channel height equal to two units and assume that the undisturbed flow is the symmetrization of the Couette flow with respect to the axis $y = 1$, the centerline of our channel. The channel wall movements induce pressure disturbances within the fluid flow. *Our goal is to derive the analytical representation of the fluid flow as it interacts with the flexible wall membrane.*

To derive the main governing equation, we start with the linearized version of the Euler momentum equation. Let $\mathbf{q}(x, y, t)$ be the velocity vector with the components $U(y) + u(x, y, t)$ and $v(x, y, t)$;

$$\mathbf{q}(x, y, t) = \begin{pmatrix} U(y) + u(x, y, t) \\ v(x, y, t) \end{pmatrix}. \tag{1.0.1}$$

The Euler momentum equation can be represented in the form

$$\frac{\mathrm{D}\mathbf{q}(x, y, t)}{\mathrm{D}t} + \nabla p(x, y, t) = 0, \tag{1.0.2}$$

where $p(x, y, t)$ is the pressure perturbation (a scalar function), $\mathbf{q}(x, y, t)$ is the velocity vector, and

$\frac{\mathrm{D}\mathbf{q}}{Dt}$ is the *total derivative*, which is defined by the following formula

$$\frac{\mathrm{D}\mathbf{q}(x,y,t)}{\mathrm{D}t} = \frac{\partial \mathbf{q}(x,y,t)}{\partial t} + \Big[\big(\mathbf{q}\cdot\nabla\big)\mathbf{q}\Big](x,y,t). \tag{1.0.3}$$

Here $\mathbf{q}\cdot\nabla$ is the formal dot-product of the velocity vector and the gradient vector operation. We need to figure out the space-time dynamics of the velocity vector, $\mathbf{q}$, which is given by $\mathbf{q}(x,y,t) = (U(y)+u(x,y,t), v(x,y,t))$, where $U(y)$ is the unperturbed flow profile. Evaluating the dot product, $(\mathbf{q}\cdot\nabla)$, we have

$$\mathbf{q}\cdot\nabla = \begin{pmatrix} U(y)+u(x,y,t) \\ v(x,y,t) \end{pmatrix}\begin{pmatrix} \frac{\partial}{\partial x} \\ \frac{\partial}{\partial y} \end{pmatrix} = \big(U(y)+u(x,y,t)\big)\frac{\partial}{\partial x} + v(x,y,t)\frac{\partial}{\partial y}. \tag{1.0.4}$$

Therefore, if we apply operation (1.0.4) to the vector $\mathbf{q}$, we obtain the following vector:

$$\begin{aligned} &\big[(\mathbf{q}\cdot\nabla)\mathbf{q}\big](x,y,t) = \\ &\begin{pmatrix} \big[U(y)+u(x,y,t)\big]\frac{\partial}{\partial x}\big[U(y)+u(x,y,t)\big] + v(x,y,t)\frac{\partial}{\partial y}\big[U(y)+u(x,y,t)\big] \\ \big[U(y)+u(x,y,t)\big]\frac{\partial}{\partial x}v(x,y,t) + v(x,y,t)\frac{\partial}{\partial y}v(x,y,t) \end{pmatrix}. \end{aligned}$$

Due to the representation (1.0.1), the above formula reduces to

$$\big[(\mathbf{q}\cdot\nabla)\mathbf{q}\big](x,y,t) = \begin{pmatrix} \big[U(y)+u(x,y,t)\big]\frac{\partial u(x,y,t)}{\partial x} + v(x,y,t)\big[U'(y)+\frac{\partial u(x,y,t)}{\partial y}\big] \\ \big[U(y)+u(x,y,t)\big]\frac{\partial v(x,y,t)}{\partial x} + v(x,y,t)\frac{\partial v(x,y,t)}{\partial y} \end{pmatrix}. \tag{1.0.5}$$

Substituting (1.0.5) into (1.0.3), we represent the Euler momentum equation (1.0.2) in the form of two coupled nonlinear differential equations,

$$\begin{aligned} &\big[U(y)+u(x,y,t)\big]u_x(x,y,t) + v(x,y,t)\big[U'(y)+u_y(x,y,t)\big] + u_t(x,y,t) + p_x(x,y,t) = 0, \\ &\big[U(y)+u(x,y,t)\big]v_x(x,y,t) + v(x,y,t)v_y(x,y,t) + v_t(x,y,t) + p_y(x,y,t) = 0. \end{aligned} \tag{1.0.6}$$

Keeping in mind that $U(y)$ is the given function representing the unperturbed flow profile, we

eliminate the nonlinear terms from system (1.0.6) and obtain the following linear system:

$$u_t(x,y,t) + U(y)\,u_x(x,y,t) + v(x,y,t)\,U'(y) + p_x(x,y,t) = 0, \tag{1.0.7}$$

$$v_t(x,y,t) + U(y)\,v_x(x,y,t) + p_y(x,y,t) = 0. \tag{1.0.8}$$

The system presented in (1.0.7) and (1.0.8) is the linearized version of the Euler momentum equation.

1.1 Mass conservation and the incompressibility condition

Dealing with a non-Newtonian fluid, we need to consider the incompressibility condition. This condition is stated as follows:

$$(\nabla \cdot \mathbf{q})(x,y,t) = 0, \tag{1.1.1}$$

which yields,

$$\frac{\partial(U(y) + u(x,y,t))}{\partial x} + \frac{\partial v(x,y,t)}{\partial y} = 0,$$

or equivalently,

$$u_x(x,y,t) + v_y(x,y,t) = 0. \tag{1.1.2}$$

From this, we pose the following lemma.

Lemma 1.1 *Let $u(x,y,t)$ and $v(x,y,t)$ be two functions with continuous partial derivatives, $u_x(x,y,t)$ and $v_y(x,y,t)$, defined on the domain $(x,y) \in \Omega \in \mathbb{R} \times [0,1]$. If these functions satisfy equation (1.1.2), then there exists a scalar function $\psi(x,y,t)$, called the stream function, such that*

$$u(x,y,t) = \psi_y(x,y,t) \quad \text{and} \quad v(x,y,t) = -\psi_x(x,y,t). \tag{1.1.3}$$

Proof. Let us define a new function by an explicit formula

$$\psi(x,y,t) = \int_{y_0}^{y} u(x,\eta,t)d\eta - \int_{x_0}^{x} v(\xi,y_0,t)d\xi. \tag{1.1.4}$$

Evaluating a partial derivative with respect to y of (1.1.4) yields

$$\psi_y(x, y, t) = u(x, y, t). \tag{1.1.5}$$

Evaluating a partial derivative with respect to x of (1.1.4) yields

$$\psi_x(x, y, t) = \int_{y_0}^{y} u_x(x, y, t)d\eta - v(x, y_0, t). \tag{1.1.6}$$

Taking into account equation (1.1.2), we proceed with (1.1.6) as follows:

$$\psi_x(x, y, t) = -\int_{y_0}^{y} v_\eta(x, \eta, t)d\eta - v(x, y_0, t) = -v(x, y, t). \tag{1.1.7}$$

Combining (1.1.5) and (1.1.7), we get the desired result (see Appendix A.1). ■

Lemma 1.1 allows us to rewrite our linearized system (1.0.7) and (1.0.8) in terms of a single function, $\psi(x, y, t)$.

In what follows, we consider a symmetric modification of the Couette flow, i.e. $U(y) = y$, $0 \leq y \leq 1$. Rewriting equations (1.0.7) and (1.0.8) in terms of the stream function, we obtain

$$\psi_{yt}(x, y, t) + y\,\psi_{xy}(x, y, t) - \psi_x(x, y, t) + p_x(x, y, t) = 0, \tag{1.1.8}$$

$$\psi_{xt}(x, y, t) + y\,\psi_{xx}(x, y, t) - p_y(x, y, t) = 0. \tag{1.1.9}$$

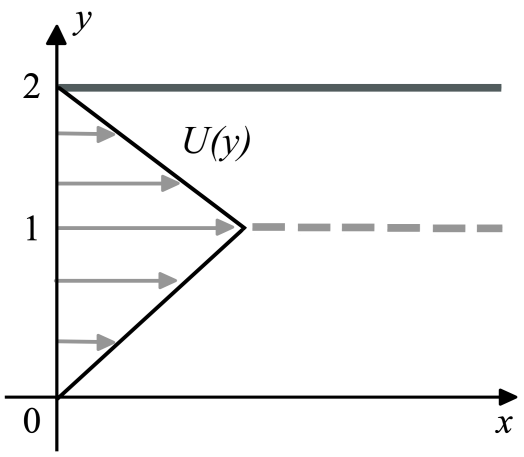

Figure 1.1: Symmetric flow profile, $U(y)$.

To eliminate pressure terms from equations (1.1.8) and (1.1.9), we differentiate (1.1.8) with respect to y and (1.1.9) with respect to x, yielding the following system:

$$\psi_{yyt}(x,y,t) + \psi_{xy}(x,y,t) + y\,\psi_{xyy}(x,y,t) - \psi_{xy}(x,y,t) + p_{xy}(x,y,t) = 0,$$
$$\psi_{xxt}(x,y,t) + y\,\psi_{xxx}(x,y,t) - p_{xy}(x,y,t) = 0,$$

which can be written in the following forms:

$$\left(\frac{\partial}{\partial t} + y\frac{\partial}{\partial x}\right)\psi_{yy}(x,y,t) + p_{xy}(x,y,t) = 0 \tag{1.1.10}$$

$$\left(\frac{\partial}{\partial t} + y\frac{\partial}{\partial x}\right)\psi_{xx}(x,y,t) - p_{xy}(x,y,t) = 0. \tag{1.1.11}$$

Summing (1.1.10) and (1.1.11) we eliminate the pressure term and obtain the following partial differential equation for the stream function:

$$\left(\frac{\partial}{\partial t} + y\frac{\partial}{\partial x}\right)\big(\psi_{xx}(x,y,t) + \psi_{yy}(x,y,t)\big) = 0. \tag{1.1.12}$$

1.2 Derivation of the boundary condition at the lower boundary

Recall that the fluid velocity is a two-component vector-valued function

$$\mathbf{q}(x, y, t) = \big(U(y) + u(x, y, t), v(x, y, t)\big)$$

where $U(y)$ is the basic, unperturbed flow profile, $u(x, y, t)$ and $v(x, y, t)$ are small perturbations. The vertical displacement of the lower wall at a position, x, and at a moment in time, t, is given by the equation $y = g(x, t)$.

To derive the lower boundary condition that is being perturbed by a traveling wave, we must derive the unit tangent and normal vectors with respect to the boundary. Let ν be the unit tangent vector at the point $(x, g(x, t))$ and $\mathbf{n}$ be the unit normal vector on the wall. We have $\nu = (\nu_1, \nu_2)$, $\nu_1^2 + \nu_2^2 = 1$, and $\nu_2 = \nu_1 g_x(x, t)$. Hence, the following representations are valid (see Appendix A.2):

$$\nu = \frac{1}{\sqrt{1 + g_x^2(x, t)}}\big(1, g_x(x, t)\big) \qquad \text{and} \qquad \mathbf{n} = \frac{1}{\sqrt{1 + g_x^2(x, t)}}\big(-g_x(x, t), 1\big). \tag{1.2.1}$$

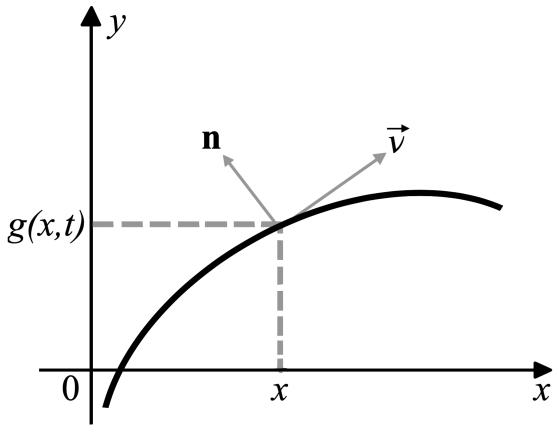

Figure 1.2: Geometry of the lower boundary.

Let $\mathbf{w}$ be the velocity of the point $(x, g(x, t))$. We assume that the wall points move only in the

vertical direction, i.e.,

$$\mathbf{w}(x,t) = \big(0, g_t(x,t)\big). \tag{1.2.2}$$

The boundary condition for the ideal fluid flow on the flexible boundary is

$$\mathbf{w} \cdot \mathbf{n} = \mathbf{q} \cdot \mathbf{n}$$

meaning that the normal components of the fluid velocity and the wall velocity are equal. Using formulas (1.2.1) and (1.2.2), we get

$$\begin{aligned}
\mathbf{w} \cdot \mathbf{n} &= \big(0, g_t(x,t)\big) \frac{\big(-g_x(x,t), 1\big)}{\sqrt{1+g_x^2(x,t)}} = \frac{g_t(x,t)}{\sqrt{1+g_x^2(x,t)}}\,, \\
\mathbf{q} \cdot \mathbf{n} &= \Big(U(y) + u(x,y,t), v(x,y,t)\Big) \frac{\big(-g_x(x,t), 1\big)}{\sqrt{1+g_x^2(x,t)}} \\
&= \frac{-\big[U(y) + u(x,y,t)\big] g_x(x,t) + v(x,y,t)}{\sqrt{1+g_x^2(x,t)}}.
\end{aligned}$$

Equating the right-hand sides of these equations, we obtain that the following equation is valid near the lower boundary

$$g_t(x,t) = -\big[U(y) + u(x,y,t)\big] g_x(x,t) + v(x,y,t). \tag{1.2.3}$$

Recall that $g(x,t)$ is the function which models the vertical displacement of the lower wall at a given position, x, and at a given moment in time, t. We assume that $g(x,t)$ is a function of small amplitude. For small values of y, we can use the following approximations for the functions $U(y)$, $u(x,y,t)$, and $v(x,y,t)$:

$$\begin{aligned}
U(y) &= U(0) + y\, U_y(0) + \frac{y^2}{2}\, U_{yy}(0) + \mathcal{O}(y^3), \\
u(x,y,t) &= u(x,0,t) + y\, u_y(x,0,t) + \frac{y^2}{2}\, u_{yy}(x,0,t) + \mathcal{O}(y^3), \\
v(x,y,t) &= v(x,0,t) + y\, v_y(x,0,t) + \frac{y^2}{2}\, v_{yy}(x,0,t) + \mathcal{O}(y^3).
\end{aligned}$$

Using the afore approximations and keeping only the zero order terms, from equation (1.2.3) we obtain the following approximation for the boundary condition:

$$g_t(x,t) + \big[U(0) + u(x,0,t)\big] g_x(x,t) = v(x,0,t). \tag{1.2.4}$$

According to the statement of the problem, $u(x,0,t) = 0$, the boundary condition at $y = 0$ can be modified as follows:

$$g_t(x,t) + U(0)\, g_x(x,t) = v(x,0,t). \tag{1.2.5}$$

Now we consider a specific function, $g(x,t)$, describing the elevation of the lower boundary.

Assumption 1.2. *The lower boundary of the channel has a long flexible section beyond which the wall is rigid. The vertical displacement of the wall, $y = g(x,t)$, satisfies the following conditions: (i) for $x \in [-R, R]$ with R being a large positive constant, the following representation is valid:*

$$g(x,t) = C_0 e^{i\omega(x-ct)}, \quad C_0 \ll 1, \quad \omega > 0, \tag{1.2.6}$$

where C_0 is a small positive amplitude, ω is a positive wave number, and c is the speed of wave propagation; (ii) there exist a positive constant r ($r \ll R$) and a twice continuously differentiable even function $g_0(x)$ such that (see Fig. 0.5 above):

$$\begin{aligned} &g(x,t) = g_0(x) e^{i\omega(x-ct)}, \quad x \in [-R-r, -R) \cup (R, R+r], \\ &g_0(-R-r) = g_0(R+r) = 0, \quad g_0(-x) = g_0(x) = C_0, \ \ x \in [-R, R], \\ &g_0(x) = 0 \ \text{ for } \ x \in (-\infty, -R-r) \cup (R+r, \infty). \end{aligned} \tag{1.2.7}$$

Using formulas (1.1.3), we rewrite (1.2.5) in terms of the stream function as

$$-i\omega c\ g(x,t) + U(0)\, g_x(x,t) = -\psi_x(x,0,t).$$

Since in our case $U(0) = 0$, we obtain,

$$\psi_x(x, 0, t) = i\omega c\ g(x, t). \tag{1.2.8}$$

In what follows, we consider (1.2.8) as *the boundary condition at* $y = 0$. Though we note that in the problem with a rigid wall channel, we would have had the condition $\psi_x(x, 0, t) = 0$.

To derive the second boundary condition, we use the fact that there is no vertical flow across the centerline: $y = 1$, due to our assumption of symmetry and thus

$$v(x, 1, t) = -\psi_x(x, 1, t) = 0. \tag{1.2.9}$$

Therefore, we consider the following initial boundary-value problem for the stream function:

$$\begin{cases} \left(\dfrac{\partial}{\partial t} + y\dfrac{\partial}{\partial x}\right)\left(\psi_{xx}(x, y, t) + \psi_{yy}(x, y, t)\right) = 0, \quad x \in (-\infty, \infty),\ 0 \le y \le 1,\ t \ge 0, & (1.2.10) \\ \psi_x(x, 0, t) = i\omega c\ g(x, t), & (1.2.11) \\ \psi_x(x, 1, t) = 0, & (1.2.12) \\ \psi(x, y, 0) = F(x, y). & (1.2.13) \end{cases}$$

CHAPTER 2

REFORMULATION OF INITIAL BOUNDARY VALUE PROBLEM

In this chapter, we apply two integral transformations to IBVP (1.2.10) – (1.2.13), which will allow us to reduce the IBVP involving a partial differential equation to the IBVP involving a parameter-dependent ordinary differential equation.

It is convenient to use the following notations. A Fourier transform, $\widetilde{f}(k)$, of a function $f(x)$, is define by

$$\widetilde{f}(k) = \int_{-\infty}^{\infty} e^{-ikx} f(x) dx, \tag{2.0.1}$$

and a Laplace transform, $\Phi(\lambda)$, of a function, $\varphi(t)$, is defined by

$$\Phi(\lambda) = \int_{0}^{\infty} e^{-\lambda t} \varphi(t) dt. \tag{2.0.2}$$

Assuming that the stream function and its higher order derivatives tend to 0 as $x \to \pm\infty$, we obtain the following formulae for the Fourier transforms:

$$\int_{-\infty}^{\infty} e^{-ikx} \left(\frac{\partial}{\partial x}\right)^n \psi(x, y, t) dx = (-ik)^n \, \widetilde{\psi}(k, y, t), \quad n = 0, 1, ..., \tag{2.0.3}$$

where $\widetilde{\psi}(k, y, t)$ is the Fourier transform of $\psi(x, y, t)$. Applying the Fourier transformation to equation (1.2.10) (see Appendix B.1.1) yields,

$$-k^2 \, \widetilde{\psi}_t(k, y, t) + \widetilde{\psi}_{yyt}(k, y, t) - ik^3 y \, \widetilde{\psi}(k, y, t) + iky \, \widetilde{\psi}_{yy}(k, y, t) = 0. \tag{2.0.4}$$

Let $\Psi(k, y, \lambda)$ be the Laplace transform of $\widetilde{\psi}(k, y, t)$ with respect to time variable, t. Applying the

Laplace transformation to both sides of equation (2.0.4) (see Appendix B.2.1) we obtain a new equation

$$-ik^3 y\,\Psi(k,y,\lambda)+iky\,\Psi_{yy}(k,y,\lambda)-\lambda k^2\,\Psi(k,y,\lambda)+\lambda\,\Psi_{yy}(k,y,\lambda)=\left(\frac{\partial^2}{\partial y^2}-k^2\right)\widetilde{\psi}(k,y,0), \quad (2.0.5)$$

which can be written in the form

$$\left(\frac{\partial^2}{\partial y^2}-k^2\right)\Psi(k,y,\lambda)=\frac{1}{\lambda+iky}\left(\frac{\partial^2}{\partial y^2}-k^2\right)\widetilde{\psi}(k,y,0), \quad (2.0.6)$$

where $\widetilde{\psi}(k,y,0)$ is the Fourier transform of the initial state. Notice, the only influence of the Couette–like flow is the "y" term in the denominator on the right-hand side of (2.0.6). If instead of Couette–like profile, we have an arbitrary axisymmetric profile, $U(y)$, then in place of y, we would have had the function, $U(y)$, and thus have a factor of $\big(\lambda+ikU(y)\big)^{-1}$ in equation (2.0.6).

The unknown function, $\Psi(k,y,\lambda)$ in (2.0.6), being a function of y, $0\le y\le 1$, depends on two complex parameters, k and λ. To justify (2.0.6) we have to impose such conditions on the wall dynamics that guarantee that the stream function and its derivatives tend to 0 as $|x|\to\infty$, and the application of the Fourier transformation is justified.

Applying the inverse Laplace transformation to both sides of equation (2.0.6) yields

$$\frac{1}{2\pi i}\int_\gamma\left(\frac{\partial^2}{\partial y^2}-k^2\right)\Psi(k,y,\lambda)\,e^{\lambda t}\,d\lambda=\frac{1}{2\pi i}\int_\gamma\frac{e^{\lambda t}}{\lambda+iky}\left(\frac{\partial^2}{\partial y^2}-k^2\right)\widetilde{\psi}(k,y,0)\,d\lambda, \quad (2.0.7)$$

where as the contour of integration can be taken as any vertical line, located in the open right half-plane of the complex λ-plane (see Fig. 2.1 below).

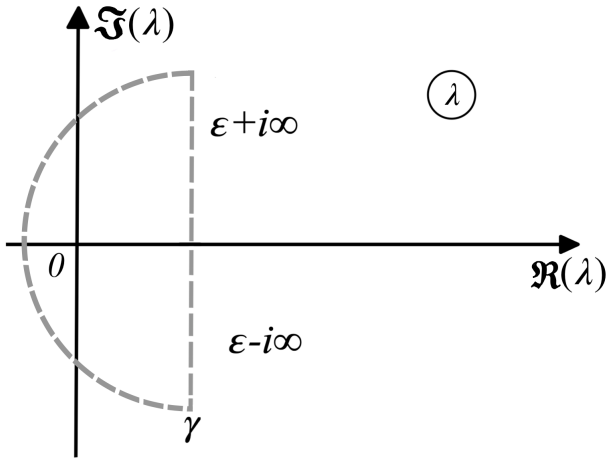

Figure 2.1: Contour for inversion of Laplace transform.

Assuming that the change of order of integration with respect to λ and differentiation with respect to y is justified, we reduce (2.0.7) to the following:

$$\left(\frac{\partial^2}{\partial y^2} - k^2\right)\widetilde{\psi}(k, y, t) = \left(\frac{\partial^2}{\partial y^2} - k^2\right)\widetilde{\psi}(k, y, 0)\left[\frac{1}{2\pi i}\int_{\gamma}\frac{e^{\lambda t}}{\lambda + iky}\, d\lambda\right]. \tag{2.0.8}$$

Closing the contour of integration in the λ-complex plane and using the Residue theorem to evaluate the contour integral at the right-hand side of equation (2.0.8), we obtain the desired form of the differential equation (see Appendix B.3):

$$\left(\frac{\partial^2}{\partial y^2} - k^2\right)\widetilde{\psi}(k, y, t) = e^{-ikyt}\left(\frac{\partial^2}{\partial y^2} - k^2\right)\widetilde{\psi}(k, y, 0). \tag{2.0.9}$$

Notice that at $t = 0$, the left and right sides of the equation are identical. Equation (2.0.9) is an *ordinary differential equation* with respect to the variable y parametrically depending on $k \in \mathbb{C}$. However, we do not have the boundary conditions for $\widetilde{\psi}(k, y, t)$; we have boundary conditions only for $\psi_x(k, y, t)$ when $y = 0$ and $y = 1$ (see (1.2.11) and (1.2.12)). Since $\psi_x(x, 1, t) = 0$, we immediately obtain the boundary condition at $y = 1$, $\widetilde{\psi}(k, 1, t) = 0$.

To derive the boundary condition at $y = 0$, we have to specify the properties of the force profile

function, $g_0(x)$ (see Assumption 1.2). According to the physical origin of the model, the channel walls are flexible for $|x| \le R+r$ and rigid for $|x| > R+r$. Let us evaluate the Fourier transformation of the boundary condition (1.2.11) (see Appendix B.1.2). Taking into account that $g_0(x)$ is an even function, we have

$$\begin{aligned} ik\,\widetilde{\psi}(k,0,t) &= i\omega c \int_{-\infty}^{\infty} g_0(\xi)\, e^{i\omega(\xi-ct)} e^{-ik\xi} d\xi \\ &= -2i\omega c\, e^{-i\omega ct} \int_R^{R+r} g_0'(\xi)\, \frac{\sin(\xi(\omega-k))}{\omega-k}\, d\xi. \end{aligned} \tag{2.0.10}$$

Collecting equation (2.0.9), boundary condition at $y = 1$ and condition (2.0.10) we obtain the following reformulation of IBVP (1.2.10) – (1.2.13) for $\widetilde{\psi}(k, y, t)$:

$$\begin{cases} \Big(\dfrac{\partial^2}{\partial y^2} - k^2\Big)\widetilde{\psi}(k,y,t) = e^{-ikyt}\Big(\dfrac{\partial^2}{\partial y^2} - k^2\Big)\widetilde{\psi}(k,y,0), \quad 0 \le y \le 1,\ k \in \mathbb{C},\ t \ge 0, & (2.0.11) \\ \widetilde{\psi}(k,0,t) = -\dfrac{2\omega c}{k}\, e^{-i\omega ct} \displaystyle\int_R^{R+r} g_0'(\xi)\, \frac{\sin(\xi(k-\omega))}{k-\omega} d\xi, & (2.0.12) \\ \widetilde{\psi}(k,1,t) = 0, & (2.0.13) \\ \widetilde{\psi}(k,y,0) = \widetilde{F}(k,y). & (2.0.14) \end{cases}$$

IBVP (2.0.11) – (2.0.14) is the main object of interest for this dissertation.

2.1 Reduction to the problem with time-independent boundary conditions.

Let us introduce a new function

$$Y(k,y,t) = e^{i\omega ct}\, \widetilde{\psi}(k,y,t). \tag{2.1.1}$$

Since $Y(k,y,0) = \widetilde{\psi}(k,y,0)$, the problem for $Y(k,y,t)$ can be represented in the form

$$\begin{cases} \left(\dfrac{\partial^2}{\partial y^2} - k^2\right) Y(k,y,t) = e^{-i(ky-\omega c)t}\left(\dfrac{\partial^2}{\partial y^2} - k^2\right) Y(k,y,0), & (2.1.2) \\ Y(k,0,t) = -\dfrac{2\omega c}{k}\displaystyle\int_R^{R+r} g_0'(\xi)\,\dfrac{\sin(\xi(k-\omega))}{k-\omega} d\xi, & (2.1.3) \\ Y(k,1,t) = 0, & (2.1.4) \\ Y(k,y,0) = \widetilde{F}(k,y). & (2.1.5) \end{cases}$$

To reduce IBVP (2.1.2) – (2.1.5) to the IBVP with homogeneous boundary conditions, we introduce the steady state solution, $Y_0(k,y)$, that satisfies the following boundary value problem:

$$\begin{cases} \left(\dfrac{\partial^2}{\partial^2 y} - k^2\right) Y_0(k,y) = 0, & (2.1.6) \\ Y_0(k,1) = 0, & (2.1.7) \\ Y_0(k,0) = -\dfrac{2\omega c}{k}\displaystyle\int_R^{R+r} g_0'(\xi)\,\dfrac{\sin(\xi(k-\omega))}{k-\omega}\, d\xi. & (2.1.8) \end{cases}$$

This problem has a unique solution that can be given by an explicit formula (see Appendix C)

$$Y_0(k,y) = -\frac{2\omega c\ \sinh(k(1-y))}{k\ \sinh(k)}\int_R^{R+r} g_0'(\xi)\,\frac{\sin(\xi(k-\omega))}{k-\omega}\, d\xi. \tag{2.1.9}$$

It can be readily seen that the steady state solution satisfies the initial boundary value problem (2.1.2) – (2.1.6), in which the initial state is simply $Y_0(k,y)$.

Now we are in a position to describe the class of initial data using the stationary solution (2.1.9).

Assumption 2.1. *We consider the initial state of the system, whose Fourier transform is a small perturbation of the steady-state solution, i.e.*

$$\widetilde{F}(k,y) = \widetilde{f}(k,y) + Y_0(k,y), \tag{2.1.10}$$

where $\widetilde{f}(k,y)$ is a smooth compactly supported function of y.

Now, let us introduce a new function, $Z(k, y, t)$, that satisfies the zero boundary conditions and therefore

$$Z(k, y, t) = Y(k, y, t) - Y_0(k, y). \tag{2.1.11}$$

Taking into account (2.1.2) and (2.1.6), we obtain the equation for $Z(k, y, t)$

$$\begin{aligned}\left(\frac{\partial^2}{\partial y^2} - k^2\right) Z(x, y, t) &= e^{-i(ky-\omega c)t}\left(\frac{\partial^2}{\partial y^2} - k^2\right) Y(k, y, 0) \\ &= e^{-i(ky-\omega c)t}\left(\frac{\partial^2}{\partial y^2} - k^2\right)\widetilde{\psi}(k, y, 0).\end{aligned} \tag{2.1.12}$$

Using (2.1.3) – (2.1.5), (2.1.7), and (2.1.8), we obtain the boundary conditions $Z(k, 0, t) = Y(k, 0, t) - Y_0(k, 0) = 0$, $Z(k, 1, t) = 0$, and from (2.1.10) and (2.1.11), we obtain the initial condition $Z(k, y, 0) = Y(k, y, 0) - Y_0(k, y) = \widetilde{f}(k, y)$.

Thus, the IBVP for $Z(k, y, t)$ can be written in the following form:

$$\begin{cases} \left(\dfrac{\partial^2}{\partial y^2} - k^2\right) Z(k, y, t) = e^{-i(ky-\omega c)t}\left(\dfrac{\partial^2}{\partial y^2} - k^2\right)\widetilde{\psi}(k, y, 0), & (2.1.13) \\ Z(k, 0, t) = Z(k, 1, t) = 0, & (2.1.14) \\ Z(k, y, 0) = \widetilde{f}(k, y). & (2.1.15) \end{cases}$$

2.2 Solving problem (2.1.13) – (2.1.15) via Green's function.

We construct an explicit solution of equation (2.1.13) satisfying the Dirichlet boundary conditions (2.1.14). The initial conditions (2.1.15) is incorporated into equation (2.1.13) in which $\widetilde{\psi}(k, y, 0) = \widetilde{f}(k, y)$.

As is known [45, 46], the solution of the boundary problem

$$W''(k, y) - k^2\, W(k, y) = \Phi(k, y), \quad W(k, 0) = W(k, 1) = 0,$$

can be given in terms of the Green's function as

$$W(k, y) = \int_0^1 G(\eta, y)\, \Phi(\eta, k)\, d\eta.$$

The following properties must be satisfied for $G(\eta, y)$ [45, 46] (see Appendix D.1):

(i) symmetry, i.e. $G(\eta, y) = G(y, \eta)$;

(ii) continuity, i.e. $G(\eta, y) \to G(y, y)$ as $\eta \to y$;

(iii) a unit jump of the derivative, i.e. $G_y(\eta, y)|_{y=\eta+0} - G_y(\eta, y)|_{y=\eta-0} = 1$;

(iv) the boundary conditions: $G(\eta, 0) = G(\eta, 1) = 0$;

(v) the equation: $G_{yy}(\eta, y) - k^2 G(\eta, y) = \delta(\eta - y)$ with $\delta(\cdot)$ being the Dirac delta function.

To derive the formula for $G(y, \eta)$ corresponding to the problem given, let

$$\begin{aligned} G(y, \eta) &= A(\eta) \sinh(ky) \quad \text{for } y < \eta, \\ G(y, \eta) &= B(\eta) \sinh(k(1 - y)) \quad \text{for } y > \eta. \end{aligned} \tag{2.2.1}$$

It is clear that $G(0, \eta) = G(1, \eta) = 0$. By continuity we require,

$$G(y, y) = A(y) \sinh(ky) = B(y) \sinh(k(1 - y)). \tag{2.2.2}$$

One can see that the derivative from the right is $-kB(\eta) \cosh(k(1 - y))$, and the derivative from the left is $kA(\eta) \cosh(ky)$. Utilizing the jump condition on the derivatives we obtain that

$$-kB(\eta) \cosh(k(1 - y)) - kA(\eta) \cosh(ky) = 1. \tag{2.2.3}$$

Combining equations (2.2.2) and (2.2.3) with $y = \eta$, we yield the following system:

$$\begin{cases} A(\eta) \sinh(ky) - B(\eta) \sinh(k(1 - y)) = 0, \\ A(\eta) \cosh(ky) + B(\eta) \cosh(k(1 - y)) = -\dfrac{1}{k}. \end{cases} \tag{2.2.4}$$

Solving this system, we obtain explicit expressions for $A(y)$ and $B(y)$ as

$$A(y) = -\frac{\sinh(k(1-y))}{k\sinh k}, \qquad B(y) = -\frac{\sinh(ky)}{k\sinh k}. \tag{2.2.5}$$

Therefore the Green's function is given by explicit formula

$$G(\eta, y) = \frac{1}{k\ \sinh(k)} \begin{cases} -\sinh(k(1-\eta))\sinh(ky), & y < \eta \\ -\sinh(k\eta)\sinh(k(1-y)), & y > \eta \end{cases} \tag{2.2.6}$$

satisfying all properties (i) – (v). Using this Green's function, we obtain the following solution of the system (2.1.13) and (2.1.14):

$$\begin{aligned} Z(k,y,t) &= e^{i\omega ct}\int_0^1 e^{-ik\eta t}\, G(y,\eta)\left(\frac{\partial^2}{\partial\eta^2} - k^2\right)\widetilde{\psi}(k,\eta,0)\, d\eta \\ &= -e^{i\omega ct}\,\frac{\sinh(k(1-y))}{k\ \sinh(k)}\int_0^y e^{-ik\eta t}\,\sinh(k\eta)\left(\frac{\partial^2}{\partial\eta^2} - k^2\right)\widetilde{\psi}(k,\eta,0)\, d\eta \\ &\quad - e^{i\omega ct}\,\frac{\sinh(ky)}{k\ \sinh(k)}\int_y^1 e^{-ik\eta t}\,\sinh(k(1-\eta))\left(\frac{\partial^2}{\partial\eta^2} - k^2\right)\widetilde{\psi}(k,\eta,0)\, d\eta \end{aligned} \tag{2.2.7}$$

which yields the desired result for $\widetilde{\psi}(k,y,t) = e^{-i\omega ct}\big[Z(k,y,t) + Y_0(k,y)\big]$:

$$\begin{aligned} \widetilde{\psi}(k,y,t) &= -\frac{\sinh(k(1-y))}{k\ \sinh(k)}\int_0^y e^{-ik\eta t}\,\sinh(k\eta)\left(\frac{\partial^2}{\partial\eta^2} - k^2\right)\widetilde{\psi}(k,\eta,0)\, d\eta \\ &\quad - \frac{\sinh(ky)}{k\ \sinh(k)}\int_y^1 e^{-ik\eta t}\,\sinh(k(1-\eta))\left(\frac{\partial^2}{\partial\eta^2} - k^2\right)\widetilde{\psi}(k,\eta,0)\, d\eta \\ &\quad - e^{-i\omega ct}\,\frac{2\omega c\ \sinh(k(1-y))}{k\ \sinh(k)}\int_R^{R+r} g_0'(\xi)\,\frac{\sin(\xi(k-\omega))}{k-\omega}\, d\xi. \end{aligned} \tag{2.2.8}$$

CHAPTER 3

EVALUATION OF THE INVERSE FOURIER TRANSFORMS

We recall that our goal is to find the space-time representation for the vertical component of the velocity perturbation $v(x, y, t)$, which is related to the derivative of the stream function by formula (1.1.3). The remaining technical challenge is to calculate the inverse Fourier transform of the function $k\,\widetilde{\psi}(k, y, t)$.

It is convenient to introduce the following notation for the inverse Fourier transform of the stream function:

$$i\psi_x(x, y, t) = \frac{1}{2\pi}\int_{-\infty}^{\infty} e^{ikx}\, k\,\widetilde{\psi}(k, y, t)\, dk \equiv I_1(k.x) + I_2(k, x) + I_3(k, x), \tag{3.0.1}$$

where

$$I_1 = -\ \frac{c\omega}{\pi}e^{-i\omega ct}\int_{-\infty}^{\infty} e^{ikx}\left[\frac{\sinh(k(1-y))}{\sinh(k)}\int_R^{R+r} g_0'(\xi)\,\frac{\sin(\xi(k-\omega))}{k-\omega}d\xi\right] dk, \tag{3.0.2}$$

$$I_2 = -\ \frac{1}{2\pi}\int_{-\infty}^{\infty} e^{ikx}\left[\frac{\sinh(k(1-y))}{\sinh(k)}\int_0^{y} e^{-ik\eta t}\sinh(k\eta)\left(\frac{\partial^2}{\partial\eta^2} - k^2\right)\widetilde{f}(k,\eta)\, d\eta\right] dk, \tag{3.0.3}$$

$$I_3 = -\ \frac{1}{2\pi}\int_{-\infty}^{\infty} e^{ikx}\left[\frac{\sinh(ky)}{\sinh(k)}\int_y^{1} e^{-ik\eta t}\sinh(k(1-\eta))\left(\frac{\partial^2}{\partial\eta^2} - k^2\right)\widetilde{f}(k,\eta)\, d\eta\right] dk. \tag{3.0.4}$$

In this section, we focus on the evaluation of the double integral (3.0.2). Assuming that the change of order of integration is justified, we represent I_1 as

$$I_1(k, x) = \ -\frac{\omega c}{\pi}\, e^{-i\omega ct}\int_R^{R+r} d\xi\; g_0'(\xi)\, \mathbb{I}_1(\xi, x),$$

where

$$\mathbb{I}_1 = \int_{-\infty}^{\infty} dk\, e^{ikx}\, \frac{\sinh(k\alpha)}{\sinh(k)}\, \frac{\sin(\xi(k-\omega))}{k-\omega}, \qquad \omega > 0, \quad 0 < \alpha \equiv 1 - y < 1. \tag{3.0.5}$$

First we prove the following technical results.

Lemma 3.1. *Let $\mathscr{A}(k)$ be the function defined by the formula*

$$\mathscr{A}(k) = \frac{\sinh(\alpha k)}{\sinh(k)}, \qquad \alpha = 1 - y < 1. \tag{3.0.6}$$

Let Γ_N be a semi-circle in the upper-half plane of the k-complex plane centered at the origin and of radius $r = \pi\left(N + \frac{1}{2}\right)$, $N \in \mathbb{N}^+$. Then for each N the following estimate holds:

$$|\mathscr{A}(k)| \leq C_0 < \infty, \qquad k \in \Gamma_N, \quad N \in \mathbb{N}^+, \tag{3.0.7}$$

with C_0 being an absolute constant. A similar estimate holds when k belongs to a symmetric semi-circle located in the lower half-plane.

Proof. Since $\mathscr{A}(-\overline{k}) = \mathscr{A}(\overline{k}) = \overline{\mathscr{A}(k)}$, it suffices to prove the lemma when k belongs to the the quarter of the circle located in the first quadrant of the complex k-plane.

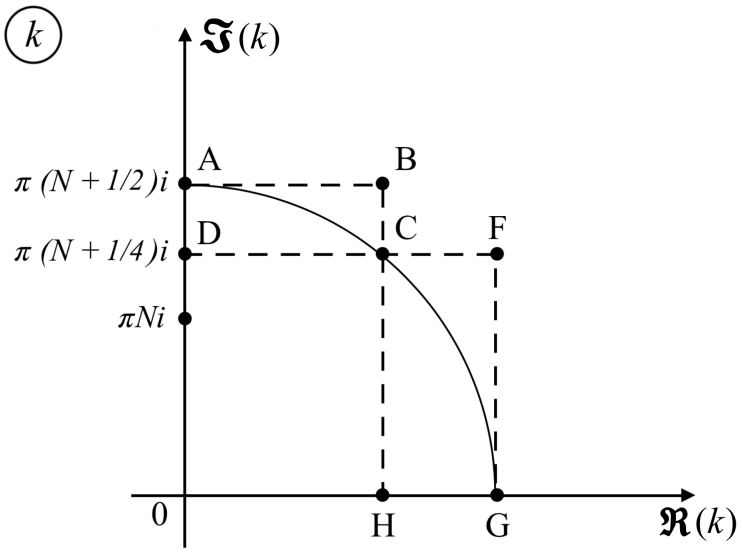

Figure 3.1: Geometrical setting for evaluation of $\mathscr{A}(k)$.

To show that $|\mathscr{A}(k)|$ is bounded along *arc* AC, we prove that $|\mathscr{A}(k)|$ is bounded along the sides of the rectangle $ABCD$, and then using analyticity of $\mathscr{A}(k)$ we obtain that $|\mathscr{A}(k)|$ is bounded inside this domain. To show that $|\mathscr{A}(k)|$ is bounded along *arc* CG, we prove that $|\mathscr{A}(k)|$ is bounded along the sides of the rectangular domain $CFGH$. Though note, tt is technically convenient to evaluate $|\mathscr{A}(k)|$ along sides of a rectangle than along an arc. In the sequel, we need the following formula for $\sinh(\alpha k)$. If $k = \xi + i\eta$, then

$$|\sinh(\alpha k)|^2 = \frac{1}{2}\,[\cosh(2\alpha\xi) - \cos(2\alpha\eta)]. \tag{3.0.8}$$

Indeed, we have: $|\sinh(\alpha(\xi + i\eta))|^2 = |\sinh(\alpha\xi)\cos(\alpha\eta) - i\cosh(\alpha\xi)\sin(\alpha\eta)|^2 =$ $\sinh^2(\alpha\xi)\cos^2(\alpha\eta) + \cosh^2(\alpha\xi)\big(1 - \cos^2(\alpha\eta)\big) = \cosh^2(\alpha\xi) - \cos^2(\alpha\eta)$, which yields formula (3.0.8). Now we prove that $|\mathscr{A}(k)|$ is bounded along each side of $ABCD$. If $k = \xi + i\eta \in AB$, then $0 \le \xi \le \pi\sqrt{N/2 + 3/16}$ and $\eta = \pi(N + 1/2)$. Using (3.0.8), one gets the estimate:

$$|\mathscr{A}(k)|^2 = \frac{\cosh(2\alpha\xi) - \cos(2\alpha\eta)}{\cosh(2\xi) - \cos(2\eta)} \le \frac{\cosh(2\alpha\xi) + 1}{\cosh(2\xi) + 1} \le 1. \tag{3.0.9}$$

If $k \in DF$, then $0 \le \xi \le \pi(N+1/2)$ and $\eta = \pi(N+1/4)$. Using (3.0.8) one gets the estimate:

$$|\mathscr{A}(k)|^2 = \frac{\cosh(2\alpha\xi) - \cos(2\alpha\eta)}{\cosh(2\xi)} \le \frac{\cosh(2\alpha\xi)}{\cosh(2\xi)} + \frac{1}{\cosh(2\xi)} \le 2. \tag{3.0.10}$$

If $k \in DA$, i.e. $k = i\eta$, and $\pi(N+1/4) \le \eta \le \pi(N+1/2)$, then one uses the fact that $\cos(2\eta) \le 0$ and gets the estimate:

$$|\mathscr{A}(k)|^2 = \frac{1 - \cos(2\alpha\eta)}{1 - \cos(2\eta)} \le \frac{1 + |\cos(2\alpha\eta)|}{1} \le 2. \tag{3.0.11}$$

If $k \in BH$, then $\xi = \pi\sqrt{N/2+3/16}$ and $0 \le \eta \le \pi(N+1/2)$. Using (3.0.6) one gets

$$\begin{aligned} |\mathscr{A}(k)|^2 &= \frac{\cosh(2\pi\sqrt{N/2+3/16}\,\alpha) - \cos(2\alpha\eta)}{\cosh(2\pi\sqrt{N/2+3/16}\,) - \cos(2\eta)} \\ &\le \frac{\cosh(2\pi\sqrt{N/2+3/16}\,\alpha) + 1}{\cosh(2\pi\sqrt{N/2+3/16}\,) - 1} \le 1 + \frac{2}{\cosh(2\pi\sqrt{N/2+3/16}\,) - 1} \le 2. \end{aligned} \tag{3.0.12}$$

If $k \in FG$, then $\xi = \pi(N+1/2)$ and $0 \le \eta \le \pi(N+1/4)$. Using (3.0.6) one gets

$$|\mathscr{A}(k)|^2 = \frac{\cosh(2\pi\,(N+1/2)\,\alpha) - \cos(2\alpha\eta)}{\cosh(2\pi\,(N+1/2)) - \cos(2\eta)} \le 1 + \frac{2}{\cosh(2\pi(N+1/2)) - 1} \le 2. \tag{3.0.13}$$

If $k \in HG$, then $|\mathscr{A}(k)|$ is bounded by 1 due to the monotonic behavior of the *sinh* function for real k. Collecting together (3.0.9) – (3.0.13), we obtain that $|\mathscr{A}(k)|$ is bounded on Γ_N uniformly with respect to N.

The lemma is proven. ■

Our goal is to represent integral $\mathbb{I}_1$ of (3.0.5) in the form of an infinite functional series using the Residue theorem. To this end, we split the derivation of the desired result into several steps.

Step 1: Reduction of the improper integral $\mathbb{I}_1(\xi, x)$ to a principal value integral. To make use of the complex analysis techniques, we represent $\mathbb{I}_1(\xi, x)$ in the form of *a limit of a sequence of contour integrals* on the complex k-plane. It can be readily seen that integral $\mathbb{I}_1(\xi, x)$ is absolutely

convergent. Indeed, for each $y > 0$, the following estimate holds for $\mathscr{A}(k)$, $k \in (-\infty, \infty)$:

$$\mathscr{A}(k) \leq \exp\{-y|k|\}, \quad k \in \mathbb{R}. \tag{3.0.14}$$

Since $\mathscr{A}(k)$ is an even function it suffices to show the convergence of (3.0.14) for $k \geq 0$. The result follows from the estimates: $\mathscr{A}(k) = \exp\{-(1-\alpha)k\}\,(1-e^{-2\alpha k})(1-e^{-2k})^{-1} \leq \exp\{-(1-\alpha)k\} = e^{-yk}$. Taking into account that the function $\dfrac{\sin(\xi(k-\omega))}{k-\omega}$ is bounded at the vicinity of $k = \omega$ and behaves as $\dfrac{1}{k}$ for large enough k, we obtain that the integral in (3.0.5) converges absolutely.

Definition 3.2. *Let P.V.(ω) be the notation for the integral that converges in the sense of the principal value "centered" at the point ω, such that for any absolutely integrable function $h(k)$, we define*

$$\text{P.V.}(\omega)\int_{-\infty}^{\infty} h(k)\,dk = \lim_{n\to\infty}\left[\int_{-\infty}^{\omega-\delta_n} + \int_{\omega+\delta_n}^{\infty}\right] h(k)dk, \tag{3.0.15}$$

for any sequence $\delta_n \to 0$ as $n \to \infty$.

Using absolute convergence of integral $\mathbb{I}_1(\xi, x)$ and Definition 4.2, we obtain

$$\mathbb{I}_1(\xi, x) = \text{P.V.}(\omega)\int_{-\infty}^{\infty} dk\; e^{ikx}\,\mathscr{A}(k)\,\frac{\sin(\xi(k-\omega))}{k-\omega}. \tag{3.0.16}$$

Step 2: Reduction of the principal value integral to the limit of a sequence of contour integrals. Let γ_n be a semi-circle in the lower half-plane centered at the point $k = \omega$ of radius δ_n, i.e., $\gamma_n = \{k:\ k = \omega + \delta_n e^{i\varphi},\ -\pi \leq \varphi \leq 0\}$; let ℓ_n be the following contour:

$$\ell_n = (-\infty, \omega - \delta_n)\ \cup\ \gamma_n\ \cup\ (\omega + \delta_n, \infty). \tag{3.0.17}$$

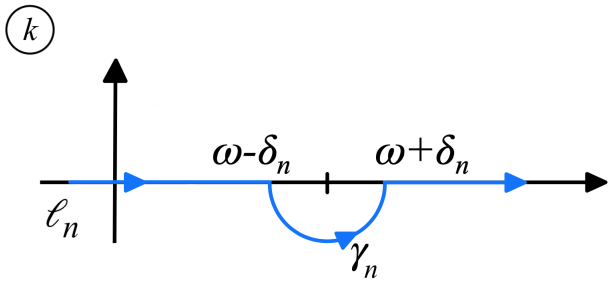

Figure 3.2: Contour of integration ℓ_n.

Lemma 3.3. *Integral $\mathbb{I}_1(\xi, x)$ of (3.0.16) can be represented as the following limit of a sequence of contour integrals:*

$$P.V.(\omega)\int_{-\infty}^{\infty} dk\; e^{ikx}\; \mathscr{A}(k)\; \frac{\sin(\xi(k-\omega))}{k-\omega} = \lim_{n\to\infty} \int_{\ell_n} dk\; e^{ikx}\; \mathscr{A}(k)\; \frac{\sin(\xi(k-\omega))}{k-\omega}. \tag{3.0.18}$$

Proof. For each n, the following decomposition holds:

$$\int_{\ell_n} dk\; e^{ikx}\; \mathscr{A}(k)\; \frac{\sin(\xi(k-\omega))}{k-\omega} = \left[\int_{-\infty}^{\omega-\delta_n} + \oint_{\gamma_n} + \int_{\omega+\delta_n}^{\infty}\right] dk\; e^{ikx}\; \mathscr{A}(k)\; \frac{\sin(\xi(k-\omega))}{k-\omega}, \tag{3.0.19}$$

where $\oint_{\gamma_n}$ is the notation for the integral along a semi-circle γ_n. Let us show that the sequence of integrals along semi-circular contours γ_n tends to 0 as $n \to \infty$ (i.e. $\delta_n \to 0$), i.e.

$$\oint_{\gamma_n} dk\; e^{ikx}\; \mathscr{A}(k)\; \frac{\sin(\xi(k-\omega))}{k-\omega} \to 0 \qquad \text{as } n \to \infty. \tag{3.0.20}$$

The proof is based on the fact that the integrand is an analytic function of k at the vicinity of $k = \omega$. Thus, if $k = \omega + \delta_n e^{i\varphi}$, then

$$\left|\oint_{\gamma_n} dk\; e^{ikx}\; \mathscr{A}(k)\; \frac{\sin(\xi(k-\omega))}{k-\omega}\right| = \left|\int_{-\pi}^{0} e^{ix(\omega+\delta_n e^{i\varphi})}\; \mathscr{A}(\omega+\delta_n e^{i\varphi})\; \sin(\xi\;\delta_n e^{i\varphi})\; d\varphi\right| \le C_0\delta_n,$$

which completes the proof.

The lemma is shown. ■

Step 3: Introducing closed contour integrals. Since each integral over ℓ_n has the domain of integration that does not pass through the point $k = \omega$, each contour integral can be split up into two integrals denoted by $\mathcal{I}_n(\xi, x)$ and $\widetilde{\mathcal{I}}_n(\xi, x)$, where:

$$\mathcal{I}_1^{(n)}(\xi, x) = \frac{1}{2i}\, e^{-i\xi\omega} J_n(\xi, x), \qquad J_n(\xi, x) \equiv \int\!\!\!\!\!\!\diagup_{\ell_n} dk\; \mathscr{A}(k)\, \frac{e^{ik(x+\xi)}}{k-\omega}, \tag{3.0.21}$$

$$\widetilde{\mathcal{I}}_1^{(n)}(\xi, x) = -\frac{1}{2i}\, e^{i\xi\omega} \widetilde{J}_n(\xi, x), \qquad \widetilde{J}_n(\xi, x) \equiv \int\!\!\!\!\!\!\diagup_{\ell_n} dk\; \mathscr{A}(k)\, \frac{e^{ik(x-\xi)}}{k-\omega}. \tag{3.0.22}$$

Assumption 3.4. *In what follows we assume that*

$$x \in [-R + \varepsilon, R - \varepsilon], \qquad \varepsilon \ll 1, \tag{3.0.23}$$

which is consistent with the physical origin of the model.

Taking into account that $\xi \in [R, R + r]$ (see (3.0.2)) and (3.0.23), we obtain the bounds on $(x + \xi)$ and $(x - \xi)$ as

$$0 < \varepsilon \le x + \xi \le 2R + r - \varepsilon, \qquad -2R - r + \varepsilon \le x - \xi \le -\varepsilon < 0. \tag{3.0.24}$$

In the sequel, these estimates will allow us to use Jordan's lemma appropriately.

In the rest of this section, we show that each integral, $J_n(\xi, x)$ and $\widetilde{J}_n(\xi, x)$, can be evaluated as a limit of a specifically chosen sequence of contour integrals. We provide a detailed proof only for the integral $J_n(\xi, x)$ since the second integral, $\widetilde{J}_n(\xi, x)$, can be treated in a similar manner.

Lemma 3.5. *Let Γ_N be a semi-circle in the upper half-plane centered at the origin of radius $\pi(N + 1/2)$, with N being a positive integer. Then on a sequence of expanding semi-circles, the following result is valid:*

$$\lim_{N\to\infty} \left(\int\!\!\!\!\!\!\diagup_{\Gamma_N} dk\; \mathscr{A}(k)\, \frac{e^{ik(x+\xi)}}{k-\omega} \right) = 0. \tag{3.0.25}$$

Let $\widetilde{\Gamma}_N$ be a symmetric semi-circle in the lower half-plane. Then on a sequence of expanding

semi-circles, the following result is valid:

$$\lim_{N\to\infty} \oint_{\tilde{\Gamma}_N} dk\, \mathscr{A}(k)\, \frac{e^{ik(x-\xi)}}{k-\omega} = 0. \tag{3.0.26}$$

The proof of the lemma is based on the straightforward application of estimates (3.0.23), Jordan's lemma [47, 48], and Lemma 3.1.

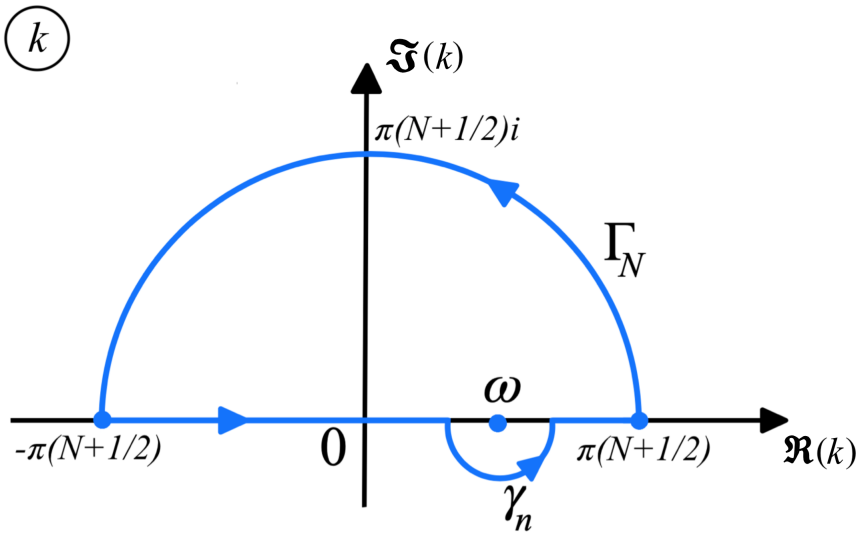

Figure 3.3: Closed contour of integration in the upper half-plane.

Let n be fixed and N be a positive integer. Consider a sequence of closed contours $\{\mathbb{\Gamma}_{N,n}\}_{N=1}^{\infty}$ in the upper half-plane defined as

$$\mathbb{\Gamma}_{N,n} = \Gamma_N \cup [-R_N, \omega-\delta_n] \cup \gamma_n \cup [\omega+\delta_n, R_N], \quad R_N = \pi(N+1/2). \tag{3.0.27}$$

Let us consider the following integral along contour $\mathbb{\Gamma}_{N,n}$:

$$\oint_{\mathbb{\Gamma}_{N,n}} dk\, \frac{e^{ik(x+\xi)}}{k-\omega}\, \mathscr{A}(k) = \left[\int_{-R_N}^{\omega-\delta_n} + \oint_{\gamma_n} + \int_{\omega+\delta_n}^{R_N} - \oint_{\Gamma_N} \right] dk\, \frac{e^{ik(x+\xi)}}{k-\omega}\, \mathscr{A}(k). \tag{3.0.28}$$

By using the Residue theorem [47, 48], we obtain for the integral that

$$\begin{aligned}\frac{1}{2\pi i}\oint_{\mathbb{\Gamma}_{N,n}} dk\ \mathscr{A}(k)\ \frac{e^{ik(x+\xi)}}{k-\omega} &= \sum_{m=1}^{N} \mathrm{Res}\left(\frac{e^{ik(x+\xi)}}{k-\omega}\ \frac{\sinh(k(1-y))}{\sinh(k)},\ \pi m i\right) \\ &\quad +\ \mathrm{Res}\left(\frac{e^{ik(x+\xi)}}{k-\omega}\ \frac{\sinh(k(1-y))}{\sinh(k)},\ \omega\right) \\ &= \sum_{m=1}^{N} \frac{e^{-\pi m(x+\xi)}}{\pi m i-\omega}\ \frac{i\ \sin(\pi m(1-y))}{\cos(\pi m)} + \frac{e^{i\omega(x+\xi)}\sinh(\omega\alpha)}{\sinh(\omega)} \\ &= -\sum_{m=1}^{N} e^{-\pi m(x+\xi)}\ \frac{\sin(\pi m y)}{\pi m+i\omega} + \frac{e^{i\omega(x+\xi)}\sinh(\omega\alpha)}{\sinh(\omega)}. \end{aligned} \tag{3.0.29}$$

Passing to the limits as $N \to \infty$ (see (3.0.25)) in (3.0.29), we arrive at the following representation for $J_n(\xi, x)$:

$$\frac{1}{2i}\ J_n(\xi,x) = \ -\pi\ \sum_{m=1}^{\infty} e^{-\pi m(x+\xi)}\ \frac{\sin(\pi m y)}{\pi m+i\omega} + \frac{\pi\ e^{i\omega(x+\xi)}\sinh(\omega\alpha)}{\sinh(\omega)}. \tag{3.0.30}$$

Now we turn to the integral $\widetilde{J}_n(\xi, x)$ from (3.0.22). Let us introduce a sequence of closed contours $\{\widetilde{\mathbb{\Gamma}}_{N,n}\}_{N=1}^{\infty}$ in the lower half-plane defined as

$$\widetilde{\mathbb{\Gamma}}_{N,n} = \ \widetilde{\Gamma}_N\ \cup\ [-R_N,\ \omega-\delta_n]\ \cup\ \gamma_n\ \cup\ [\omega+\delta_n, R_N], \quad R_N = \pi(N+1/2), \tag{3.0.31}$$

where $\widetilde{\Gamma}_N$ is a semi-circle in the lower half-plane (in the clockwise direction).

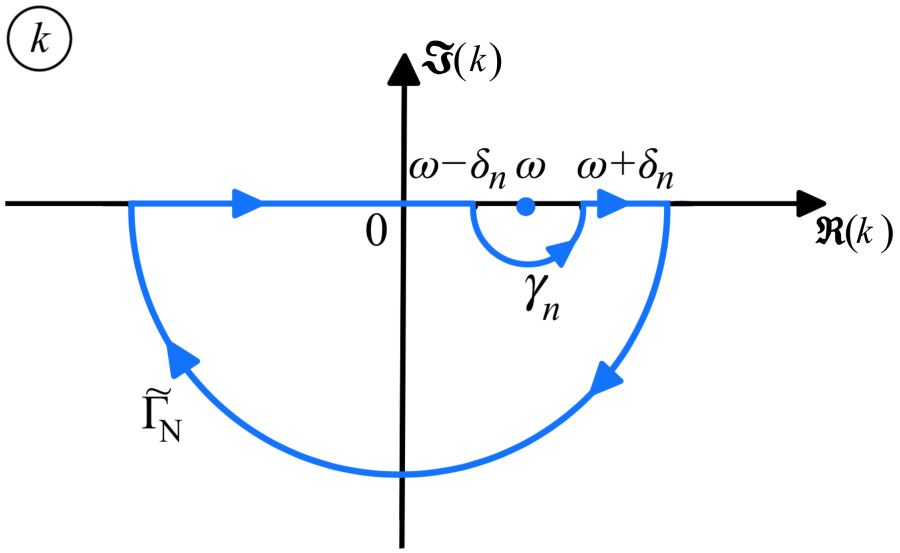

Figure 3.4: Closed contour of integration in the lower half-plane.

Evaluation of the integral along the closed contour $\widetilde{\mathbb{\Gamma}}_{N,n}$ yields

$$\begin{aligned}\oint_{\widetilde{\mathbb{\Gamma}}_{N,n}} dk\, \mathscr{A}(k)\, \frac{e^{ik(x-\xi)}}{k-\omega} &\equiv -\oint_{\widetilde{\mathbb{\Gamma}}_{N,n}} dk\, \mathscr{A}(k)\, \frac{e^{ik(x-\xi)}}{k-\omega} \\ &= -\left[\int_{-R_N}^{\omega-\delta_n} + \oint_{\gamma_n} + \int_{\omega+\delta_n}^{R_N} - \oint_{\widetilde{\Gamma}_N}\right] dk\, \mathscr{A}(k)\, \frac{e^{ik(x-\xi)}}{k-\omega}. \end{aligned} \tag{3.0.32}$$

Using the Residue theorem, we obtain for the same integral

$$\begin{aligned}\frac{1}{2\pi i}\oint_{\mathbb{\Gamma}_{N,n}} dk\, \mathscr{A}(k)\, \frac{e^{ik(x-\xi)}}{k-\omega} &= \sum_{m=1}^{N} \mathrm{Res}\left(\frac{e^{ik(x-\xi)}}{k-\omega}\,\frac{\sinh(k(1-y))}{\sinh(k)},\ -\pi mi\right) \\ &= \sum_{m=1}^{N} \frac{e^{\pi m(x-\xi)}}{\pi mi+\omega}\,\frac{i\,\sin(\pi m(1-y))}{\cos(\pi mi)} \\ &= -\sum_{m=1}^{N} e^{\pi m(x-\xi)}\,\frac{\sin(\pi my)}{\pi m - i\omega}. \end{aligned} \tag{3.0.33}$$

Passing to the limit when $N \to \infty$ (see 3.0.26)) in (3.0.33), we have from (3.0.32) and (3.0.33)

$$\frac{1}{2i}\,\widetilde{J}_n(\xi,x) = \pi \sum_{m=1}^{\infty} e^{\pi m(x-\xi)}\,\frac{\sin(\pi my)}{\pi m - i\omega}. \tag{3.0.34}$$

Substituting (3.0.30) into formula (3.0.21) for $\mathcal{I}_n(\xi, x)$ and (3.0.34) into formula (3.0.22) for $\widetilde{\mathcal{I}}_n(\xi, x)$, we obtain

$$(\mathcal{I}_n + \widetilde{\mathcal{I}}_n) = \pi\, e^{i\omega x}\, \frac{\sinh(\omega(1-y))}{\sinh(\omega)} - \pi \sum_{m=1}^{\infty} e^{-\pi m\xi}\, \sin(\pi m y) \left\{ \frac{e^{-\pi m x}\, e^{-i\xi\omega}}{\pi m + i\omega} + \frac{e^{\pi m x}\, e^{i\xi\omega}}{\pi m - i\omega} \right\}$$
$$= \pi\, e^{i\omega x}\, \frac{\sinh(\omega(1-y))}{\sinh(\omega)} - 2 \sum_{m=1}^{\infty} e^{-\pi m\xi} \sin(\pi m y) \times$$
$$\left\{ \frac{\pi m\, \cosh(\pi m x + i\xi\omega) - i\omega\, \sinh(\pi m x + i\xi\omega)}{\pi^2 m^2 + \omega^2} \right\}. \quad (3.0.35)$$

Now we use formulae (3.0.16), (3.0.18), and (3.0.35) to obtain the formula for $\mathbb{I}_1(\xi, x)$

$$\mathbb{I}_1(\xi, x) = \lim_{n\to\infty} (\mathcal{I}_n + \widetilde{\mathcal{I}}_n)(\xi, x) = \pi\, e^{i\omega x}\, \frac{\sinh(\omega(1-y))}{\sinh(\omega)}$$
$$- 2 \sum_{m=1}^{\infty} e^{-\pi m\xi} \sin(\pi m y) \left\{ \frac{\pi m\, \cosh(\pi m x + i\xi\omega) - i\omega\, \sinh(\pi m x + i\xi\omega)}{\pi^2 m^2 + \omega^2} \right\}. \quad (3.0.36)$$

Summarizing the results of this section, we formulate the following statement.

Theorem 3.6. *The following explicit formulae holds the for the term I_1 from the decomposition (3.0.1) :*

$$I_1 = -\omega c\, e^{i\omega(x-ct)}\, g_0(R)\, \frac{\sinh(\omega(1-y))}{\sinh(\omega)} - 2\omega c\, e^{-i\omega c t} \sum_{m=1}^{\infty} \frac{\sin \pi m y}{\pi^2 m^2 + \omega^2} \times$$
$$\int_R^{R+r} d\xi\, g_0'(\xi)\, e^{-\pi m\xi} \left[\pi m\, \cosh(\pi m x + i\xi\omega) - i\omega\, \sinh(\pi m x + i\xi\omega) \right], \quad (3.0.37)$$

with the series being absolutely convergent for any $x \in (-R, R)$, $0 < y < 1$, and $-\infty < t < \infty$.

CHAPTER 4

EVALUATION OF INTEGRALS I_2 AND I_3.

4.1 Evaluation of Integrals I_2 and I_3 from (3.0.3) and (3.0.4)

Our goal in this section is to evaluate the integrals I_2 and I_3 using the Residue theorem. To simplify further calculations, we denote

$$\mathbb{I}_2 \equiv -2\pi\ I_2 \qquad \text{and} \qquad \mathbb{I}_3 \equiv -2\pi\ I_3, \tag{4.1.1}$$

where

$$\mathbb{I}_2 = \int_{-\infty}^{\infty} dk\ e^{ikx} \left[\frac{\sinh(k(1-y))}{\sinh(k)}\right] \int_0^y d\eta\ e^{-ik\eta t}\ \sinh(k\eta) \left[\widetilde{f}_{\eta\eta}(k,\eta) - k^2 \widetilde{f}(k,\eta)\right], \tag{4.1.2}$$

$$\mathbb{I}_3 = \int_{-\infty}^{\infty} dk\ e^{ikx} \left[\frac{\sinh(ky)}{\sinh(k)}\right] \int_y^1 d\eta\ e^{-ik\eta t}\ \sinh(k(1-\eta)) \left[\widetilde{f}_{\eta\eta}(k,\eta) - k^2 \widetilde{f}(k,\eta)\right]. \tag{4.1.3}$$

Integrating by parts twice the integral along $(0, y)$ we modify $\mathbb{I}_2$ to the following form:

$$\begin{aligned}\mathbb{I}_2 = \int_{-\infty}^{\infty} dk\ \frac{e^{ikx}}{\sinh(k)} \sinh(k(1-y)) \Big\{ & e^{-iky t} \sinh(ky)\ \widetilde{f}_y(k,y) \\ & + (ikt)\ e^{-iky t} \sinh(ky)\ \widetilde{f}(k,y) - k\ e^{-iky t} \cosh(ky)\ \widetilde{f}(k,y) + k\ \widetilde{f}(k,0) \\ & + \int_0^y d\eta\ \widetilde{f}(k,\eta) \left(\frac{\partial^2}{\partial \eta^2} - k^2\right) \left[e^{-ik\eta t} \sinh(k\eta)\right] \Big\}.\end{aligned} \tag{4.1.4}$$

Integrating by parts twice the integral along $(y, 1)$ we modify $\mathbb{I}_3$ to the following form:

$$\begin{aligned}\mathbb{I}_3 = \int_{-\infty}^{\infty} dk\, \frac{e^{ikx}}{\sinh(k)}\, \sinh(ky)\Big\{ & - e^{-ikyt} \sinh(k(1-y))\, \widetilde{f}_y(k, y) \\ & + k\, e^{-ikt}\, \widetilde{f}(k, 1) - ikt\, e^{-ikyt}\, \sinh(k(1-y))\widetilde{f}(k, y) \\ & - k\, e^{-ikyt}\, \cosh(k(1-y))\widetilde{f}(k, y) \\ & + \int_y^1 d\eta\, \widetilde{f}(k, \eta) \left(\frac{\partial^2}{\partial \eta^2} - k^2\right)\left[e^{-ik\eta t} \sinh(k(1-\eta))\right]\Big\}. \end{aligned} \tag{4.1.5}$$

Without loss of generality to simplify further calculations, we assume that $f(x, 0) = f(x, 1) = 0$ and obtain the following representation for the sum $\mathbb{I}_2 + \mathbb{I}_3$:

$$\mathbb{I}_2 + \mathbb{I}_3 = - \int_{-\infty}^{\infty} dk\, k\, e^{ikx} e^{-ikyt}\, \widetilde{f}(k, y) + \mathbf{I}, \tag{4.1.6}$$

where

$$\begin{aligned}\mathbf{I} = \int_{-\infty}^{\infty} dk\, \frac{e^{ikx}}{\sinh(k)}\Big\{ & \sinh(k(1-y)) \int_0^y d\eta\, \widetilde{f}(k, \eta) \left(\frac{\partial^2}{\partial \eta^2} - k^2\right)\left[e^{-ik\eta t} \sinh(k\eta)\right] \\ & + \sinh(ky) \int_y^1 d\eta\, \widetilde{f}(k, \eta) \left(\frac{\partial^2}{\partial \eta^2} - k^2\right)\left[e^{-ik\eta t} \sinh(k(1-\eta))\right]\Big\}. \end{aligned} \tag{4.1.7}$$

Remark 4.1. One can readily check that the integral of (4.1.6) generates the following result:

$$- \int_{-\infty}^{\infty} dk\, k\, e^{ik(x-yt)}\, \widetilde{f}(k, y) = \, i f_x(x - yt, y).$$

If we fix y for $0 < y < 1$ and consider x and t such that $x - yt = C$, where C is some constant, then the function $f_x(x - yt, y)$ is also equal to a constant. It means that the perturbation velocity moves with the speed y along the x-axis.

One can readily check that the integral $\mathbf{I}$ defined in (4.1.6) can be represented in the form:

$\mathbf{I} \equiv \sum_{j=1}^{4} \mathbf{I}_j$, where

$$
\begin{aligned}
\mathbf{I}_1 &= \int_0^y d\eta \int_{-\infty}^{\infty} dk\; e^{ik(x-\eta t)}\; \widetilde{f}(k,\eta)\,(-k^2t^2)\;\frac{\sinh(k(1-y))}{\sinh(k)}\;\sinh(k\eta),\\
\mathbf{I}_2 &= \int_0^y d\eta \int_{-\infty}^{\infty} dk\; e^{ik(x-\eta t)}\; \widetilde{f}(k,\eta)\,(-2i\;k^2t)\;\frac{\sinh(k(1-y))}{\sinh(k)}\;\cosh(k\eta),\\
\mathbf{I}_3 &= \int_y^1 d\eta \int_{-\infty}^{\infty} dk\; e^{ik(x-\eta t)}\; \widetilde{f}(k,\eta)\,(-k^2t^2)\;\frac{\sinh(ky)}{\sinh(k)}\;\sinh(k(1-\eta)),\\
\mathbf{I}_4 &= -\int_y^1 d\eta \int_{-\infty}^{\infty} dk\; e^{ik(x-\eta t)}\; \widetilde{f}(k,\eta)\,(-2i\;k^2t)\;\frac{\sinh(ky)}{\sinh(k)}\;\cosh(k(1-\eta)).
\end{aligned}
\tag{4.1.8}
$$

In this work, we make the following assumptions on the perturbation of $f(x,y)$.

Assumption 4.2. *Let $f(\cdot,y)$ be a smooth function with compact support, i.e.,*

$$
\operatorname{supp}\{f(\cdot,y)\} \in (0,r_0), \qquad r_0 > 0. \tag{4.1.9}
$$

Assume that $f(x,y)$ has the first three partial derivatives in x equal to zero for $x \le 0$ and $x \ge r_0$, i.e.,

$$
\begin{aligned}
f_x(0,y) = f_{xx}(0,y) = f_{xxx}(0,y) = 0,\\
f_x(r_0,y) = f_{xx}(r_0,y) = f_{xxx}(r_0,y) = 0.
\end{aligned}
\tag{4.1.10}
$$

Using of Assumption 4.2, from (4.1.10) one can obtain that

$$
\widetilde{f}(k,y) = \frac{i}{k^3}\int_0^{r_0} dx\; e^{-ikx} f_{xxx}(x,y) \equiv \frac{1}{k^3}\,\widetilde{\chi}(k,y), \quad \text{where } \chi(x,y) = i\; f_{xxx}(x,y), \tag{4.1.11}
$$

(see Appendix D.2). It is convenient to present the integrals $\mathbf{I}_j$, $j = 1,2,3,4$ from (4.1.8) in the forms

$$
\mathbb{I}_{2j-1} = -t^2\,\widehat{\mathbf{I}}_{2j-1},\; j=1,2 \quad \text{and} \quad \mathbb{I}_{2j} = -2it\,\widehat{\mathbf{I}}_{2j},\; j=1,2. \tag{4.1.12}
$$

Taking into account definition (4.1.11) we obtain that the following representations are valid for

$\widehat{\mathbf{I}}_j$, $j = 1, 2, 3, 4$:

$$\widehat{\mathbf{I}}_1 = \int_0^{r_0} d\xi \int_0^{y} d\eta\ \chi(\xi,\eta) \int_{-\infty}^{\infty} dk\ e^{ik(x-\eta t-\xi)}\ \frac{\sinh(k(1-y))\sinh(k\eta)}{k\ \sinh(k)}, \tag{4.1.13}$$

$$\widehat{\mathbf{I}}_2 = \int_0^{r_0} d\xi \int_0^{y} d\eta\ \chi(\xi,\eta)\ \text{P.V.} \int_{-\infty}^{\infty} dk\ e^{ik(x-\eta t-\xi)}\ \frac{\sinh(k(1-y))\cosh(k\eta)}{k\ \sinh(k)}, \tag{4.1.14}$$

$$\widehat{\mathbf{I}}_3 = \int_0^{r_0} d\xi \int_y^{1} d\eta\ \chi(\xi,\eta) \int_{-\infty}^{\infty} dk\ e^{ik(x-\eta t-\xi)}\ \frac{\sinh(k(1-\eta))\sinh(ky)}{k\ \sinh(k)}, \tag{4.1.15}$$

$$\widehat{\mathbf{I}}_4 = -\int_0^{r_0} d\xi \int_y^{1} d\eta\ \chi(\xi,\eta)\ \text{P.V.} \int_{-\infty}^{\infty} dk\ e^{ik(x-\eta t-\xi)}\ \frac{\sinh(ky)\cosh(k(1-\eta))}{k\ \sinh(k)}. \tag{4.1.16}$$

Our goal is to evaluate the improper integrals from (4.1.13) – (4.1.16) by representing each of them as a limit of a sequence of closed contour integrals on the complex k-plane and then using the Residue theorem. It turns out that the derivation of the desired result for the sum $\left(\widehat{\mathbf{I}}_1 + \widehat{\mathbf{I}}_3\right)$ is technically different than the derivation of the result for the sum $\left(\widehat{\mathbf{I}}_2 + \widehat{\mathbf{I}}_4\right)$. For the rest of this chapter we will focus on the results for $\left(\widehat{\mathbf{I}}_1 + \widehat{\mathbf{I}}_3\right)$.

We have to consider two separate cases: $x \leq r_0$ and $x \geq r_0$. In what follows, we provide a detailed analysis for the case $x \leq r_0$. The case $x \geq r_0$ remains an open question and can be analyzed in a similar manner. The first result is concerned with the sum $\left(\widehat{\mathbf{I}}_1 + \widehat{\mathbf{I}}_3\right)$.

Theorem 4.3 *For $x \geq r_0$, the following representation is valid for $\widehat{\mathbf{I}}_1 + \widehat{\mathbf{I}}_3$:*

$$\widehat{\mathbf{I}}_1 + \widehat{\mathbf{I}}_3 = 2\pi \int_0^{r_0} d\xi \int_0^{1} d\eta\ \chi(\xi,\eta) \sum_{m=1}^{\infty} e^{-\pi m|x-\eta t-\xi|}\ \frac{\sin(\pi m y)\ \sin(\pi m \eta)}{\pi m}. \tag{4.1.17}$$

Proof. To prove the result we consider three different subintervals for time t. The case when $\infty > t \geq \frac{x}{y}$, will be called Case A; the case when $\frac{x}{y} > t \geq \frac{x-r_0}{y}$, will be called Case B, and the case when $\frac{x-r_0}{y} > t \geq x - r_0$, will be called Case C.

Case A. For this case, we provide a detailed proof. We consider separately the subcases (i) $t = \frac{x}{y}$ and (ii) $t > \frac{x}{y}$ and denote them as Case A(i) and Case A(ii). Let us evaluate the integral $\widehat{\mathbf{I}}_1$ for the moment in time, $t = \frac{x}{y}$. The domain of integration with respect to ξ and η in $\widehat{\mathbf{I}}_1$ of (4.1.13) can be given as $[0, r_0] \times [0, y]$.

A straight line defined as $x - \eta t - \xi = 0$ passes through the points B with coordinates ($\xi = x, \eta = 0$) and D with the coordinates ($\xi = 0, \eta = y$) (see Fig. 4.1).

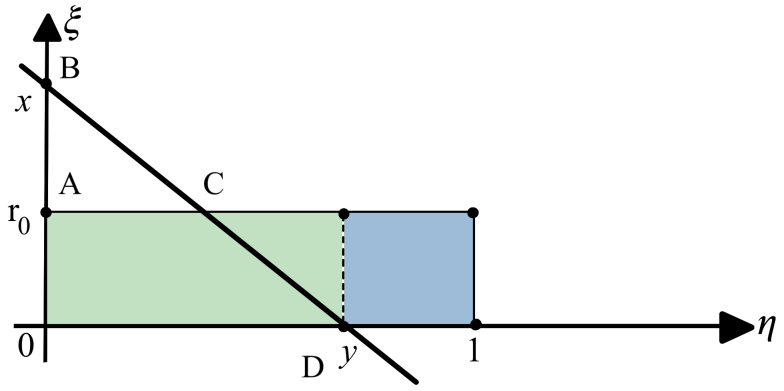

Figure 4.1: Position of the straight line for Case A.

For all points located above the line BD, one has $x - \eta t - \xi < 0$ and for all points located below the line BD, one has $x - \eta t - \xi > 0$. The line BD splits the domain of integration of $(0, y)$ into two subdomains: the triangular subdomain above the line and the trapezoidal subdomain below the line. Therefore, we have for the integral of (4.1.13) the following decomposition:

$$\frac{1}{2\pi i}\,\widehat{\mathbf{I}}_1 = \widehat{\mathcal{I}}_1 + \widehat{\mathcal{I}}_2,$$

where

$$\widehat{\mathcal{I}}_1 = \frac{1}{2\pi i}\int_0^{r_0} d\xi \int_0^{\frac{x-\xi}{t}} d\eta\ \chi(\xi,\eta) \int_{-\infty}^{\infty} dk\ e^{ik(x-\eta t-\xi)}\ \frac{\sinh(k(1-y))\sinh(k\eta)}{k\ \sinh(k)},$$

$$\widehat{\mathcal{I}}_2 = \frac{1}{2\pi i}\int_0^{r_0} d\xi \int_{\frac{x-\xi}{t}}^{y} d\eta\ \chi(\xi,\eta) \int_{-\infty}^{\infty} dk\ e^{ik(x-\eta t-\xi)}\ \frac{\sinh(k(1-y))\sinh(k\eta)}{k\ \sinh(k)}. \tag{4.1.18}$$

First we evaluate $\widehat{\mathcal{I}}_1$ in which $x - \eta t - \xi \geq 0$. Let us show that the improper integral with respect to k can be represented as a limit of a sequence of contour integrals in the closed upper half-plane.

Let $\mathscr{B}(k)$ be an analytic function defined by

$$\mathscr{B}(k) = \frac{\sinh(k(1-y))\ \sinh(k\eta)}{k\ \sinh(k)}. \tag{4.1.19}$$

Let Γ_N be a semi-circle in the upper half-plane of the complex k-plane centered at the origin of radius $r = \pi(N + \frac{1}{2})$, where N is a large positive integer. It can be readily shown that when $\eta \leq y$, the following result holds:

$$|\mathscr{B}(k)| \to 0 \ \text{ when } \ k \in \Gamma_N \ \text{ and } \ N \to \infty. \tag{4.1.20}$$

Using the Jordan's lemma and (4.1.20) yields

$$\lim_{N\to\infty} \int_{\Gamma_N} e^{ik(x-\eta t-\xi)}\, \mathscr{B}(k) \to 0 \ \text{ as } \ N \to \infty, \tag{4.1.21}$$

where $\int_{\Gamma_N}$ denotes the integral along Γ_N. Consider a sequence $\left\{\mathbb{\Gamma}_N\right\}_{N=1}^{\infty}$ of closed contours defined by $\mathbb{\Gamma}_N = \Big[-\pi(N+\frac{1}{2}), \pi(N+\frac{1}{2})\Big] \bigcup \Gamma_N$. Based on (4.1.21) we obtain that the following relation holds for the improper integral from $\widehat{\mathcal{I}}_1$:

$$\begin{aligned}\int_{-\infty}^{\infty} dk\ e^{ik(x-\eta t-\xi)}\ &\frac{\sinh(k(1-y))\ \sinh(k\eta)}{k\ \sinh(k)} \\ &= \lim_{N\to\infty} \oint_{\mathbb{\Gamma}_N} dk\ e^{ik(x-\eta t-\xi)}\ \frac{\sinh(k(1-y))\ \sinh(k\eta)}{k\ \sinh(k)}.\end{aligned} \tag{4.1.22}$$

Using the Residue theorem and relationship (4.1.22), we evaluate the integral $\widehat{\mathcal{I}}_1$ and have

$$\begin{aligned}\widehat{\mathcal{I}}_1 &= \int_0^{r_0} d\xi \int_0^{\frac{x-\xi}{t}} d\eta\ \chi(\xi,\eta) \sum_{m=1}^{\infty} \text{Res}\left\{ e^{ik(x-\eta t-\xi)}\ \frac{\sinh(k(1-y))\sinh(k\eta)}{k\ \sinh(k)},\ \pi m i \right\} \\ &= -i \int_0^{r_0} d\xi \int_0^{\frac{x-\xi}{t}} d\eta\ \chi(\xi,\eta) \sum_{m=1}^{\infty} e^{-\pi m(x-\eta t-\xi)}\ \frac{\sin(\pi m y)\ \sin(\pi m\eta)}{\pi m}.\end{aligned} \tag{4.1.23}$$

For the second integral $\widehat{\mathcal{I}}_2$, in which $x - \eta t - \xi < 0$, we can consider a sequence $\left\{\widetilde{\mathbb{\Gamma}}_N\right\}_{N=1}^{\infty}$ of contours in the lower half-plane which is symmetric to the sequence $\left\{\mathbb{\Gamma}_N\right\}_{N=1}^{\infty}$ (see Fig. 4.2 (b)).

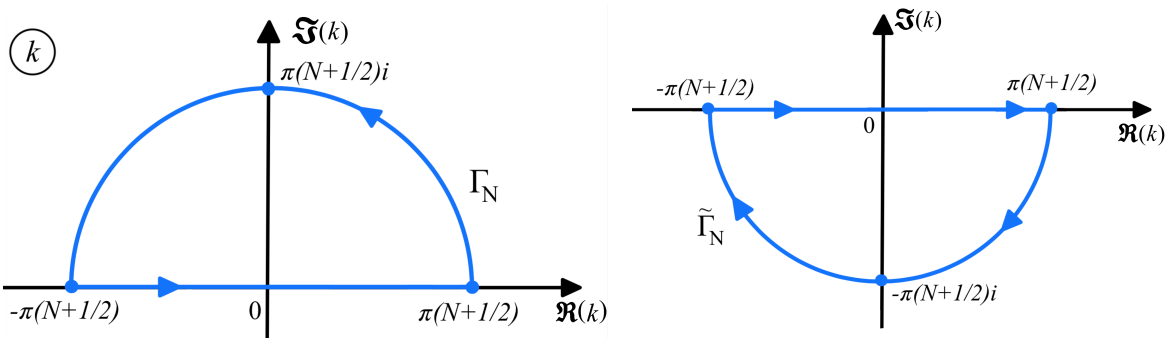

(a) (b)

Figure 4.2: Closed contours of integration for the integrals $\widehat{I}_1$ (a) and $\widehat{I}_2$ (b).

Evaluating the corresponding limit as $N \to \infty$, we obtain

$$\begin{aligned}\widehat{I}_2 &= -\int_0^{r_0} d\xi \int_{\frac{x-\xi}{t}}^{y} d\eta\ \chi(\xi,\eta) \sum_{m=1}^{\infty} \mathrm{Res}\left\{ e^{ik(x-\eta t-\xi)}\ \frac{\sinh(k(1-y))\sinh(k\eta)}{k\ \sinh(k)},\ -\pi m i \right\} \\ &= -i\int_0^{r_0} d\xi \int_{\frac{x-\xi}{t}}^{y} d\eta\ \chi(\xi,\eta) \sum_{m=1}^{\infty} e^{\pi m(x-\eta t-\xi)}\ \frac{\sin(\pi m y)\ \sin(\pi m\eta)}{\pi m}. \end{aligned} \tag{4.1.24}$$

Summing the integrals (4.1.23) and (4.1.24) together, we find

$$\widehat{\mathbf{I}}_1 = 2\pi \int_0^{r_0} d\xi \int_0^{y} d\eta\ \chi(\xi,\eta) \sum_{m=1}^{\infty} e^{-\pi m|x-\eta t-\xi|}\ \frac{\sin(\pi m y)\ \sin(\pi m\eta)}{\pi m}. \tag{4.1.25}$$

To evaluate $\widehat{\mathbf{I}}_3$, we notice that for the entire domain of integration the following estimate holds: $x - \eta t - \xi < 0$. We proceed with a sequence of steps similar to the steps we used for evaluation of the second integral of $\widehat{\mathbf{I}}_1$. Namely, we introduce a sequence of expanding contours closed in the

lower half-plane and have

$$
\begin{aligned}
-\frac{1}{2\pi i}\int_0^{r_0} d\xi \int_y^1 d\eta\ \chi(\xi,\eta) \int_{-\infty}^{\infty} dk\ e^{ik(x-\eta t-\xi)}\ \frac{\sinh(k(1-\eta))\ \sinh(ky)}{k\ \sinh(k)} \\
&= -\int_0^{r_0} d\xi \int_y^1 d\eta\ \chi(\xi,\eta) \sum_{m=1}^{\infty} \mathrm{Res}\left\{ e^{ik(x-\eta t-\xi)}\ \frac{\sinh(k(1-\eta))\sinh(ky)}{k\ \sinh(k)},\ -\pi m i \right\} \\
&= -\int_0^{r_0} d\xi \int_y^1 d\eta\ \chi(\xi,\eta) \sum_{m=1}^{\infty} e^{\pi m(x-\eta t-\xi)}\ \frac{\sinh(-\pi m i(1-\eta))\sinh(-\pi m i y)}{(-\pi m i)\ \cosh(-\pi m i)} \\
&= -i\int_0^{r_0} d\xi \int_y^1 d\eta\ \chi(\xi,\eta) \sum_{m=1}^{\infty} e^{-\pi m|x-\eta t-\xi|}\ \frac{\sin(\pi m y)\ \sin(\pi m\eta)}{\pi m}.
\end{aligned}
$$

Thus, for $\widehat{\mathbf{I}}_3$ the following representation holds:

$$
\widehat{\mathbf{I}}_3 = 2\pi \int_0^{r_0} d\xi \int_y^1 d\eta\ \chi(\xi,\eta) \sum_{m=1}^{\infty} e^{-\pi m|x-\eta t-\xi|}\ \frac{\sin(\pi m y)\ \sin(\pi m\eta)}{\pi m}. \tag{4.1.26}
$$

Collecting together representations (4.1.25) and (4.1.26), we obtain

$$
\widehat{\mathbf{I}}_1 + \widehat{\mathbf{I}}_3 = 2\pi \int_0^{r_0} d\xi \int_0^1 d\eta\ \chi(\xi,\eta) \sum_{m=1}^{\infty} e^{-\pi m|x-\eta t-\xi|}\ \frac{\sin(\pi m y)\ \sin(\pi m\eta)}{\pi m}. \tag{4.1.27}
$$

Therefore, Case A(i) is proven. We notice that in what follows, the case Case B(i) and Case C(i) will be shown first and then the results of Case A(ii), Case B(ii), and Case C(ii) will follow.

Case B. We start with Case B (i), which corresponds to $t = \frac{x-r_0}{y}$. The line $x - \eta t - \xi = 0$ passes through the points B with coordinates $(x, 0)$ and E with the coordinates $(\xi = r_0, \eta = y)$.

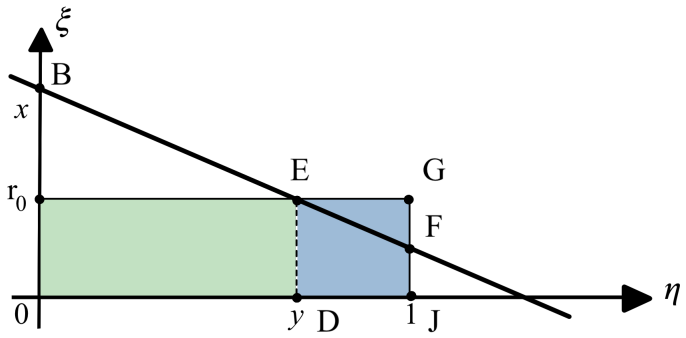

Figure 4.3: Position of the straight line BEF corresponding to $t = \frac{x-r_0}{y}$.

To evaluate $\widehat{\mathbf{I}}_1$, we notice that the domain of integration when $\eta \in (0, y)$ is located below the line BE, and thus $x - \eta t - \xi > 0$. Therefore, we choose a sequence of closed contours with semi-circle parts in the upper half-plane. We have

$$\begin{aligned}
&\frac{1}{2\pi i}\int_0^{r_0} d\xi \int_0^{y} d\eta\ \chi(\xi,\eta) \int_{-\infty}^{\infty} dk\ e^{ik(x-\eta t-\xi)}\ \frac{\sinh(k(1-y))\sinh(k\eta)}{k\ \sinh(k)} \\
&\quad = \int_0^{r_0} d\xi \int_0^{y} d\eta\ \chi(\xi,\eta) \sum_{m=1}^{\infty} \mathrm{Res}\left\{ e^{ik(x-\eta t-\xi)}\ \frac{\sinh(k(1-y))\sinh(k\eta)}{k\ \sinh(k)},\ \pi m i \right\} \\
&\quad = \int_0^{r_0} d\xi \int_0^{y} d\eta\ \chi(\xi,\eta) \sum_{m=1}^{\infty} e^{i(\pi m i)(x-\eta t-\xi)}\ \frac{\sinh(\pi m i(1-y))\sinh(\eta\ \pi m i)}{(\pi m i)\ \cosh(\pi m i)} \\
&\quad = -\,i \int_0^{r_0} d\xi \int_0^{y} d\eta\ \chi(\xi,\eta) \sum_{m=1}^{\infty} e^{-\pi m|x-\eta t-\xi|}\ \frac{\sin(\pi m y)\ \sin(\pi m\eta)}{\pi m}.
\end{aligned} \tag{4.1.28}$$

Thus again we obtain

$$\widehat{\mathbf{I}}_1 = 2\pi \int_0^{r_0} d\xi \int_0^{y} d\eta\ \chi(\xi,\eta) \sum_{m=1}^{\infty} e^{-\pi m|x-\eta t-\xi|}\ \frac{\sin(\pi m y)\ \sin(\pi m\eta)}{\pi m}. \tag{4.1.29}$$

To evaluate $\widehat{\mathbf{I}}_3$ we have to consider two subdomains: the trapezoidal subdomain $DEFJ$ and

triangular subdomain, EGF which yields the decomposition

$$\frac{1}{2\pi i}\,\widehat{\mathbf{I}}_3 = \frac{1}{2\pi i}\int_0^{r_0} d\xi \int_y^{\frac{x-\xi}{t}} d\eta\ \chi(\xi,\eta) \int_{-\infty}^{\infty} dk\ e^{ik(x-\eta t-\xi)}\ \frac{\sinh(k(1-y))\sinh(k\eta)}{k\ \sinh(k)} + \frac{1}{2\pi i}\int_0^{r_0} d\xi \int_{\frac{x-\xi}{t}}^{1} d\eta\ \chi(\xi,\eta) \int_{-\infty}^{\infty} dk\ e^{ik(x-\eta t-\xi)}\ \frac{\sinh(k(1-y))\sinh(k\eta)}{k\ \sinh(k)}.$$

For the first integral, where $x-\eta t-\xi > 0$, we choose a sequence of closed contours with semi-circles in the upper half-plane. For the second integral, where $x-\eta t-\xi < 0$, we choose a sequence of closed contours with semi-circles in the lower half-plane. Evaluating the first integral, we find

$$\begin{aligned}
&\frac{1}{2\pi i}\int_0^{r_0} d\xi \int_y^{\frac{x-\xi}{t}} d\eta\ \chi(\xi,\eta) \int_{-\infty}^{\infty} dk\ e^{ik(x-\eta t-\xi)}\ \frac{\sinh(k(1-y))\sinh(k\eta)}{k\ \sinh(k)} \\
&\quad = \frac{1}{2\pi i}\int_0^{r_0} d\xi \int_y^{\frac{x-\xi}{t}} d\eta\ \chi(\xi,\eta)\ \mathrm{Res}\left\{ e^{ik(x-\eta t-\xi)}\ \frac{\sinh(k(1-y))\sinh(k\eta)}{k\ \sinh(k)}, \pi m i \right\} \\
&\quad = -i\int_0^{r_0} d\xi \int_y^{\frac{x-\xi}{t}} d\eta\ \chi(\xi,\eta) \sum_{m=1}^{\infty} e^{-\pi m|x-\eta t-\xi|}\ \frac{\sin(\pi m y)\sin(\pi m\eta)}{\pi m}.
\end{aligned}$$

Evaluating the second integral, we find

$$\begin{aligned}
&\frac{1}{2\pi i}\int_0^{r_0} d\xi \int_{\frac{x-\xi}{t}}^{1} d\eta\ \chi(\xi,\eta) \int_{-\infty}^{\infty} dk\ e^{ik(x-\eta t-\xi)}\ \frac{\sinh(k(1-y))\sinh(k\eta)}{k\ \sinh(k)} \\
&\quad = \frac{1}{2\pi i}\int_0^{r_0} d\xi \int_{\frac{x-\xi}{t}}^{1} d\eta\ \chi(\xi,\eta)\ \mathrm{Res}\left\{ e^{ik(x-\eta t-\xi)}\ \frac{\sinh(k(1-y))\sinh(k\eta)}{k\ \sinh(k)}, \ -\pi m i \right\} \\
&\quad = -i\int_0^{r_0} d\xi \int_{\frac{x-\xi}{t}}^{1} \eta\ \chi(\xi,\eta) \sum_{m=1}^{\infty} e^{-\pi m|x-\eta t-\xi|}\ \frac{\sin(\pi m y)\sin(\pi m\eta)}{\pi m}.
\end{aligned}$$

Summing the two integrals, we obtain the result for $\widehat{\mathbf{I}}_3$ similar to (4.1.26), i.e.

$$\widehat{\mathbf{I}}_3 = 2\pi \int_0^{r_0} d\xi \int_y^{1} d\eta\ \chi(\xi,\eta) \sum_{m=1}^{\infty} e^{-\pi m|x-\eta t-\xi|}\ \frac{\sin(\pi m y)\ \sin(\pi m\eta)}{\pi m}. \tag{4.1.30}$$

Adding the results (4.1.29) for $\widehat{\mathbf{I}}_1$ and (4.1.30) for $\widehat{\mathbf{I}}_3$, we obtain the result for $\widehat{\mathbf{I}}_1 + \widehat{\mathbf{I}}_3$ similar to (4.1.27).

Case C. We start with Case C(i), which corresponds to $t = x - r_0$. The line $x - nt - \xi = 0$ passes through the points $B\ (x, 0)$ and $G\ (r_0, 1)$.

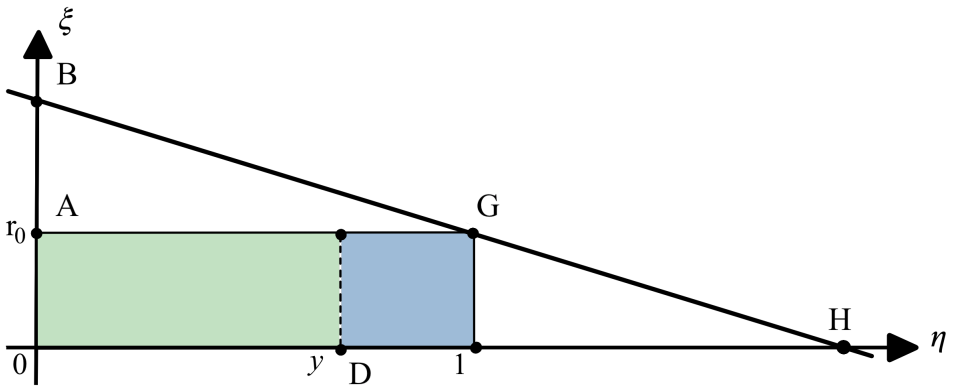

Figure 4.4: Position of straight line BGH corresponding to $t = x - r_0$.

For both $\widehat{\mathbf{I}}_1$ and $\widehat{\mathbf{I}}_3$ in this case, all points in their respective subdomains are below the line $x - \eta t - \xi = 0$, where $x - \eta t - \xi > 0$. For both integrals we choose a sequence of closed contours with semi-circle parts in the upper half-plane. Again, we find the results similar to (4.1.17)

$$\widehat{\mathbf{I}}_1 = 2\pi \int_0^{r_0} d\xi \int_0^{y} d\eta\ \chi(\xi,\eta) \sum_{m=1}^{\infty} e^{-\pi m|x-\eta t-\xi|}\ \frac{\sin(\pi m y)\ \sin(\pi m\eta)}{\pi m}\,, \tag{4.1.31}$$

$$\widehat{\mathbf{I}}_3 = 2\pi \int_0^{r_0} d\xi \int_y^{1} d\eta\ \chi(\xi,\eta) \sum_{m=1}^{\infty} e^{-\pi m|x-\eta t-\xi|}\ \frac{\sin(\pi m y)\ \sin(\pi m\eta)}{\pi m}. \tag{4.1.32}$$

Summing up these results, we obtain

$$\begin{aligned}\widehat{\mathbf{I}}_1 + \widehat{\mathbf{I}}_3 = 2\pi \Bigg[&\int_0^{r_0} d\xi \int_0^{y} d\eta\ \chi(\xi,\eta) \sum_{m=1}^{\infty} e^{-\pi m|x-\eta t-\xi|}\ \frac{\sin(\pi m y)\ \sin(\pi m\eta)}{\pi m} \\ &+ \int_0^{r_0} d\xi \int_y^{1} d\eta\ \chi(\xi,\eta) \sum_{m=1}^{\infty} e^{-\pi m|x-\eta t-\xi|}\ \frac{\sin(\pi m y)\ \sin(\pi m\eta)}{\pi m}\Bigg] \\ = 2\pi &\int_0^{r_0} d\xi \int_0^{1} d\eta\ \chi(\xi,\eta) \sum_{m=1}^{\infty} e^{-\pi m|x-\eta t-\xi|}\ \frac{\sin(\pi m y)\ \sin(\pi m\eta)}{\pi m}. \end{aligned} \tag{4.1.33}$$

Remark 4.4. Comparing formulas for $\widehat{\mathbf{I}}_1 + \widehat{\mathbf{I}}_3$ evaluated for three different time moments, i.e.

$t_1 = \frac{x}{y}$, $t_2 = \frac{(x-r_0)}{y}$, and $t_3 = x - r_0$, one can see that they are the same.

4.1.1 *Evaluation of integrals* $\widehat{\mathbf{I}}_1$ *and* $\widehat{\mathbf{I}}_3$ *for an arbitrary moment of time t.*

In this subsection we show that the result (4.1.17) of Theorem 4.3 obtained for $\widehat{\mathbf{I}}_1$ and $\widehat{\mathbf{I}}_3$ is valid for any arbitrary position of the straight line. We will consider three cases when the line $x - \eta t - \xi = 0$ is located between the lines $BA0$ and BCD, between the lines BCD and BEF, and lastly, between BEF and BGH.

Case A: Domain defined by a line between $BA0$ and BCD.

Let BKL be a straight line located between the lines $BA0$ and BCD, which corresponds to $t > t_1$, $t_1 = \frac{x}{y}$.

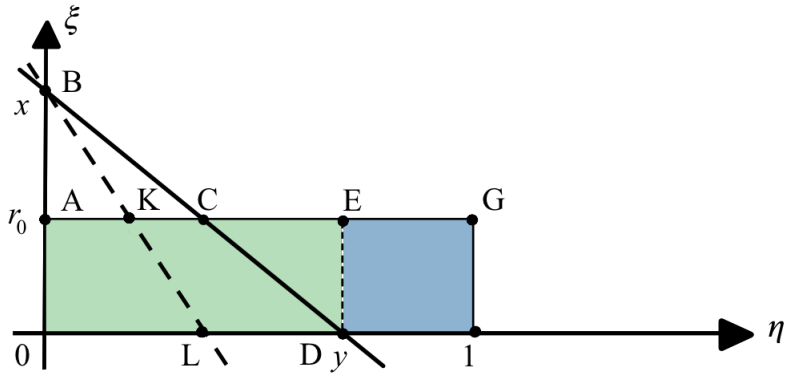

Figure 4.5: Position of the straight line between $BA0$ and BCD corresponding to $t > \frac{x}{y}$.

The point of intersection of BKL with the η-axis is $L\left(\frac{x}{t}, 0\right)$. The domain of integration of $\widehat{\mathbf{I}}_1$ consists of two trapezoidal subdomains, $AKL0$ and $KEDL$, while the domain of integration of

the integral $\widehat{\mathbf{I}}_3$ stays the same as long as the line BKL is located below BCD. Therefore, we have

$$\begin{aligned}\frac{1}{2\pi i}\,\widehat{\mathbf{I}}_1 &= \frac{1}{2\pi i}\int_0^{r_0} d\xi \int_0^{y} d\eta\ \chi(\xi,\eta) \int_{-\infty}^{\infty} dk\ e^{ik(x-\eta t-\xi)}\ \frac{\sinh(k(1-y))\ \sinh(k\eta)}{k\ \sinh(k)} \\ &= \frac{1}{2\pi i}\int_0^{r_0} d\xi \int_0^{\frac{x-\xi}{t}} d\eta\ \chi(\xi,\eta) \int_{-\infty}^{\infty} dk\ e^{ik(x-\eta t-\xi)}\ \frac{\sinh(k(1-y))\ \sinh(k\eta)}{k\ \sinh(k)} \\ &+ \frac{1}{2\pi i}\int_0^{r_0} d\xi \int_{\frac{x-\xi}{t}}^{y} d\eta\ \chi(\xi,\eta) \int_{-\infty}^{\infty} dk\ e^{ik(x-\eta t-\xi)}\ \frac{\sinh(k(1-y))\ \sinh(k\eta)}{k\ \sinh(k)}.\end{aligned} \tag{4.1.34}$$

In the trapezoidal subdomain, $AKL0$, we have $x-\eta t-\xi>0$ and in the trapezoidal subdomain $KEDL$, we have $x-\eta t-\xi<0$. To evaluate the integral from (4.1.34) involving the integration over $\left(0,\frac{(x-\xi)}{t}\right)$, we consider a sequence of expanding contours in the upper half-plane and get the result

$$-i\int_0^{r_0} d\xi \int_0^{\frac{x-\xi}{t}} d\eta\ \chi(\xi,\eta) \sum_{m=1}^{\infty} e^{-\pi m(x-\eta t-\xi)}\ \frac{\sin(\pi m y)\ \sin(\pi m\eta)}{\pi m}. \tag{4.1.35}$$

To evaluate the integral from (4.1.34) involving the integration over $\left(\frac{(x-\xi)}{t},y\right)$, we consider a sequence of expanding contours in the lower half-plane and get the result

$$-i\int_0^{r_0} d\xi \int_{\frac{x-\xi}{t}}^{y} d\eta\ \chi(\xi,\eta) \sum_{m=1}^{\infty} e^{\pi m(x-\eta t-\xi)}\ \frac{\sin(\pi m y)\ \sin(\pi m\eta)}{\pi m}. \tag{4.1.36}$$

Summing up (4.1.35) and (4.1.36), we obtain

$$\widehat{\mathbf{I}}_1 = 2\pi\int_0^{r_0} d\xi \int_0^{y} d\eta\ \chi(\xi,\eta) \sum_{m=1}^{\infty} e^{-\pi m|x-\eta t-\xi|}\ \frac{\sin(\pi m y)\ \sin(\pi m\eta)}{\pi m}. \tag{4.1.37}$$

As follows from Fig. 4.5, to evaluate $\widehat{\mathbf{I}}_3$, for any straight line below BCD, the domain of integration is located above the afore line. Now we repeat the argument that has been used to justify representation (4.1.26) and have

$$\frac{1}{2\pi i}\widehat{\mathbf{I}}_3 = \frac{1}{2\pi i}\int_0^{r_0} d\xi \int_y^{1} d\eta\ \chi(\xi,\eta) \int_{-\infty}^{\infty} dk\ e^{-ik(x-\eta t-\xi)}\ \frac{\sinh(k(1-\eta))\ \sinh(ky)}{k\ \sinh(k)},$$

which yields

$$\widehat{\mathbf{I}}_3 = 2\pi \int_0^{r_0} d\xi \int_y^1 d\eta\ \chi(\xi,\eta) \sum_{m=1}^{\infty} e^{-\pi m|x-\eta t-\xi|}\ \frac{\sin(\pi m y)\ \sin(\pi m\eta)}{\pi m}. \tag{4.1.38}$$

Combining (4.1.37) and (4.1.38) we obtain that for all $t > \frac{x}{y}$ the following result holds:

$$\widehat{\mathbf{I}}_1 + \widehat{\mathbf{I}}_3 = 2\pi \int_0^{r_0} d\xi \int_0^1 d\eta\ \chi(\xi,\eta) \sum_{m=1}^{\infty} e^{-\pi m|x-\eta t-\xi|}\ \frac{\sin(\pi m y)\ \sin(\pi m\eta)}{\pi m}. \tag{4.1.39}$$

Case B: Domain defined by a line between BCD and BEF.

Let BMP be a straight line located between BCD and BEF. The position of BMP corresponds to t such that

$$\frac{x-r_0}{y} < t < \frac{x}{y}. \tag{4.1.40}$$

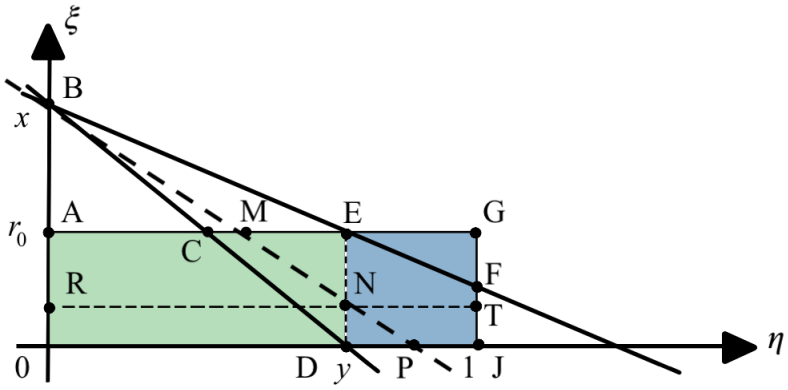

Figure 4.6: Position of the straight line between BCD and BEF corresponding to $\left(\frac{(x-r_0)}{y}\right) < t < \frac{x}{y}$.

To evaluate $\widehat{\mathbf{I}}_1$, we notice that the domain of integration when $\eta \in (0, y)$ consists of three subdomains: a rectangular subdomain $0RND$, a trapezoidal subdomain $RAMN$, and a triangular

subdomain MEN. Evaluating the integral over the rectangle $0RND$ yields

$$\frac{1}{2\pi i}\int_0^R d\xi \int_0^y d\eta\ \chi(\xi,\eta) \int_\infty^\infty dk\ e^{ik(x-\eta t-\xi)}\ \frac{\sinh(k(1-y))\ \sinh(k\eta)}{k\ \sinh(k)}$$
$$= -i\int_0^R d\xi \int_0^y d\eta\ \chi(\xi,\eta) \sum_{m=1}^\infty e^{-\pi m(x-\eta t-\xi)}\ \frac{\sin(\pi m y)\ \sin(\pi m\eta)}{\pi m}. \tag{4.1.41}$$

Evaluating the integral over the trapezoid $RAMN$ yields

$$\frac{1}{2\pi i}\int_R^{r_0} d\xi \int_0^{\frac{x-\xi}{t}} d\eta\ \chi(\xi,\eta) \int_\infty^\infty dk\ e^{ik(x-\eta t-\xi)}\ \frac{\sinh(k(1-y))\ \sinh(k\eta)}{k\ \sinh(k)}$$
$$= -i\int_R^{r_0} d\xi \int_0^{\frac{x-\xi}{t}} d\eta\ \chi(\xi,\eta) \sum_{m=1}^\infty e^{-\pi m(x-\eta t-\xi)}\ \frac{\sin(\pi m y)\ \sin(\pi m\eta)}{\pi m}. \tag{4.1.42}$$

Evaluating the integral over the triangle MEN yields

$$\frac{1}{2\pi i}\int_R^{r_0} d\xi \int_{\frac{x-\xi}{t}}^y d\eta\ \chi(\xi,\eta) \int_\infty^\infty dk\ e^{ik(x-\eta t-\xi)}\ \frac{\sinh(k(1-y))\ \sinh(k\eta)}{k\ \sinh(k)}$$
$$= -i\int_R^{r_0} d\xi \int_{\frac{x-\xi}{t}}^y d\eta\ \chi(\xi,\eta) \sum_{m=1}^\infty e^{\pi m(x-\eta t-\xi)}\ \frac{\sin(\pi m y)\ \sin(\pi m\eta)}{\pi m}. \tag{4.1.43}$$

Summing the results of (4.1.41) - (4.1.43), we obtain

$$\widehat{\mathbf{I}}_1 = 2\pi\int_0^{r_0} d\xi \int_0^y d\eta\ \chi(\xi,\eta) \sum_{m=1}^\infty e^{-\pi m|x-\eta t-\xi|}\ \frac{\sin(\pi m y)\ \sin(\pi m\eta)}{\pi m}. \tag{4.1.44}$$

To evaluate the integral $\widehat{\mathbf{I}}_3$, we notice that for t satisfying (4.1.40) the domain of integration of $(y,1)$ is a union of three subdomains: a rectangular subdomain $NEGT$, a trapezoidal subdomain $NTJP$, and a triangular subdomain DNP. For the triangular subdomain, we consider a sequence of expanding contours in the upper half-plane and for the two remaining subdomains, we consider a sequence of expanding contours in the lower half-plane. Evaluating the integral over the domain

DNP yields

$$\frac{1}{2\pi i}\int_0^N d\xi \int_y^{\frac{x-\xi}{t}} d\eta\ \chi(\xi,\eta)\ \int_{-\infty}^{\infty} dk\ e^{-ik(x-\eta t-\xi)}\ \frac{\sinh(k(1-\eta))\ \sinh(ky)}{k\ \sinh(k)}$$
$$= -i\int_0^N d\xi \int_y^{\frac{x-\xi}{t}} d\eta\ \chi(\xi,\eta)\ \sum_{m=1}^{\infty} e^{-\pi m(x-\eta t-\xi)}\ \frac{\sin(\pi m y)\ \sin(\pi m\eta)}{\pi m}. \tag{4.1.45}$$

Evaluating the integral over the domain $NTJP$ yields

$$\frac{1}{2\pi i}\int_0^N d\xi \int_{\frac{x-\xi}{t}}^1 d\eta\ \chi(\xi,\eta)\ \int_{-\infty}^{\infty} dk\ e^{-ik(x-\eta t-\xi)}\ \frac{\sinh(k(1-\eta))\ \sinh(ky)}{k\ \sinh(k)}$$
$$= -i\int_0^N d\xi \int_{\frac{x-\xi}{t}}^1 d\eta\ \chi(\xi,\eta)\ \sum_{m=1}^{\infty} e^{\pi m(x-\eta t-\xi)}\ \frac{\sin(\pi m y)\ \sin(\pi m\eta)}{\pi m}. \tag{4.1.46}$$

Summing (4.1.45) and (4.1.46) yields

$$-i\int_0^N d\xi \int_y^1 d\eta\ \chi(\xi,\eta)\ \sum_{m=1}^{\infty} e^{-\pi m|x-\eta t-\xi|}\ \frac{\sin(\pi m y)\ \sin(\pi m\eta)}{\pi m}. \tag{4.1.47}$$

Evaluating the integral over the domain $NEGT$ yields

$$\frac{1}{2\pi i}\int_N^E d\xi \int_y^1 d\eta\ \chi(\xi,\eta)\ \int_{-\infty}^{\infty} dk\ e^{-ik(x-\eta t-\xi)}\ \frac{\sinh(k(1-\eta))\ \sinh(ky)}{k\ \sinh(k)}$$
$$= -i\int_N^E d\xi \int_y^1 d\eta\ \chi(\xi,\eta)\ \sum_{m=1}^{\infty} e^{-\pi m|x-\eta t-\xi|}\ \frac{\sin(\pi m y)\ \sin(\pi m\eta)}{\pi m}. \tag{4.1.48}$$

Summing (4.1.47) and (4.1.48) we find the following result:

$$\widehat{\mathbf{I}}_3 = 2\pi\int_0^{r_0} d\xi\ \int_y^1 d\eta\ \chi(\xi,\eta)\ \sum_{m=1}^{\infty} e^{-\pi m|x-\eta t-\xi|}\ \frac{\sin(\pi m y)\ \sin(\pi m\eta)}{\pi m}. \tag{4.1.49}$$

Summing (4.1.48) and (4.1.49), we again attain the result for t from (4.1.40), which is similar to the result (4.1.39).

Case C: Domain defined by a line between BEF and BGH.

Let BQS be a straight line located between BEF and BGH. The position of BQS corresponds

to t such that

$$x - r_0 < t < \frac{x - r_0}{y} \tag{4.1.50}$$

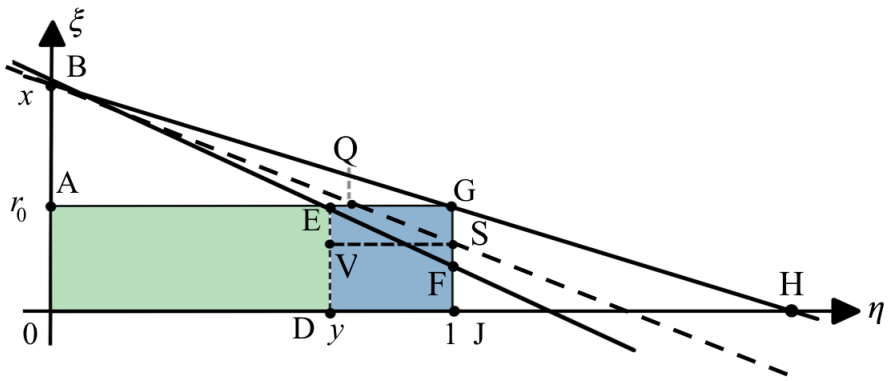

Figure 4.7: Position of the straight line between BEF and BGH corresponding to $(x - r_0) < t < \frac{(x-r_0)}{y}$.

It can be readily checked that the evaluation of $\widehat{\mathbf{I}}_1$, for any position of the line $x - \eta t - \xi = 0$ above BEF, yields the result similar to (4.1.44):

$$\widehat{\mathbf{I}}_1 = 2\pi \int_0^{r_0} d\xi \int_0^{y} d\eta \; \chi(\xi, \eta) \sum_{m=1}^{\infty} e^{-\pi m|x-\eta t-\xi|} \frac{\sin(\pi m y) \; \sin(\pi m \eta)}{\pi m}. \tag{4.1.51}$$

To evaluate $\widehat{\mathbf{I}}_3$ for any t of (4.1.50) we split the domain of integration of $(y, 1)$ into three subdomains: a rectangular subdomain $DVSJ$, a trapezoidal subdomain $VEQS$, and a triangular subdomain QGS (Fig. 4.7). To evaluate $\widehat{I}_3$ on the subdomains $DVSJ$ and $VEQS$, we consider a sequence of expanding contours in the upper half-plane and for the subdomain QGS, we consider a sequence of expanding contours in the lower-half plane. Evaluating the integral over the domain

$DVSJ$ yields

$$\frac{1}{2\pi i}\int_0^V d\xi \int_y^1 d\eta\ \chi(\xi,\eta)\ \int_{-\infty}^{\infty} dk\ e^{-ik(x-\eta t-\xi)}\ \frac{\sinh(k(1-\eta))\ \sinh(ky)}{k\ \sinh(k)}$$
$$= -i\int_0^V d\xi \int_y^1 d\eta\ \chi(\xi,\eta)\ \sum_{m=1}^{\infty} e^{-\pi m(x-\eta t-\xi)}\ \frac{\sin(\pi m y)\ \sin(\pi m\eta)}{\pi m}. \tag{4.1.52}$$

Evaluating the integral over the domain $VEQS$ yields

$$\frac{1}{2\pi i}\int_V^E d\xi \int_y^{\frac{x-\xi}{t}} d\eta\ \chi(\xi,\eta)\ \int_{-\infty}^{\infty} dk\ e^{-ik(x-\eta t-\xi)}\ \frac{\sinh(k(1-\eta))\ \sinh(ky)}{k\ \sinh(k)}$$
$$= -i\int_V^E d\xi \int_y^{\frac{x-xi}{t}} d\eta\ \chi(\xi,\eta)\ \sum_{m=1}^{\infty} e^{-\pi m(x-\eta t-\xi)}\ \frac{\sin(\pi m y)\ \sin(\pi m\eta)}{\pi m}. \tag{4.1.53}$$

Evaluating the integral on the domain QGS yields

$$\frac{1}{2\pi i}\int_V^{r_0} d\xi \int_{\frac{x-\xi}{t}}^1 d\eta\ \chi(\xi,\eta)\ \int_{-\infty}^{\infty} dk\ e^{-ik(x-\eta t-\xi)}\ \frac{\sinh(k(1-\eta))\ \sinh(ky)}{k\ \sinh(k)}$$
$$= -i\int_V^{r_0} d\xi \int_{\frac{x-\xi}{t}}^1 d\eta\ \chi(\xi,\eta)\ \sum_{m=1}^{\infty} e^{\pi m(x-\eta t-\xi)}\ \frac{\sin(\pi m y)\ \sin(\pi m\eta)}{\pi m}. \tag{4.1.54}$$

Therefore summing (4.1.53) and (4.1.54) we obtain,

$$-i\int_V^{r_0} d\xi \int_y^1 d\eta\ \chi(\xi,\eta)\ \sum_{m=1}^{\infty} e^{-\pi m|x-\eta t-\xi|}\ \frac{\sin(\pi m y)\ \sin(\pi m\eta)}{\pi m}. \tag{4.1.55}$$

Lastly, summing (4.1.52) and (4.1.54) we again find the result similar to (4.1.38). Finally summing the results for $\widehat{\mathbf{I}}_1$ and $\widehat{\mathbf{I}}_3$ we find the results similar to (4.1.39).

The proof of Theorem 4.3 is complete. ■

CHAPTER 5

EVALUATION OF INTEGRALS $\widehat{\mathbf{I}}_2$ AND $\widehat{\mathbf{I}}_4$ OF (4.1.14) AND (4.1.16)

This chapter is devoted to the technical details used for evaluation of the integrals $\widehat{\mathbf{I}}_2$ and $\widehat{\mathbf{I}}_4$. We focus on the case $x > r_0$. Our goal is to show that both integrals can be evaluated by using the Residue Theorem. Let ℓ_n be a notation for a contour on the complex k-plane defined by

$$\ell_n = \{k : k \in (-\infty, -\delta_n) \cup \gamma_n \cup (\delta_n, \infty), \gamma_n = \delta_n e^{i\varphi}, \ -\pi \leq \varphi \leq 0\}. \tag{5.0.1}$$

Without any confusion, we use the same notation ℓ_n for the contour defined in (5.0.1) as we use for another contour defined in (3.0.17). Our first statement in this section is:

Lemma 5.1. *The following representations hold for the integrals $\widehat{\mathbf{I}}_2$ and $\widehat{\mathbf{I}}_4$:*

$$\begin{aligned}
\widehat{\mathbf{I}}_2 &= \int_0^{r_0} d\xi \int_0^y d\eta \ \chi(\xi,\eta) \ P.V. \int_{-\infty}^{\infty} dk \ e^{ik(x-\eta t-\xi)} \ \frac{\sinh(k(1-y))\cosh(k\eta)}{k \ \sinh(k)} \\
&= \lim_{\delta_n \to 0} \int_0^{r_0} d\xi \int_0^y d\eta \ \chi(\xi,\eta) \int_{\ell_n} dk \ e^{ik(x-\eta t-\xi)} \ \frac{\sinh(k(1-y))\cosh(k\eta)}{k \ \sinh(k)} \\
&\quad - \pi i \ (1-y) \int_0^{r_0} d\xi \int_0^y d\eta \ \chi(\xi,\eta),
\end{aligned} \tag{5.0.2}$$

and

$$\begin{aligned}
\widehat{\mathbf{I}}_4 &= -\int_0^{r_0} d\xi \int_y^1 d\eta \ \chi(\xi,\eta) \ P.V. \int_{-\infty}^{\infty} dk \ e^{ik(x-\eta t-\xi)} \ \frac{\sinh(ky)\cosh(k(1-\eta))}{k \ \sinh(k)} \\
&= \lim_{\delta_n \to 0} \int_0^{r_0} d\xi \int_y^1 d\eta \ \chi(\xi,\eta) \int_{\ell_n} dk \ e^{ik(x-\eta t-\xi)} \ \frac{\sinh(ky)\cosh(k(1-\eta))}{k \ \sinh(k)} \\
&\quad + \pi i \ y \int_0^{r_0} d\xi \int_y^1 d\eta \ \chi(\xi,\eta).
\end{aligned} \tag{5.0.3}$$

Proof. Using the definition of principal value integral [46, 47], we represent the formula for $\widehat{\mathbf{I}}_2$ as follows:

$$\begin{aligned}\widehat{\mathbf{I}}_2 = &\lim_{\delta_n\to 0}\int_0^{r_0} d\xi \int_0^{y} d\eta\ \chi(\xi,\eta) \int\!\!\!\!\!\!\diagup_{\ell_n} dk\ e^{ik(x-\eta t-\xi)}\ \frac{\sinh(k(1-y))\cosh(k\eta)}{k\ \sinh(k)}\\ &-\lim_{\delta_n\to 0}\int_0^{r_0} d\xi \int_0^{y} d\eta\ \chi(\xi,\eta) \int\!\!\!\!\!\!\diagup_{\gamma_n} dk\ e^{ik(x-\eta t-\xi)}\ \frac{\sinh(k(1-y))\cosh(k\eta)}{k\ \sinh(k)},\end{aligned} \tag{5.0.4}$$

where $\int\!\!\!\!\!\!\diagup_{\ell_n}$ denotes the integral along a semi-circle in the lower half-plane. To evaluate the integral over γ_n we can use the asymptotic approximations [48] at the vicinity of $k = 0$: $\sinh(k(1-y)) = k(1-y) + \mathcal{O}((1-y)^3k^3)$ and $\cosh(k\eta) = 1 + \mathcal{O}(\eta^2k^2)$. We have

$$\begin{aligned}&\lim_{\delta_n\to 0}\int_0^{r_0} d\xi \int_0^{y} d\eta\ \chi(\xi,\eta) \int_{-\pi}^{0} \frac{k\big[(1-y)+\mathcal{O}((1-y)^3k^3)\big]\big[1+\mathcal{O}((\eta^2k^2)\big]}{k+\mathcal{O}(k^3)}\ i\ d\varphi\\ &\quad = \pi i(1-y)\int_0^{r_0} d\xi \int_0^{y} d\eta\ \chi(\xi,\eta).\end{aligned} \tag{5.0.5}$$

Thus, formula (5.0.4) for $\widehat{\mathbf{I}}_2$can be modified as

$$\begin{aligned}\frac{1}{2\pi i}\,\widehat{\mathbf{I}}_2 = &\frac{1}{2\pi i}\lim_{\delta_n\to 0}\int_0^{r_0} d\xi \int_0^{y} d\eta\ \chi(\xi,\eta) \int\!\!\!\!\!\!\diagup_{\ell_n} dk\ e^{ik(x-\eta t-\xi)}\ \frac{\sinh(k(1-y))\cosh(k\eta)}{k\ \sinh(k)}\\ &-\frac{(1-y)}{2}\int_0^{r_0} d\xi \int_0^{y} d\eta\ \chi(\xi,\eta),\end{aligned} \tag{5.0.6}$$

which yields formula (5.0.2).

Using the definition of principle value integral [46, 47], we represent the integral for $\widehat{\mathbf{I}}_4$ of (4.1.16) in the form

$$\begin{aligned}\widehat{\mathbf{I}}_4 = &-\lim_{\delta_n\to 0}\int_0^{r_0} d\xi \int_y^{1} d\eta\ \chi(\xi,\eta) \int\!\!\!\!\!\!\diagup_{\ell_n} dk\ e^{ik(x-\eta t-\xi)}\ \frac{\sinh(ky)\cosh(k(1-\eta))}{k\ \sinh(k)}\\ &+\lim_{\delta_n\to 0}\int_0^{r_0} d\xi \int_y^{1} d\eta\ \chi(\xi,\eta) \int\!\!\!\!\!\!\diagup_{\gamma_n} dk\ e^{ik(x-\eta t-\xi)}\ \frac{\sinh(ky)\cosh(k(1-\eta))}{k\ \sinh(k)}.\end{aligned} \tag{5.0.7}$$

Evaluating the integral involving γ_n, we obtain for small $|k|$ the following result:

$$\lim_{\delta_n\to 0}\int_0^{r_0} d\xi \int_y^1 d\eta\, \chi(\xi,\eta) \int_{-\pi}^0 \frac{\left[ky+\mathcal{O}(y^3k^3)\right]\left[1+\mathcal{O}((1-\eta)^2k^2)\right]}{k+\mathcal{O}(k^3)}\, i\, d\varphi = \pi i y \int_0^{r_0} d\xi \int_y^1 d\eta\, \chi(\xi,\eta). \tag{5.0.8}$$

which yields (5.0.3).

The lemma is shown. ■

Theorem 5.2. *Let $\mathfrak{S}(x,y,t)$ be defined as*

$$\mathfrak{S}(x,y,t) = \; -2\pi i \int_0^{r_0} d\xi \int_0^1 d\eta\; \chi(\xi,\eta)\, \frac{x-\eta t-\xi}{|x-\eta t-\xi|} \sum_{m=1}^{\infty} e^{-\pi m|x-\eta t-\xi|} \frac{\sin(\pi m y)\cos(\pi m\eta)}{\pi m}. \tag{5.0.9}$$

For $x \geq r_0$ the following representation is valid for the sum $(\widehat{\mathbf{I}}_2+\widehat{\mathbf{I}}_4)$:

(a) When $t \geq \frac{x}{y}$, then

$$\widehat{\mathbf{I}}_2+\widehat{\mathbf{I}}_4 = \mathfrak{S}(x,y,t) + 2\pi i\,(1-y)\int_0^{r_0} d\xi \int_0^{\frac{x-\xi}{t}} d\eta\; \chi(\xi,\eta) - \\ \pi i\,(1-y)\int_0^{r_0} d\xi \int_0^{y} d\eta\; \chi(\xi,\eta) \; + \pi i\, y \int_0^{r_0} d\xi \int_y^1 d\eta\; \chi(\xi,\eta).$$

(b) When $\frac{x}{y} > t \geq \frac{(x-r_0)}{y}$, then

$$\widehat{\mathbf{I}}_2+\widehat{\mathbf{I}}_4 = \mathfrak{S}(x,y,t) - 2\pi i\, y \int_0^{R} d\xi \int_y^{\frac{x-\xi}{t}} d\eta\; \chi(\xi,\eta) + \\ 2\pi i\,(1-y)\int_0^{R} d\xi \int_0^{y} d\eta\; \chi(\xi,\eta) + 2\pi i\,(1-y)\int_R^{r_0} d\xi \int_0^{\frac{x-\xi}{t}} d\eta\; \chi(\xi,\eta) + \\ \pi i\, y \int_0^{r_0} d\xi \int_y^1 d\eta\; \chi(\xi,\eta) + \pi i\,(1-y)\int_0^{r_0} d\xi \int_0^{y} d\eta\; \chi(\xi,\eta), \qquad R = x-yt.$$

(c) When $\frac{(x-r_0)}{y} > t \geq (x - r_0)$*, then*

$$\widehat{\mathbf{I}}_2 + \widehat{\mathbf{I}}_4 = \mathfrak{S}(x, y, t) - 2\pi i\ y \int_0^V d\xi \int_y^1 d\eta\ \chi(\xi, \eta) + \pi i\ (1 - y) \int_0^{r_0} d\xi \int_0^y d\eta\ \chi(\xi, \eta) -$$
$$2\pi i\ y \int_V^{r_0} d\xi \int_y^{\frac{x-\xi}{t}} d\eta\ \chi(\xi, \eta) + \pi i\ y \int_0^{r_0} d\xi \int_y^1 d\eta\ \chi(\xi, \eta), \qquad V = x - t.$$

Proof. To prove the result we consider three different time intervals, that we call Cases A, B, and C (see the beginning of the proof of Theorem 4.3).

Case A. We start with evaluation of the integrals $\widehat{\mathbf{I}}_2$ and $\widehat{\mathbf{I}}_4$ for $t = \frac{x}{y}$. To evaluate the integral along ℓ_n, we notice that the line BCD splits the domain of integration into two subdomains (Fig. 4.1), which results in the following decomposition:

$$\frac{1}{2\pi i}\,\widehat{\mathbf{I}}_2 = \frac{1}{2\pi i}\ \lim_{n\to\infty} \int_0^{r_0} d\xi \int_0^{\frac{x-\xi}{t}} d\eta\ \chi(\xi, \eta) \int_{\ell_n} dk\ e^{ik(x-\eta t-\xi)}\ \frac{\sinh(k(1-y))\cosh(k\eta)}{k\ \sinh(k)}$$
$$+\ \frac{1}{2\pi i}\ \lim_{n\to\infty} \int_0^{r_0} d\xi \int_{\frac{x-\xi}{t}}^{y} d\eta\ \chi(\xi, \eta) \int_{\ell_n} dk\ e^{ik(x-\eta t-\xi)}\ \frac{\sinh(k(1-y))\cosh(k\eta)}{k\ \sinh(k)}$$
$$-\ \frac{(1-y)}{2} \int_0^{r_0} d\xi \int_0^y d\eta\ \chi(\xi, \eta). \tag{5.0.10}$$

We will evaluate the first two integrals in (5.0.10), which are the triple integrals. Therefore, for the first integral in (5.0.10), we have $x - \eta t - \xi > 0$. Therefore, this integral can be evaluated as a limit of a sequence of contour integrals, with each contour being closed in the upper half-plane. For each ℓ_n, we obtain that

$$\frac{1}{2\pi i} \int_0^{r_0} d\xi \int_0^{\frac{x-\xi}{t}} d\eta\ \chi(\xi, \eta) \int_{\ell_n} dk\ e^{ik(x-\eta t-\xi)}\ \frac{\sinh(k(1-y))\cosh(k\eta)}{k\ \sinh(k)}$$
$$= \lim_{N\to\infty} \int_0^{r_0} d\xi \int_0^{\frac{x-\xi}{t}} d\eta\ \chi(\xi, \eta) \sum_{m=0}^{N} \operatorname{Res}\left\{ e^{ik(x-\eta t-\xi)}\ \frac{\sinh(k(1-y))\cosh(k\eta)}{k\ \sinh(k)},\ \pi m i \right\}$$
$$= -\int_0^{r_0} d\xi \int_0^{\frac{x-\xi}{t}} d\eta\ \chi(\xi, \eta) \sum_{m=1}^{\infty} e^{-\pi m(x-\eta t-\xi)}\ \frac{\sin(\pi m y)\cos(\pi m \eta)}{\pi m}$$
$$+ (1 - y) \int_0^{r_0} d\xi \int_0^{\frac{x-\xi}{t}} d\eta\ \chi(\xi, \eta). \tag{5.0.11}$$

Evaluating the second triple integral from (5.0.10), where $x-\eta t-\xi<0$, we can use a sequence of contours closed in the lower half-plane. Taking into account the direction on the contour ℓ_n, we get

$$\begin{aligned}
&\frac{1}{2\pi i}\int_0^{r_0} d\xi \int_{\frac{x-\xi}{t}}^{y} d\eta\ \chi(\xi,\eta)\ \oint_{\ell_n} dk\ e^{ik(x-\eta t-\xi)}\ \frac{\sinh(k(1-y))\cosh(k\eta)}{k\ \sinh(k)}\\
&\quad=-\lim_{N\to\infty}\int_0^{r_0} d\xi \int_{\frac{x-\xi}{t}}^{y} d\eta\ \chi(\xi,\eta)\sum_{m=1}^{N}\ \mathrm{Res}\left\{ e^{ik(x-\eta t-\xi)}\ \frac{\sinh(k(1-y))\cosh(k\eta)}{k\ \sinh(k)},\ -\pi m i\right\}\\
&\quad=-\lim_{N\to\infty}\int_0^{r_0} d\xi \int_{\frac{x-\xi}{t}}^{y} d\eta\ \chi(\xi,\eta)\sum_{m=1}^{N}\ e^{-\pi m|x-\eta t-\xi|}\ \frac{\sin(\pi m(1-y))\cos(\pi m\eta)}{\pi m\ \cos(\pi m)}\\
&\quad=\int_0^{r_0} d\xi \int_{\frac{x-\xi}{t}}^{y} d\eta\ \chi(\xi,\eta)\sum_{m=1}^{\infty}\ e^{-\pi m|x-\eta t-\xi|}\ \frac{\sin(\pi m y)\cos(\pi m\eta)}{\pi m}. \qquad (5.0.12)
\end{aligned}$$

Substituting (5.0.11) and (5.0.12) into (5.0.10) and using Lemma 5.1, we obtain

$$\begin{aligned}
\frac{1}{2\pi i}\,\widehat{\mathbf{I}}_2 &= (1-y)\int_0^{r_0} d\xi \int_0^{\frac{x-\xi}{t}} d\eta\ \chi(\xi,\eta)\\
&\quad-\int_0^{r_0} d\xi \int_0^{y} d\eta\ \chi(\xi,\eta)\ \frac{x-\eta t-\xi}{|x-\eta t-\xi|}\ \sum_{m=1}^{\infty}\ e^{-\pi m|x-\eta t-\xi|}\ \frac{\sin(\pi m y)\cos(\pi m\eta)}{\pi m}\\
&\quad-\frac{(1-y)}{2}\int_0^{r_0} d\xi \int_0^{y} d\eta\ \chi(\xi,\eta). \qquad (5.0.13)
\end{aligned}$$

To evaluate the integral $\widehat{\mathbf{I}}_4$, we notice that the domain of integration corresponds to the case $x-\eta t-\xi<0$. Therefore, we can use a sequence of contours closed in the lower half-plane and have (see (5.0.7)) and evaluate this integral as a corresponding limit

$$\begin{aligned}
&\frac{1}{2\pi i}\ \lim_{\delta_n\to 0}\int_0^{r_0} d\xi \int_{y}^{1} d\eta\ \chi(\xi,\eta)\ \oint_{\ell_n} dk\ e^{ik(x-\eta t-\xi)}\ \frac{\sinh(ky)\cosh(k(1-\eta))}{k\ \sinh(k)}\\
&\quad=-\int_0^{r_0} d\xi \int_{y}^{1} d\eta\ \chi(\xi,\eta)\sum_{m=1}^{\infty}\ \mathrm{Res}\left\{ e^{ik(x-\eta t-\xi)}\ \frac{\sinh(ky)\cosh(k(1-\eta))}{k\ \sinh(k)},\ -\pi m i\right\}\\
&\quad=-\int_0^{r_0} d\xi \int_{y}^{1} d\eta\ \chi(\xi,\eta)\sum_{m=1}^{\infty} e^{-\pi m|x-\eta t-\xi|}\ \frac{\sin(\pi m y)\cos(\pi m\eta)}{\pi m}. \qquad (5.0.14)
\end{aligned}$$

Combining formulas (5.0.3) and (5.0.14) we obtain,

$$\begin{aligned}\frac{1}{2\pi i}\,\widehat{\mathbf{I}}_4 = &-\int_0^{r_0} d\xi \int_y^1 d\eta\ \chi(\xi,\eta) \sum_{m=1}^{\infty} e^{-\pi m|x-\eta t-\xi|}\ \frac{\sin(\pi m y)\cos(\pi m\eta)}{\pi m} \\ &+\ \frac{y}{2}\int_0^{r_0} d\xi \int_y^1 d\eta\ \chi(\xi,\eta) \\ =&-\int_0^{r_0} d\xi \int_y^1 d\eta\ \chi(\xi,\eta)\ \frac{x-\eta t-\xi}{|x-\eta t-\xi|}\ \sum_{m=1}^{\infty} e^{-\pi m|x-\eta t-\xi|}\ \frac{\sin(\pi m y)\cos(\pi m\eta)}{\pi m} \\ &+\ \frac{y}{2}\int_0^{r_0} d\xi \int_y^1 d\eta\ \chi(\xi,\eta). \end{aligned} \tag{5.0.15}$$

Summing (5.0.13) and (5.0.15) yields

$$\begin{aligned}\widehat{\mathbf{I}}_2+\widehat{\mathbf{I}}_4 = &\ 2\pi i\,(1-y)\int_0^{r_0} d\xi \int_0^{\frac{x-\xi}{t}} d\eta\ \chi(\xi,\eta)\ -\pi i(1-y)\int_0^{r_0} d\xi \int_0^{y} d\eta\ \chi(\xi,\eta) \\ &+\pi i\ y\int_0^{r_0} d\xi \int_y^1 d\eta\ \chi(\xi,\eta) \\ &-2\pi i\int_0^{r_0} d\xi \int_0^1 d\eta\ \chi(\xi,\eta)\ \frac{x-\eta t-\xi}{|x-\eta t-\xi|}\ \sum_{m=1}^{\infty} e^{-\pi m|x-\eta t-\xi|}\ \frac{\sin(\pi m y)\cos(\pi m\eta)}{\pi m}. \end{aligned} \tag{5.0.16}$$

On the next step we show that formula (5.0.16) is valid for any moment of time t such that $t > \frac{x}{y}$. Let BKL (the dashed line on Fig. 4.5) be the straight line $x-\eta t-\xi$ corresponding to such t. The point of intersection of BKL with the η-axis has the coordinates ($\xi = \frac{x}{t}, \eta = 0$). As one can see from Fig. 4.5, the domain of integration of $\widehat{\mathbf{I}}_2$ consists of two trapezoidal subdomains, $AKL0$ and $KEDL$. To evaluate the integral on the subdomains $AKL0$, we consider a sequence of expanding

contours closed in the upper half-plane. After passing to the limit we arrive at the following result:

$$\begin{aligned}
&\frac{1}{2\pi i}\int_0^{r_0} d\xi \int_0^{\frac{x-\xi}{t}} d\eta\ \chi(\xi,\eta)\ \text{P.V.}\int_{-\infty}^{\infty} dk\ e^{ik(x-\eta t-\xi)}\ \frac{\sinh(k(1-y))\cosh(k\eta)}{k\ \sinh(k)} \\
&\qquad = \int_0^{r_0} d\xi \int_0^{\frac{x-\xi}{t}} d\eta\ \chi(\xi,\eta) \sum_{m=0}^{\infty} \text{Res}\left\{ e^{ik(x-\eta t-\xi)}\ \frac{\sinh(k(1-y))\cosh(k\eta)}{k\ \sinh(k)},\ \pi m i \right\} \\
&\qquad = -\int_0^{r_0} d\xi \int_0^{\frac{x-\xi}{t}} d\eta\ \chi(\xi,\eta)\ \sum_{m=1}^{\infty} e^{-\pi m(x-\eta t-\xi)}\ \frac{\sin(\pi m y)\cos(\pi m\eta)}{\pi m} \\
&\qquad\quad + (1-y)\int_0^{r_0} d\xi \int_0^{\frac{x-\xi}{t}} d\eta\ \chi(\xi,\eta). \qquad (5.0.17)
\end{aligned}$$

We notice that this result coincides with (5.0.11).

To evaluate the integral on the subdomain $KEDL$, we consider a sequence of expanding contours closed in the lower half-plane. After passing to the limit, we arrive at the following result:

$$\begin{aligned}
&\frac{1}{2\pi i}\int_0^{r_0} d\xi \int_{\frac{x-\xi}{t}}^{y} d\eta\ \chi(\xi,\eta)\ \text{P.V.}\int_{-\infty}^{\infty} dk\ e^{ik(x-\eta t-\xi)}\ \frac{\sinh(k(1-y))\cosh(k\eta)}{k\ \sinh(k)} \\
&\qquad = -\int_0^{r_0} d\xi \int_{\frac{x-\xi}{t}}^{y} d\eta\ \chi(\xi,\eta) \sum_{m=0}^{\infty} \text{Res}\left\{ e^{ik(x-\eta t-\xi)}\ \frac{\sinh(k(1-y))\cosh(k\eta)}{k\ \sinh(k)},\ -\pi m i \right\} \\
&\qquad = \int_0^{r_0} d\xi \int_{\frac{x-\xi}{t}}^{y} d\eta\ \chi(\xi,\eta)\ \sum_{m=1}^{\infty} e^{\pi m(x-\eta t-\xi)}\ \frac{\sin(\pi m y)\cos(\pi m\eta)}{\pi m}. \qquad (5.0.18)
\end{aligned}$$

This result coincides with (5.0.12). Summing equations (5.0.17) and (5.0.18) and using Lemma 5.1, we obtain

$$\begin{aligned}
\frac{1}{2\pi i}\,\widehat{\mathbf{I}}_2 = &-\int_0^{r_0} d\xi \int_0^{y} d\eta\ \chi(\xi,\eta)\ \frac{x-\eta t-\xi}{|x-\eta t-\xi|}\ \sum_{m=1}^{\infty} e^{-\pi m|x-\eta t-\xi|}\ \frac{\sin(\pi m y)\cos(\pi m\eta)}{\pi m} \\
&+ (1-y)\int_0^{r_0} d\xi \int_0^{\frac{x-\xi}{t}} d\eta\ \chi(\xi,\eta)\ -\ \frac{(1-y)}{2}\int_0^{r_0} d\xi \int_0^{y} d\eta\ \chi(\xi,\eta). \qquad (5.0.19)
\end{aligned}$$

To evaluate $\widehat{\mathbf{I}}_4$, we notice that the entire domain is located above the line $x-\eta t-\xi=0$. Thus, we

consider a sequence of closed contours in the lower half-plane, pass to the limit and get

$$
\begin{aligned}
-\frac{1}{2\pi i}\int_0^{r_0} d\xi \int_y^1 d\eta\ \chi(\xi,\eta)\ \text{P.V.}\int_{-\infty}^{\infty} dk\ e^{ik(x-\eta t-\xi)}\ \frac{\sinh(ky)\cosh(k(1-\eta))}{k\ \sinh(k)} \\
= \int_0^{r_0} d\xi \int_y^1 d\eta\ \chi(\xi,\eta) \sum_{m=1}^{\infty} \text{Res}\left\{ e^{ik(x-\eta t-\xi)}\ \frac{\sinh(ky)\cosh(k(1-\eta))}{k\ \sinh(k)},\ -\pi m i \right\} \\
= \int_0^{r_0} d\xi \int_y^1 d\eta\ \chi(\xi,\eta)\ \sum_{m=1}^{\infty} e^{\pi m(x-\eta t-\xi)}\ \frac{\sin(\pi m y)\cos(\pi m\eta)}{\pi m}. \qquad (5.0.20)
\end{aligned}
$$

Therefore, using (5.0.20) and Lemma 5.1, we obtain

$$
\begin{aligned}
\widehat{\mathbf{I}}_4 = -2\pi i \int_0^{r_0} d\xi \int_y^1 d\eta\ \chi(\xi,\eta)\ \frac{x-\eta t-\xi}{|x-\eta t-\xi|} \sum_{m=1}^{\infty} e^{-\pi m|x-\eta t-\xi|}\ \frac{\sin(\pi m y)\cos(\pi m\eta)}{\pi m} \\
+ \pi i\ y \int_0^{r_0} d\xi \int_y^1 d\eta\ \chi(\xi,\eta). \qquad (5.0.21)
\end{aligned}
$$

This formula is essentially the same as (5.0.15).

Summing equations (5.0.19) and (5.0.21) together yields the result

$$
\begin{aligned}
\widehat{\mathbf{I}}_2 + \widehat{\mathbf{I}}_4 = -2\pi i \int_0^{r_0} d\xi \int_0^1 d\eta\ \chi(\xi,\eta)\ \frac{x-\eta t-\xi}{|x-\eta t-\xi|} \sum_{m=1}^{\infty} e^{-\pi m|x-\eta t-\xi|}\ \frac{\sin(\pi m y)\cos(\pi m\eta)}{\pi m} \\
+ 2\pi i\ (1-y) \int_0^{r_0} d\xi \int_0^{\frac{x-\xi}{t}} d\eta\ \chi(\xi,\eta)\ -\ \pi i(1-y) \int_0^{r_0} d\xi \int_0^{y} d\eta\ \chi(\xi,\eta) \\
+ \pi i\ y \int_0^{r_0} d\xi \int_y^1 d\eta\ \chi(\xi,\eta). \qquad (5.0.22)
\end{aligned}
$$

We notice that formulas (5.0.16) and (5.0.22) coincide. Case A is shown.

Case B. Let us evaluate the integrals for $\widehat{\mathbf{I}}_2$ and $\widehat{\mathbf{I}}_4$ for the time moment $t = \frac{(x-r_0)}{y}$. A straight line $x - \eta t - \xi = 0$ passes through the points B and E with the coordinates $(\xi = r_0, \eta = y)$ (see Fig. 4.6).

To evaluate $\widehat{\mathbf{I}}_2$, we notice that the domain of integration corresponds to the case $x - \eta t - \xi > 0$. Therefore, the integral along ℓ_n can be evaluated as a limit of a sequence of contour integrals, with

each contour being closed in the upper half-plane using Lemma 5.1. We have

$$\begin{aligned}\frac{1}{2\pi i}\,\widehat{\mathbf{I}}_2 &= \frac{1}{2\pi i}\,\lim_{\delta_n\to 0}\int_0^{r_0} d\xi \int_0^{y} d\eta\ \chi(\xi,\eta)\ \oint_{\ell_n} dk\ e^{ik(x-\eta t-\xi)}\ \frac{\sinh(k(1-y))\cosh(k\eta)}{k\ \sinh(k)} \\ &\quad - \frac{(1-y)}{2}\int_0^{r_0} d\xi \int_0^{y} d\eta\ \chi(\xi,\eta) \\ &= (1-y)\int_0^{r_0} d\xi \int_0^{y} d\eta\ \chi(\xi,\eta) - \frac{(1-y)}{2}\int_0^{r_0} d\xi \int_0^{y} d\eta\ \chi(\xi,\eta) \\ &\quad - \int_0^{r_0} d\xi \int_0^{y} d\eta\ \chi(\xi,\eta)\ \frac{x-\eta t-\xi}{|x-\eta t-\xi|}\ \sum_{m=1}^{\infty} e^{-\pi m|x-\eta t-\xi|}\ \frac{\sin(\pi m y)\cos(\pi m\eta)}{\pi m},\end{aligned}$$

which yields

$$\begin{aligned}\frac{1}{2\pi i}\,\widehat{\mathbf{I}}_2 = \ & \frac{(1-y)}{2}\int_0^{r_0} d\xi \int_0^{y} d\eta\ \chi(\xi,\eta) \\ & - \int_0^{r_0} d\xi \int_0^{y} d\eta\ \chi(\xi,\eta)\ \frac{x-\eta t-\xi}{|x-\eta t-\xi|}\ \sum_{m=1}^{\infty} e^{-\pi m|x-\eta t-\xi|}\ \frac{\sin(\pi m y)\cos(\pi m\eta)}{\pi m}. \quad (5.0.23)\end{aligned}$$

To evaluate $\widehat{\mathbf{I}}_4$ we consider two different subdomains: the trapezoidal subdomains $EDJF$ and the triangular subdomain EGF, which yields the decomposition

$$\begin{aligned}\frac{1}{2\pi i}\,\widehat{\mathbf{I}}_4 = \ & -\frac{1}{2\pi i}\,\lim_{\delta_n\to 0}\int_0^{r_0} d\xi \int_y^{\frac{x-\xi}{t}} d\eta\ \chi(\xi,\eta)\ \oint_{\ell_n} dk\ e^{ik(x-\eta t-\xi)}\ \frac{\sinh(ky)\cosh(k(1-\eta))}{k\ \sinh(k)} \\ & - \frac{1}{2\pi i}\,\lim_{\delta_n\to 0}\int_0^{r_0} d\xi \int_{\frac{x-\xi}{t}}^{1} d\eta\ \chi(\xi,\eta)\ \oint_{\ell_n} dk\ e^{ik(x-\eta t-\xi)}\ \frac{\sinh(ky)\cosh(k(1-\eta))}{k\ \sinh(k)} \\ & + \frac{y}{2}\int_0^{r_0} d\xi \int_y^{1} d\eta\ \chi(\xi,\eta). \quad (5.0.24)\end{aligned}$$

To evaluate the first integral of (5.0.24), we notice that $x-\eta t-\xi > 0$. We consider a sequence of

contours closed in the upper half-plane and get after passing to a limit

$$\int_0^{r_0} d\xi \int_y^{\frac{x-\xi}{t}} d\eta\ \chi(\xi,\eta)\ \sum_{m=0}^{\infty} \mathrm{Res}\left\{ e^{ik(x-\eta t-\xi)}\ \frac{\sinh(ky)\cosh(k(1-\eta))}{k\ \sinh(k)},\ \pi i m \right\}$$
$$= \int_0^{r_0} d\xi \int_y^{\frac{x-\xi}{t}} d\eta\ \chi(\xi,\eta)\ \sum_{m=1}^{\infty} e^{-\pi m|x-\eta t-\xi|}\ \frac{\sin(\pi m y)\cos(\pi m\eta)}{\pi m}$$
$$+\ y \int_0^{r_0} d\xi \int_y^{\frac{x-\xi}{t}} d\eta\ \chi(\xi,\eta). \tag{5.0.25}$$

To evaluate the second integral of (5.0.24) we notice that $x-\eta t-\xi<0$. We consider a sequence of contours closed in the lower half-plane and get after passing to a limit

$$-\int_0^{r_0} d\xi \int_{\frac{x-\xi}{t}}^1 d\eta\ \chi(\xi,\eta)\ \sum_{m=0}^{\infty} \mathrm{Res}\left\{ e^{ik(x-\eta t-\xi)}\ \frac{\sinh(ky)\cosh(k(1-\eta))}{k\ \sinh(k)},\ -\pi i m \right\}$$
$$= -\int_0^{r_0} d\xi \int_{\frac{x-\xi}{t}}^1 d\eta\ \chi(\xi,\eta)\ \sum_{m=1}^{\infty} e^{\pi m(x-\eta t-\xi)}\ \frac{\sin(\pi m y)\cos(\pi m\eta)}{\pi m}$$
$$= \int_0^{r_0} d\xi \int_{\frac{x-\xi}{t}}^1 d\eta\ \chi(\xi,\eta)\ \frac{x-\eta t-\xi}{|x-\eta t-\xi|}\ \sum_{m=1}^{\infty} e^{-\pi m|x-\eta t-\xi|}\ \frac{\sin(\pi m y)\cos(\pi m\eta)}{\pi m}. \tag{5.0.26}$$

Combining (5.0.25) and (5.0.26) yields,

$$\int_0^{r_0} d\xi \int_y^1 d\eta\ \chi(\xi,\eta)\ \frac{x-\eta t-\xi}{|x-\eta t-\xi|}\ \sum_{m=1}^{\infty} e^{-\pi m|x-\eta t-\xi|}\ \frac{\sin(\pi m y)\cos(\pi m\eta)}{\pi m}$$
$$+\ y \int_0^{r_0} d\xi \int_y^{\frac{x-\xi}{t}} d\eta\ \chi(\xi,\eta). \tag{5.0.27}$$

Taking into account (5.0.3), we have

$$\frac{1}{2\pi i}\,\widehat{\mathbf{I}}_4 = -\int_0^{r_0} d\xi \int_y^1 d\eta\ \chi(\xi,\eta)\ \frac{x-\eta t-\xi}{|x-\eta t-\xi|}\ \sum_{m=1}^{\infty} e^{-\pi m|x-\eta t-\xi|}\ \frac{\sin(\pi m y)\cos(\pi m\eta)}{\pi m}$$
$$-\ y \int_0^{r_0} d\xi \int_y^{\frac{x-\xi}{t}} d\eta\ \chi(\xi,\eta) + \frac{y}{2} \int_0^{r_0} d\xi \int_y^1 d\eta\ \chi(\xi,\eta). \tag{5.0.28}$$

Combining together (5.0.23) and (5.0.28), we obtain

$$\begin{aligned}\widehat{\mathbf{I}}_2+\widehat{\mathbf{I}}_4 = & -2\pi i\int_0^{r_0} d\xi\int_0^1 d\eta\ \chi(\xi,\eta)\ \frac{x-\eta t-\xi}{|x-\eta t-\xi|}\ \sum_{m=1}^{\infty} e^{-\pi m|x-\eta t-\xi|}\ \frac{\sin(\pi m y)\cos(\pi m\eta)}{\pi m}\\ & -2\pi i\ y\int_0^{r_0} d\xi\int_y^{\frac{x-\xi}{t}} d\eta\ \chi(\xi,\eta)+\pi i\ y\int_0^{r_0} d\xi\int_y^1 d\eta\ \chi(\xi,\eta)\\ & +\pi i\ (1-y)\int_0^{r_0} d\xi\int_0^y d\eta\ \chi(\xi,\eta). \end{aligned} \tag{5.0.29}$$

On the next step, we derive the formula for $(\widehat{\mathbf{I}}_2+\widehat{\mathbf{I}}_4)$ for any moment of time t such that $\frac{x}{y} > t \geq \frac{(x-r_0)}{y}$ and show that the afore formula (see (5.0.38) below) coincides with (5.0.38) when $t=\frac{(x-r_0)}{y}$. Let BMP (the dashed line on Fig. 4.6) be the straight line $x-\eta t-\xi=0$ corresponding to such t, i.e. located between BCD and BEF.

As one can see from Fig. 4.6, the domain of integration for $\widehat{\mathbf{I}}_2$ can be is broken into three subdomains: a rectangular subdomain $0RDN$, a trapezoidal subdomain $RAMN$, and a triangular subdomain MEN. For both subdomains, $0RND$ and $RAMN$, the contours of integration for $\widehat{\mathbf{I}}_2$ can be closed in the upper half-plane. Thus evaluating $\widehat{\mathbf{I}}_2$ over $0RND$ yields,

$$\begin{aligned}\frac{1}{2\pi i}\int_0^R d\xi\int_0^y d\eta\ \chi(\xi,\eta)\ \text{P.V.}\int_{-\infty}^{\infty} dk\ e^{ik(x-\eta t-\xi)}\ \frac{\sinh(k(1-y))\cosh(k\eta)}{k\ \sinh(k)}\\ =-\int_0^R d\xi\int_0^y d\eta\ \chi(\xi,\eta)\ \sum_{m=1}^{\infty} e^{-\pi m(x-\eta t-\xi)}\ \frac{\sin(\pi m y)\cos(\pi m\eta)}{\pi m}\\ +(1-y)\int_0^R d\xi\int_0^y d\eta\ \chi(\xi,\eta). \end{aligned} \tag{5.0.30}$$

Evaluating $\widehat{\mathbf{I}}_2$ over the subdomain $RAMN$ yields

$$\begin{aligned}\frac{1}{2\pi i}\int_R^{r_0} d\xi\int_0^{\frac{x-\xi}{t}} d\eta\ \chi(\xi,\eta)\ \text{P.V.}\int_{-\infty}^{\infty} dk\ e^{ik(x-\eta t-\xi)}\ \frac{\sinh(k(1-y))\cosh(k\eta)}{k\ \sinh(k)}\\ =-\int_R^{r_0} d\xi\int_0^{\frac{x-\xi}{t}} d\eta\ \chi(\xi,\eta)\ \sum_{m=1}^{\infty} e^{-\pi m(x-\eta t-\xi)}\ \frac{\sin(\pi m y)\cos(\pi m\eta)}{\pi m}\\ +(1-y)\int_R^{r_0} d\xi\int_0^{\frac{x-\xi}{t}} d\eta\ \chi(\xi,\eta). \end{aligned} \tag{5.0.31}$$

Evaluating $\widehat{\mathbf{I}}_2$ over the subdomain MEN and closing the corresponding contours of integration downward yields

$$\frac{1}{2\pi i}\int_R^{r_0} d\xi \int_{\frac{x-\xi}{t}}^{y} d\eta\ \chi(\xi,\eta)\ \text{P.V.}\int_{-\infty}^{\infty} dk\ e^{ik(x-\eta t-\xi)}\ \frac{\sinh(k(1-y))\cosh(k\eta)}{k\ \sinh(k)}$$
$$= -\int_R^{r_0} d\xi \int_{\frac{x-\xi}{t}}^{y} d\eta\ \chi(\xi,\eta)\ \sum_{m=1}^{\infty} e^{\pi m(x-\eta t-\xi)}\ \frac{\sin(\pi m y)\cos(\pi m\eta)}{\pi m}. \tag{5.0.32}$$

Summing equations (5.0.30) – (5.0.32) and using Lemma 5.1, we find

$$\widehat{\mathbf{I}}_2 = -2\pi i \int_0^{r_0} d\xi \int_0^{y} d\eta\ \chi(\xi,\eta)\ \frac{x-\eta t-\xi}{|x-\eta t-\eta|}\ \sum_{m=1}^{\infty} e^{-\pi m|x-\eta t-\xi|}\ \frac{\sin(\pi m y)\cos(\pi m\eta)}{\pi m}$$
$$+ 2\pi i\ (1-y)\int_0^{R} d\xi \int_0^{y} d\eta\ \chi(\xi,\eta) + 2\pi i\ (1-y)\int_R^{r_0} d\xi \int_0^{\frac{x-\xi}{t}} d\eta\ \chi(\xi,\eta)$$
$$- \pi i\ (1-y)\int_0^{r_0} d\xi \int_0^{y} d\eta\ \chi(\xi,\eta). \tag{5.0.33}$$

Before we move to evaluation of $\widehat{\mathbf{I}}_4$, let us check that formula (5.0.33) is consistent with the previous results for $\widehat{\mathbf{I}}_2$. Namely, let t change in such a way that the straight line BMP moves towards the line BCD. In this case, $R \to 0$ and formula (5.0.33) becomes:

$$\mathfrak{S}(x,y,t) + 2\pi i\ (1-y)\int_0^{r_0} d\xi \int_0^{\frac{x-\xi}{t}} d\eta\ \chi(\xi,\eta) - \pi i\ (1-y)\int_0^{r_0} d\xi \int_0^{y} \chi(\xi,\eta)$$

which coincides with formula (5.0.23).

Now we turn to evaluation of $\widehat{\mathbf{I}}_4$ and notice that (see Fig. 4.6) the domain of integration can be broken into three subdomains: a rectangular subdomain $NEGT$, a trapezoidal subdomain $NTJP$, and a triangular subdomain NPD. For the triangular subdomain, the approximating contours of integration can be closed upward and for the remaining two subdomains the contours of integration

can be closed downward. For the triangular subdomain NPD we obtain the result

$$
\begin{aligned}
-\frac{1}{2\pi i}\int_0^N d\xi \int_y^{\frac{x-\xi}{t}} d\eta\ \chi(\xi,\eta)\ \text{P.V.}\int_{-\infty}^{\infty} dk\ e^{ik(x-\eta t-\xi)}\ \frac{\sinh(ky)\cosh(k(1-\eta))}{k\ \sinh(k)} \\
= -\int_0^N d\xi \int_y^{\frac{x-\xi}{t}} d\eta\ \chi(\xi,\eta)\ \sum_{m=1}^{\infty} e^{-\pi m(x-\eta t-\xi)}\ \frac{\sin(\pi m y)\cos(\pi m\eta)}{\pi m} \\
- y\int_0^N d\xi \int_y^{\frac{x-\xi}{t}} d\eta\ \chi(\xi,\eta). \qquad (5.0.34)
\end{aligned}
$$

For the trapezoidal subdomain $NTHP$ we find

$$
\begin{aligned}
-\frac{1}{2\pi i}\int_0^N d\xi \int_{\frac{x-\xi}{t}}^1 d\eta\ \chi(\xi,\eta)\ \text{P.V.}\int_{-\infty}^{\infty} dk\ e^{ik(x-\eta t-\xi)}\ \frac{\sinh(ky)\cosh(k(1-\eta))}{k\ \sinh(k)} \\
= \int_0^N d\xi \int_{\frac{x-\xi}{t}}^1 d\eta\ \chi(\xi,\eta)\ \sum_{m=1}^{\infty} e^{-\pi m|x-\eta t-\xi|}\ \frac{\sin(\pi m y)\cos(\pi m\eta)}{\pi m}. \qquad (5.0.35)
\end{aligned}
$$

For the rectangular subdomain $NEGT$ we find

$$
\begin{aligned}
-\frac{1}{2\pi i}\int_N^{r_0} d\xi \int_y^1 d\eta\ \chi(\xi,\eta)\ \text{P.V.}\int_{-\infty}^{\infty} dk\ e^{ik(x-\eta t-\xi)}\ \frac{\sinh(ky)\cosh(k(1-\eta))}{k\ \sinh(k)} \\
= \int_N^{r_0} d\xi \int_y^1 d\eta\ \chi(\xi,\eta)\ \sum_{m=1}^{\infty} e^{-\pi m|x-\eta t-\xi|}\ \frac{\sin(\pi m y)\cos(\pi m\eta)}{\pi m}. \qquad (5.0.36)
\end{aligned}
$$

Therefore, summing equations (5.0.34) – (5.0.36) together and using Lemma 5.1 yields the following result:

$$
\begin{aligned}
\widehat{\mathbf{I}}_4 = -2\pi i\int_0^{r_0} d\xi \int_y^1 d\eta\ \chi(\xi,\eta)\ \frac{x-\eta t-\xi}{|x-\eta t-\xi|}\ \sum_{m=1}^{\infty} e^{-\pi m|x-\eta t-\xi|}\ \frac{\sin(\pi m y)\cos(\pi m\eta)}{\pi m} \\
-2\pi i\ y\int_0^R d\xi \int_y^{\frac{x-\xi}{t}} d\eta\ \chi(\xi,\eta) + \pi i y\int_0^{r_0} d\xi \int_y^1 d\eta\ \chi(\xi,\eta). \qquad (5.0.37)
\end{aligned}
$$

Now we verify that formula (5.0.37) is consistent with the previous results obtained for $\widehat{\mathbf{I}}_4$. Let t change in such a way that the straight line BMP moves towards the line BCD. In this case, $R \to 0$ and formula (5.0.37) coincides with formula (5.0.16). Let t change in such a way that the straight

line BMP moves towards the line BEF. In this case, $R \to r_0$, and formula (5.0.37) coincides with formula (5.0.28).

Lastly, summing equations (5.0.33) and (5.0.37) together yields the result:

$$\begin{aligned}\widehat{\mathbf{I}}_2 + \widehat{\mathbf{I}}_4 = &-2\pi i \int_0^{r_0} d\xi \int_0^1 d\eta\ \chi(\xi,\eta)\ \frac{x-\eta t-\xi}{|x-\eta t-\xi|} \sum_{m=1}^{\infty} e^{-\pi m|x-\eta t-\xi|} \frac{\sin(\pi m y)\cos(\pi m\eta)}{\pi m} \\ &+ 2\pi i\,(1-y) \int_0^R d\xi \int_0^y d\eta\ \chi(\xi,\eta) + 2\pi i\,(1-y) \int_R^{r_0} d\xi \int_0^{\frac{x-\xi}{t}} d\eta\ \chi(\xi,\eta) \\ &- \pi i\,(1-y) \int_0^{r_0} d\xi \int_0^y d\eta\ \chi(\xi,\eta) - 2\pi i\ y \int_0^R d\xi \int_y^{\frac{x-\xi}{t}} d\eta\ \chi(\xi,\eta) \\ &+ \pi i\ y \int_0^{r_0} d\xi \int_y^1 d\eta\ \chi(\xi,\eta). \end{aligned} \tag{5.0.38}$$

One can see that the value of R corresponds to the value of the ξ-coordinate at the point of intersection of the straight lines $x-\eta t-\xi = 0$ and $\eta = y$, i.e. $R = x - yt$. Case B is shown.

Remark 5.3. One can check that when check that when $t = \frac{x}{y}$, then $R = 0$ and formula (5.0.38) coincides with formula (a) of Theorem 5.2. When $t = \frac{(x-r_0)}{y}$, then $R = r_0$ and formula (5.0.38) coincides with formula (c) of Theorem 5.2.

Case C. Let us evaluate the integrals $\widehat{\mathbf{I}}_2$ and $\widehat{\mathbf{I}}_4$ for the time moment $t = x - r_0$. The domains of integration for both $\widehat{\mathbf{I}}_2$ and $\widehat{\mathbf{I}}_4$ are located below the straight line $x-\eta t-\xi = 0$. Therefore, for both integrals the approximating contours of integration can be closed in the upper half-plane (see Fig. 4.7). Evaluating $\widehat{\mathbf{I}}_2$ yields

$$\begin{aligned}\frac{1}{2\pi i}\,\widehat{\mathbf{I}}_2 = &\int_0^{r_0} d\xi \int_0^y d\eta\ \chi(\xi,\eta) \sum_{m=0}^{\infty} \operatorname{Res}\left\{ e^{ik(x-\eta t-\xi)}\ \frac{\sinh(k(1-y))\cosh(k\eta)}{k\ \sinh(k)},\ i\pi m \right\} \\ &- \frac{(1-y)}{2} \int_0^{r_0} d\xi \int_0^y d\eta\ \chi(\xi,\eta) \\ = &\ \frac{(1-y)}{2} \int_0^{r_0} d\xi \int_0^y d\eta\ \chi(\xi,\eta) \\ &- \int_0^{r_0} d\xi \int_0^y d\eta\ \chi(\xi,\eta) \sum_{m=1}^{\infty} e^{-\pi m(x-\eta t-\xi)}\ \frac{\sin(\pi m y)\cos(\pi m\eta)}{\pi m}. \end{aligned} \tag{5.0.39}$$

Evaluating $\widehat{\mathbf{I}}_4$ yields,

$$\begin{aligned}\frac{1}{2\pi i}\,\widehat{\mathbf{I}}_4 = &-\int_0^{r_0} d\xi \int_y^1 d\eta\ \chi(\xi,\eta)\ \sum_{m=0}^{\infty}\ \text{Res}\left\{ e^{ik(x-\eta t-\xi)}\ \frac{\sinh(ky)\cosh(k(1-\eta))}{k\ \sinh(k)},\ i\pi m\right\}\\ &+\ \frac{y}{2}\int_0^{r_0} d\xi \int_y^1 d\eta\ \chi(\xi,\eta)\\ =&-\int_0^{r_0} d\xi \int_y^1 d\eta\ \chi(\xi,\eta)\ \sum_{m=1}^{\infty} e^{-\pi m(x-\eta t-\xi)}\ \frac{\sin(\pi m y)\cos(\pi m\eta)}{\pi m}\\ &-\frac{y}{2}\int_0^{r_0} d\xi \int_y^1 d\eta\ \chi(\xi,\eta).\end{aligned} \tag{5.0.40}$$

Collecting (5.0.39) and (5.0.40), we obtain the following result:

$$\begin{aligned}\widehat{\mathbf{I}}_2+\widehat{\mathbf{I}}_4 = \pi i\ (1-y)\int_0^{r_0} d\xi \int_0^{y} d\eta\ \chi(\xi,\eta)\ -\pi i\ y\int_0^{r_0} d\xi \int_y^{1} d\eta\ \chi(\xi,\eta)\\ -2\pi i\int_0^{r_0} d\xi \int_0^{1} d\eta\ \chi(\xi,\eta)\ \frac{x-\eta t-\xi}{|x-\eta t-\xi|}\ \sum_{m=1}^{\infty} e^{-\pi m|x-\eta t-\xi|}\ \frac{\sin(\pi m y)\cos(\pi m\eta)}{\pi m}.\end{aligned} \tag{5.0.41}$$

On the next step we derive the formula for $(\widehat{\mathbf{I}}_2+\widehat{\mathbf{I}}_4)$ for any moment of time t such that $\frac{(x-r_0)}{y} > t \geq x-r_0$. We show that formula (5.0.41) is a particular case of the general formula (5.0.46) derived below. Let BQS (the dashed line on Fig. 4.7) be the straight line $x-\eta t-\xi=0$ located between BEF and BGH. As one can see (Fig. 4.7), the domain of integration for $\widehat{\mathbf{I}}_2$ is positioned entirely below the line $x-\eta t-\xi=0$. Therefore the result for $\widehat{\mathbf{I}}_2$ coincides with (5.0.23).

The domain of integration for $\widehat{\mathbf{I}}_4$ can be split into three subdomains: a rectangular subdomain $VSJD$, a trapezoidal subdomain $EQSV$, and a triangular subdomain QGS. For the subdomains $VSJD$ and $EQSV$, the approximating contours of integration can be closed upward while for the subdomain, QGS the contours of integration can be closed downward. Evaluating $\widehat{\mathbf{I}}_4$ over the

subdomain $VSJD$, we obtain

$$
\begin{aligned}
&-\frac{1}{2\pi i}\int_0^V d\xi \int_y^1 d\eta\ \chi(\xi,\eta)\ \text{P.V.}\int_{-\infty}^{\infty} dk\ e^{ik(x-\eta t-\xi)}\ \frac{\sinh(ky)\cosh(k(1-\eta))}{k\ \sinh(k)}\\
&\quad=-\int_0^V d\xi \int_y^1 d\eta\ \chi(\xi,\eta)\ \sum_{m=1}^{\infty} e^{-\pi m(x-\eta t-\xi)}\ \frac{\sin(\pi m y)\cos(\pi m\eta)}{\pi m}\\
&\qquad- y\int_0^V d\xi \int_y^1 d\eta\ \chi(\xi,\eta).
\end{aligned}
\tag{5.0.42}
$$

Evaluating $\widehat{\mathbf{I}}_4$ over the subdomain $EQSV$, we obtain

$$
\begin{aligned}
&-\frac{1}{2\pi i}\int_V^{r_0} d\xi \int_y^{\frac{x-\xi}{t}} d\eta\ \chi(\xi,\eta)\ \text{P.V.}\int_{-\infty}^{\infty} dk\ e^{ik(x-\eta t-\xi)}\ \frac{\sinh(ky)\cosh(k(1-\eta))}{k\ \sinh(k)}\\
&\quad=-\int_V^{r_0} d\xi \int_y^{\frac{x-\xi}{t}} d\eta\ \chi(\xi,\eta)\ \sum_{m=1}^{\infty} e^{-\pi m|x-\eta t-\xi|}\ \frac{\sin(\pi m y)\cos(\pi m\eta)}{\pi m}\\
&\qquad- y\int_V^{r_0} d\xi \int_y^{\frac{x-\xi}{t}} d\eta\ \chi(\xi,\eta).
\end{aligned}
\tag{5.0.43}
$$

Evaluating $\widehat{\mathbf{I}}_4$ over the subdomain QGS, we obtain

$$
\begin{aligned}
&-\frac{1}{2\pi i}\int_V^{r_0} d\xi \int_{\frac{x-\xi}{t}}^1 d\eta\ \chi(\xi,\eta)\ \text{P.V.}\int_{-\infty}^{\infty} dk\ e^{ik(x-\eta t-\xi)}\ \frac{\sinh(ky)\cosh(k(1-\eta))}{k\ \sinh(k)}\\
&\qquad=\int_V^{r_0} d\xi \int_{\frac{x-\xi}{t}}^1 d\eta\ \chi(\xi,\eta)\ \sum_{m=1}^{\infty} e^{-\pi m|x-\eta t-\xi|}\ \frac{\sin(\pi m y)\cos(\pi m\eta)}{\pi m}.
\end{aligned}
\tag{5.0.44}
$$

Summing equations (5.0.42) – (5.0.44) and using Lemma 5.1 yield

$$
\begin{aligned}
\widehat{\mathbf{I}}_4 =&-2\pi i\int_0^{r_0} d\xi \int_y^1 d\eta\ \chi(\xi,\eta)\ \frac{x-\eta t-\xi}{|x-\eta t-\xi|}\ \sum_{m=1}^{\infty} e^{-\pi m|x-\eta t-\xi|}\ \frac{\sin(\pi m y)\cos(\pi m\eta)}{\pi m}\\
&-2\pi i\ y\int_0^V d\xi \int_y^1 d\eta\ \chi(\xi,\eta)-2\pi i\ y\int_V^{r_0} d\xi \int_y^{\frac{x-\xi}{t}} d\eta\ \chi(\xi,\eta)\\
&+\pi i\ y\int_0^{r_0} d\xi \int_y^1 d\eta\ \chi(\xi,\eta).
\end{aligned}
\tag{5.0.45}
$$

Lastly, summing equations (5.0.23) and (5.0.45) together yields the result

$$\widehat{\mathbf{I}}_2 + \widehat{\mathbf{I}}_4 = \mathfrak{S}(x, y, t) + i\pi\,(1-y)\int_0^{r_0} d\xi \int_0^{y} d\eta\ \chi(\xi,\eta) - 2\pi i\ y \int_0^{V} d\xi \int_y^{1} d\eta\ \chi(\xi,\eta)$$
$$- 2\pi i\ y \int_V^{r_0} d\xi \int_y^{\frac{x-\xi}{t}} d\eta\ \chi(\xi,\eta) + \pi i\ y \int_0^{r_0} d\xi \int_y^{1} d\eta\ \chi(\xi,\eta). \tag{5.0.46}$$

The value of V is defined as the ξ-coordinate of the point of intersection of the straight lines $x - \eta t - \xi = 0$ and $\eta = 1$, i.e. $V = x - t$. Case C is shown.

The proof of Theorem 5.2 is complete. ■

CHAPTER 6

SUMMARY

The present dissertation is devoted to the problem of stability of the fluid flow moving in a channel with flexible walls and interacting with the walls. The walls of the vessel are subject to traveling waves. Experimental data shows that the energy of the flowing fluid can be transferred and consumed by the structure (the walls), inducing traveling wave flutter. The problem of stability of fluid-structure interaction splits into two parts:

(1) stability of fluid flow in the channel with harmonically moving walls and

(2) stability of solid structure participating in the energy exchange with the flow. Stability of fluid flow, the main focus of the research, is obtained by solving the initial boundary value problem for the *stream function*. The main findings of this research are the following (i) – (iv):

(i) rigorous formulation of the initial boundary problem for the stream function, $\psi(x, y, t)$, induced by the fluid-structure interaction model, which takes into account the axisymmetric pattern of the flow and the "no-slip" condition near the channel walls;

(ii) application of a double integral transformation (the Fourier transformation and Laplace transformation) to both the equation and boundary and initial conditions, which reduces the original IBVP involving a partial differential equation to an IBVP involving a parameter dependent ordinary differential equation;

(iii) derivation of the *explicit* formula for the Fourier transform of the stream function, $\widetilde{\psi}(k, y, t)$;

(iv) evaluation of the inverse Fourier transform of $\widetilde{\psi}(k, y, t)$ and proving that reconstruction of $\psi(x, y, t)$ can be obtained through a limiting process in the complex k-plane, which allows us to

use the Residue theorem and represent the solution in the form of an infinite series of residues. The main result of this research is an analytical solution of a mathematical model describing blood flowing through a channel with flexible walls that are being perturbed in the form of a traveling wave.

In Chapter 1 we formulate the initial boundary value problem describing the dynamics of pressure perturbation in the horizontal channel. The upper boundary condition reflects an assumption on the axial symmetry of the unperturbed problem with respect to the centerline of the channel (see equation (1.2.9)). We consider general behavior of the channel walls and use the equation that relates the vertical component of the flow velocity and the velocity of the points of a solid boundary of the channel (see equation (1.2.4)). We emphasize that we do not impose any restrictions on the function describing the elevation of the boundary, which means that equation (1.2.4) can be used to analyze non-harmonic movement of the channel wall. In the present work, we assume that the channel is a horizontal tube with the following properties of the walls reflecting the physical origin of the model. There exists a large positive number R ($R \gg 1$) such that within the symmetric interval $(-R, R)$ the wall is flexible and the lower boundary moves "almost harmonically" in accordance with the law:

$$g(x,t) = C_0\, e^{i\omega(x-ct)}, \quad \omega > 0, \quad x \in [-R, R],$$

where ω is the wave number and c is the speed of the wave crest propagation; $g(x,t)$ denotes the transverse displacement of the channel wall at location x and moment in time t; C_0 is a small positive constant. We also assume that (i) there exists a small positive number, r : $r \ll R$, and r is such that outside the interval $[-R-r, R+r]$, the wall is rigid, i.e. the vertical displacement on $\mathbb{R}\backslash[-R-r, R+r]$ is zero; and (ii) there exists a smooth function, $g_0(x)$, that governs the transition of displacement $g(x,t)$ to zero, i.e. we set

$$g(x,t) = g_0(x)e^{i\omega(x-ct)}, \quad |g_0(x)| \ll 1, \ \ \omega > 0, \quad -R-r \le x \le R+r, \ \ r \ll 1,$$

with $\text{supp}\{g_0(x)\} \in [-R-r, R+r]$ and $g_0(x) = g_0(0) = C_0$ for $x \in [-R, R]$ (see Fig. 0.5 above).

We present the IBVP given by (1.2.10) – (1.2.13) for the stream function $\psi(x, y, t)$, in which the harmonic behavior of the wall is addressed. If one knows the stream function, then the components of the velocity vector can be reconstructed (see formulas (1.1.3) above).

In Chapter 2, we modified the IBVP given by (1.2.10) – (1.2.13) and reduce it to a more tractable form. First, we apply the Fourier transformation to the equation and the boundary and initial conditions. As the result, we obtain an equation in which the partial derivatives, with respect to the x-variable, are replaced with polynomials with respect to the Fourier transform parameter, k (see equation (2.0.11)). Second, we apply the Laplace transformation with respect to the time variable, t. The second integral transformation allows us to take into account the explicit expression for the unperturbed flow velocity profile, $U(y)$. After incorporating $U(y)$, we reduce IBVP (1.2.10) – (1.2.13) to the new formulation (2.1.2) – (2.1.5). The main equation (2.1.2) is an ordinary differential equation with respect to the variable y parametrically depending on the complex parameter k (the result of the Fourier transformation). This equation has time-dependent right-hand side and non-homogeneous boundary conditions. We conclude this section by deriving the boundary problem for the stationary solution (2.1.9). With the help of the stationary solution we reduce IBVP to the problem with homogeneous boundary conditions (2.1.13) – (2.1.15). Finally, we use the Green's function for the problem with homogeneous boundary conditions and present a closed-form expression for the Fourier transform of the stream function denoted by $\widetilde{\psi}(k, y, t)$ (see formula (2.2.8)).

To examine the behavior of the stream function as a function of variable x, we have to evaluate the inverse Fourier transform of (2.2.8). Chapter 3 – 5 present our technical results. The Fourier transform of the stream function, $\widetilde{\psi}(k, y, t)$, is represented as a sum of three terms. The inverse Fourier transform, which is the stream function ψ itself, also contains three terms denoted by I_1, I_2, and I_3 (see formulae (3.0.2) – (3.0.4)). The main results of the paper are Theorem 3.6, Theorem 4.3, and Theorem 5.2. These theorems provide the desired representation for the stream function as a function of time and space. To obtain such representations one has to split $\widetilde{\psi}(k, y, t)$ into several

terms and prove that each term, containing the improper integral with respect to k can be extended into the complex k-plane and evaluated by using the Residue theorem. The series representing the solution converge at exponential rates. It means that one can take only several terms from each series and attain the desired level of accuracy, which is important for practical applications.

Based on already obtained results, one can proceed with the research in the following directions. As our solution represents the fluid flow influenced by the boundary dynamics, the problem of flexible wall deformation still remains open, i.e. finding the solution of the problem describing displacement of flexible wall structure as the result of fluid flow pressure perturbation. The second direction is to compare the analytical solution to previous numerical research of this model. An advantage of our results is that the infinite functional series can be truncated to a finite number of terms without compromising the accuracy of the solution. This is due to the exponential decay of the individual terms as the number of a term tends to infinity.

The next step of this research is to generate a numerical scheme corresponding to the analytically derived solution. Then, the second part of this research, regarding the stability of the channel wall structure as it participates in the energy exchange with the fluid flow, still remains open. This research problem would be concerning the pressure imposed on the channel wall as it undergoes perturbations in the form of a traveling wave. This problem could be addresses as strictly a fluid-structure interaction, or by analyzing this question as an immersed boundary problem.

Additionally, there are natural extensions and variations such as modifying boundary conditions to represent varying blood vessels and plaque build up, introducing foreign bodies within the blood vessel to obstruct fluid flow, and removing symmetry assumptions to encompass Neumann and Neumann-Dirichlet boundary conditions. To further validate findings, generating a numerical model of the analytical solution can allow for adaptions to the model.

From current findings, one interesting direction would be to weaken the channel wall's membrane causing the wall to rupture or bulge. This could lead to understanding the formation of a brain aneurysm or hypotension, or from an industrial viewpoint, the weakening of a pipeline's wall. This research has potential to connect to the physics of micro-fluids and drug delivery.

Another area of interest are the impacts and flow dynamics of micro-plastics and flow of stiff bodies in impacting micro-filtration.

6.1 Summary of technical tools

The goal of this research is to derive the analytical closed form solution of a biologically motivated fluid-structure interaction problem. We begin by formulating our system of equations to represent the symmetries and assumptions within our model. By utilizing the definition of a stream function, our system of equations can be written as a single partial differential equation with corresponding boundary and initial conditions. Having the stream function allows us to obtain the vertical and horizontal components of the velocity vector. Then, using the Navier-Stokes equations, we are able to find the analytical representation of the pressure distribution.

For derivation of the boundary conditions, symmetry of the geometry of our model is leveraged. The flow is symmetric with respect to the centerline of the channel and it obeys the "no-slip" condition which means that the velocity of the wall is the same as the velocity to the fluid near the wall. Thus, there is no relative movement between the wall and the near wall fluid.

We use the Laplace transform with respect to t and the Fourier transform with respect to x to reformulate the IBVP. The advantage of the respective transforms is the ability to write the partial differential equation as an ordinary differential equation with respect to y, parametrically depending on the complex argument k. This generates the IBVP (2.0.11) – (2.0.14), which remains the focus for the dissertation.

By using the stationary solution, we reduce the IBVP to the system with homogeneous boundary conditions. From this moment, we take advantage of the explicit Green's function to solve the system of equations. The last remaining transform is to apply the *inverse Fourier transform* to the stream function $\widetilde{\psi}(k, y, t)$. Reconstruction of the stream function, $\psi(x, y, t)$, from its Fourier transform is the most challenging technical step in the research as $\widetilde{\psi}(k, y, t)$ is represented as the sum

$$\widetilde{\psi}(k, y, t) = \widetilde{I}_1(k, y, t) + \widetilde{I}_2(k, y, t) + \widetilde{I}_3(k, y, t),$$

requiring the inversion of each $\widetilde{I}_n,\ n = 1, 2, 3$ term.

The evaluation of the afore integrals are split as follows: (i) the evaluation of $\widetilde{I}_1(k, y, t)$, and (ii) the evaluation of the sum $\widetilde{I}_2(k, y, t) + \widetilde{I}_3(k, y, t)$. The evaluation begins with (a) splitting the function $\sin(\xi(k-\omega))$ into two exponentials and prove that each of the resulting integrals (denoted by $\mathcal{I}$ and $\widetilde{\mathcal{I}}$ respectively) converges in the sense of the *principle value*; (b) each integral, $\mathcal{I}$ and $\widetilde{\mathcal{I}}$, can be approximated by the sequence of closed contour integrals in the complex k-plane; (c) using the Residue theorem, each closed contour integral can be evaluated and represented as a finite sum of residues.

In the conclusion, we represent the main formulas derived in the paper. We recall from (1.1.3) that $v(x, y, t) = -\psi_x(x, y, t)$. As follows from (3.0.1), (4.1.1),

$$i\psi_x(x, y, t) = I_1 + I_2 + I_3 \qquad \psi_x(x, y, t) \equiv -iI_1 + \frac{i}{2\pi}(\mathbb{I}_2 + \mathbb{I}_3). \tag{6.1.1}$$

For the second term in (6.1.1), from (4.1.6) – (4.1.8), and (4.1.12), we find

$$\frac{i}{2\pi}(\mathbb{I}_2 + \mathbb{I}_3) = -\frac{i}{2\pi}\int_{-\infty}^{\infty} dk\ k\ e^{ikx}e^{-ikyt}\ \widetilde{f}(x, y) - \frac{it^2}{2\pi}(\widehat{\mathbf{I}}_1 + \widehat{\mathbf{I}}_3) + \frac{t}{\pi}(\widehat{\mathbf{I}}_2 + \widehat{\mathbf{I}}_4). \tag{6.1.2}$$

Let $\mathbf{I}^*_{(2k)} = \frac{t}{\pi}\widehat{\mathbf{I}}_{2k}$ and $\mathbf{I}^*_{(2k-1)} = -\frac{it^2}{2\pi}\widehat{\mathbf{I}}_{(2k-1)}$ for $k = 1, 2$ and from (5.0.9), $\mathfrak{S}^*(x, y, t) = \frac{t}{\pi}\mathfrak{S}(x, y, t)$. Therefore we can conclude for $x \geq r_0$ that

$$\begin{aligned}\psi_x(x, y, t) = i\omega c\ e^{i\omega(x-ct)}\ g_0(R)\ \frac{\sinh(\omega(1-y))}{\sinh(\omega)} + 2\omega c\ e^{-i\omega ct}\ \sum_{m=1}^{\infty}\frac{\sin\pi my}{\pi^2m^2+\omega^2}\times\\ \int_R^{R+r} d\xi\ g_0'(\xi)\ e^{-\pi m\xi}\left[\pi m\ \cosh(i\pi mx + i\xi\omega) + \omega\ \sinh(\pi mx + i\xi\omega)\right]\\ -\frac{i}{2\pi}\int_{-\infty}^{\infty} dk\ k\ e^{ikx}e^{-ikyt}\ \widetilde{f}(x, y) + (\mathbf{I}^*_1 + \mathbf{I}^*_3) + (\mathbf{I}^*_2 + \mathbf{I}^*_4),\end{aligned} \tag{6.1.3}$$

where for all t:

$$\mathbf{I}^*_1 + \mathbf{I}^*_3 = -it^2\int_0^{r_0} d\xi\int_0^1 d\eta\ \chi(\xi, \eta)\ \sum_{m=1}^{\infty} e^{-\pi m|x-\eta t-\xi|}\ \frac{\sin(\pi my)\ \sin(\pi m\eta)}{\pi m}$$

and when $t \geq \frac{x}{y}$, then

$$\mathbf{I}_2^* + \mathbf{I}_4^* = \mathfrak{S}^*(x,y,t) + 2it\,(1-y)\int_0^{r_0} d\xi \int_0^{\frac{x-\xi}{t}} d\eta\ \chi(\xi,\eta) - \\ it\,(1-y)\int_0^{r_0} d\xi \int_0^{y} d\eta\ \chi(\xi,\eta)\ + it\,y\int_0^{r_0} d\xi \int_y^{1} d\eta\ \chi(\xi,\eta);$$

when $\frac{x}{y} > t \geq \frac{x-r_0}{y}$, then

$$\mathbf{I}_2^* + \mathbf{I}_4^* = \mathfrak{S}^*(x,y,t) - 2it\,y\int_0^{R} d\xi \int_y^{\frac{x-\xi}{t}} d\eta\ \chi(\xi,\eta) + \\ 2it\,(1-y)\int_0^{R} d\xi \int_0^{y} d\eta\ \chi(\xi,\eta) + 2it\,(1-y)\int_R^{r_0} d\xi \int_0^{\frac{x-\xi}{t}} d\eta\ \chi(\xi,\eta) + \\ it\,y\int_0^{r_0} d\xi \int_y^{1} d\eta\ \chi(\xi,\eta) + it\,(1-y)\int_0^{r_0} d\xi \int_0^{y} d\eta\ \chi(\xi,\eta), \qquad R = x - yt;$$

and lastly when $\frac{(x-r_0)}{y} > t \geq (x - r_0)$, then

$$\mathbf{I}_2^* + \mathbf{I}_4^* = \mathfrak{S}^*(x,y,t) - 2it\,y\int_0^{V} d\xi \int_y^{1} d\eta\ \chi(\xi,\eta) + it\,(1-y)\int_0^{r_0} d\xi \int_0^{y} d\eta\ \chi(\xi,\eta) - \\ 2it\,y\int_V^{r_0} d\xi \int_y^{\frac{x-\xi}{t}} d\eta\ \chi(\xi,\eta) + it\,y\int_0^{r_0} d\xi \int_y^{1} d\eta\ \chi(\xi,\eta), \qquad V = x - t.$$

The analytical solution, ψ_x represents the velocity component, $v(x,y,t)$, of the fluid flowing through a channel with flexible walls being perturbed by a traveling wave.

LIST OF REFERENCES

[1] P.W. Carpenter and A.D. Garrad. The hydrodynamic stability of flow over Kramer-type compliant surfaces. Part 2. Flow-induced surface instabilities. *J. Fluid Mech.*, 170:199–232, 1986.

[2] M. Heil and O.E. Jensen. Flows in deformable tubes and channels. In *Ann. R. Coll. Surg. Engl.*, volume 75, pages 15–49. 2003.

[3] P.G. Larose and J.B. Grotberg. Flutter and long-wave instabilities in compliant channels conveying developing flows. *J. Fluid Mech.*, 331:37–58, 1997.

[4] J. P. Armitstead, C.D. Bertram, and Oliver E. Jensen. A study of the bifurcation behaviour of a model of flow through a collapsible tube. *Bull. Math. Biol.*, 58(4):611–641, jul 1996.

[5] L. Huang. Reversal of the Bernoulli effect and channel flutter. *J. Fluids Struct.*, 12(2):131–151, 1998.

[6] T. Aittokallio, M. Gyllenberg, and O. Polo. A model of a snorer's upper airway. *Turku Cent. Comput. Sci. Tech. Rep.*, (266), 1999.

[7] Y. Aurégan and C. Depollier. Snoring: linear stability analysis and in-vitro experiments. *J. Sound Vib.*, 188(1):39–53, 1995.

[8] R. Beck, M. Odeh, A. Oliven, and N. Gavriely. The acoustic properties of snores. *Eur. Respir. J.*, 8(12):2120–2128, 1995.

[9] J.B. Grotberg and N. Gavriely. Flutter in collapsible tubes: a theoretical model of wheezes. *J. Appl. Physiol.*, 66(5):2262–2273, 1989.

[10] Z.S. Liu, X.Y. Luo, H.P. Lee, and C. Lu. Snoring source identification and snoring noise prediction. *J. Biomech.*, 40(4):861–870, 2007.

[11] D. Pevernagie, R.M. Aarts, and M. De Meyer. The acoustics of snoring. *Sleep Med. Rev.*, 14(2):131–144, 2010.

[12] J. Wang, G.A. Tetlow, and A.D. Lucey. Flow-structure interaction in the upper airway: Motions of a cantilevered flexible plate in channel flow with flexible walls. *Proc. 16th Australas. Fluid Mech. Conf.*, (January):342–345, 2007.

[13] R.J. Whittaker, M. Heil, O.E. Jensen, and S. L. Waters. Predicting the onset of high-frequency self-excited oscillations in elastic-walled tubes. *Proc. R. Soc. A Math. Phys. Eng. Sci.*, 466(2124):3635–3657, 2010.

[14] K.N. Karagiozis, M.P. Païdoussis, M. Amabili, and A.K. Misra. Nonlinear stability of cylindrical shells subjected to axial flow: Theory and experiments. *J. Sound Vib.*, 309(3-5):637–676, 2008.

[15] M.P. Païdoussis and J.P. Denise. Flutter of thin cylindrical shells conveying fluid. *J. Sound Vib.*, 20(1):9–26, 1972.

[16] M.P. Païdoussis and T.P. Luu. Dynamics of a pipe aspirating fluid such as might be used in ocean mining. *J. Energy Resour. Technol.*, 107(2):250–255, 1985.

[17] M.P. Païdoussis. Some unresolved issues in fluid-structure interactions. *J. Fluids Struct.*, 20(6):871–890, 2005.

[18] C.D. Bertram. Unstable equilibrium behaviour in collapsible tubes. *J. Biomech.*, 19(1):61–69, 1986.

[19] C.D. Bertram. The effects of wall thickness, axial strain and end proximity on the pressure-area relation of collapsible tubes. *J. Biomech.*, 20(9):863–876, 1987.

[20] C.D. Bertram, C.J. Raymond, and T.J. Pedley. Mapping of instabilities for flow through collapsed tubes of differing length. *J. Fluids Struct.*, 4(2):125–153, 1990.

[21] C. Cancelli and T.J. Pedley. A separated-flow model for collapsible-tube oscillations. *J. Fluid Mech.*, 157:375–404, 1985.

[22] O.E. Jensen and T.J. Pedley. The existence of steady flow in a collapsed tube. *J. Fluid Mech.*, 206:339–374, 1989.

[23] V. Kumaran. Stability of the flow of a fluid through a flexible tube at intermediate Reynolds number. *J. Fluid Mech.*, 357:123–140, 1998.

[24] C.D. Bertram. Flow-induced oscillation of collapsed tubes and airway structures. *Respir. Physiol. Neurobiol.*, 163(1-3):256–265, 2008.

[25] P.D.M. Ellis, J.E.F. Williams, and J.M. Shneerson. Surgical relief of snoring due to palatal flutter: a preliminary report. *Ann. R. Coll. Surg. Engl.*, 75(4):286–90, 1993.

[26] O.E. Jensen and M. Heil. High-frequency self-excited oscillations in a collapsible-channel flow. *J. Fluid Mech.*, 481(481):235–268, 2003.

[27] L. Huang and J.E.F. Williams. Neuromechanical interaction in human snoring and upper airway obstruction. *J. Appl. Physiol.*, 86(6):1759–1763, 1999.

[28] P.S. Stewart, S.L. Waters, and O.E. Jensen. Local and global instabilities of flow in a flexible-walled channel. *Eur. J. Mech. - B/Fluids*, 28(4):541–557, 2009.

[29] K.M. Case. Stability of inviscid plane Couette flow. *Phys. Fluids*, 3(2):143–148, 1960.

[30] K.M. Case. Hydrodynamic stability and the initial-value problems. *Proc. Symp. Appl. Math.*, 13:25–33, 1962.

[31] B.K. Shivamoggi. Stability of inviscid plane couette flow. *Acta Mech.*, 44(3-4):327–329, 1982.

[32] P. Krindel and A. Silberberg. Flow through gel-walled tubes. *J. Colloid Interface Sci.*, 71(1):39–50, 1979.

[33] V. Kumaran. Stability of inviscid flow in a flexible tube. *J. Fluid Mech.*, 320:1–17, 1996.

[34] P.G. Drazin and W.H. Reid. *Hydrodynamic Stability*, volume 124. Cambridge University Press, Cambridge, 1981.

[35] M.P. Païdoussis and G.X. Li. Pipes conveying fluid: a model dynamical problem. *J. Fluids Struct.*, 7(2):137–204, 1993.

[36] H. Ashley and G. Haviland. Bending vibrations of a pipeline containing flowing fluid. *J. Appl. Mech.*, 17:229–232, 1950.

[37] M. Amabili, F. Pellicano, and M.P. Païdoussis. Non-linear dynamics and stability of circular cylindrical shells conveying flowing fluid. *J. Sound Vib.*, 225(4):655–699, 1999.

[38] M.P. Païdoussis, C. Semler, and M. Wadham-Gagnon. A reappraisal of why aspirating pipes do not flutter at infinitesimal flow. *J. Fluids Struct.*, 20(1):147–156, 2005.

[39] M.P. Païdoussis. Aspirating pipes do not flutter at infinitesimally small flow. *J. Fluids Struct.*, 13(3):419–425, 1999.

[40] K. Bach, H. Hetzler, and W. Seemann. Stability of a steady flow guided by flexible walls. *PAMM*, 10(1):353–354, 2010.

[41] K. Bach, H. Hetzler, and W. Seemann. On stability and self-excited vibrations in fluid-structure-interaction. *PAMM*, 11(1):309–310, 2011.

[42] K. Bach, H. Hetzler, and W. Seemann. Oscillations of a channel with a flexible wall conveying viscous flow. *PAMM*, 12(1):245–246, 2012.

[43] J.W. Miles. On the generation of surface waves by shear flows. *J. Fluid Mech.*, 3(02):185–204, 1957.

[44] L. Huang. Viscous flutter of a finite elastic membrane in Poiseuille Flow. *J. Fluids Struct.*, 15(7):1061–1088, 2001.

[45] G.F. Roach. *Green's Functions*. Cambridge Univ. Press, Cambridge, 2nd edition, 1995.

[46] I. Stakgold. *Green's Functions and Boundary Value Problems*. John Wiley & Sons, Inc., Hoboken, NJ, USA, 2011.

[47] A. Jeffrey. *Complex Analysis and Applications*. Chapman and Hall/CRC, Boca Raton, London, 2nd edition, 2006.

[48] E.B. Saff and A.D. Snyder. *Fundamentals of Complex Analysis with Applications to Engineering and Science*. Pearson Hall, Upper Saddle River, NJ, USA, 3rd edition, 2003.

APPENDIX A

INITIAL DERIVATIONS

A.1 Stream function

Recall that $u_x(x, y, t) + v_y(x, y, t) = 0$.

(i). Let

$$\psi(x, y, t) = \int_{y_0}^{y} u(x, \eta, t)\, d\eta - \int_{x_0}^{x} v(\xi, y_0, t)\, d\xi.$$

Then by assumption, let $\psi_y(x, y, t) = u(x, y, t)$. Therefore

$$\begin{aligned}
\psi_x(, x, y, t) &= \frac{\partial}{\partial x}\Big(\int_{y_0}^{y} u_x(x, \eta, t)\, dt - v(x, y_0, t) \Big) \\
&= (-v_\eta(x, \eta, t))\, d\eta - v(x, y_0, t) \\
&= -v(x, y, t) + v(x, y_0, t) - v(, x, y_0, t) \\
\psi_x(x, y, t) &= -v(x, y, t).
\end{aligned}$$

(ii). Let

$$\psi(x, y, t) = \int_{y_0}^{y} u(x_0, y, t)\, d\eta - \int_{x_0}^{x} v(\xi, y, t)\, d\xi.$$

Then by assumption, let $\psi_x(x, y, t) = -v(x, y, t)$.

$$\begin{aligned}
\psi_y(x, y, t) &= \frac{\partial}{\partial y}\Big(\int_{y_0}^{y} u(x_0, \eta, t)\, d\eta - \int_{x_0}^{x} v(\xi, ymt)\, d\xi \\
&= u(x_0, y, t) - \int_{x_0}^{x} v_y(\xi, y, t)\, d\xi \\
&= u(x_0, y, t,) + \int_{x_0}^{x} u_{\xi}(\xi, y, t)\, d\xi \\
&= u(x_0, y, t) + u(x, y, t) - u(x_0, y, t) \\
\psi_y(x, y, t) &= u(x, y, t).
\end{aligned}$$

Therefore we conclude that $\psi_x(x, y, t) = -v(x, y, t)$ and $\psi_y(x, y, t) = u(x, y, t)$.

A.2 Derivation of Normal and Unit Tangent Vectors

Let ν be the unit tangent vector and $\mathbf{n}$ be the unit normal vector the point $(x, g(x, t))$ on the wall. Specifically, let ν be at point (ν_1, ν_2), where $\nu_2 = \nu_1 g_x(x, t)$ and $\mathbf{n}$ be at the point (n_1, n_2). Two conditions exist,

(1) by orthogonality: $n_1\nu_1 + n_2\nu_2 = 0$

(2) by normalization: $n_1^2 + n_2^2 = 1$.

Solving for a_1 in condition (2),

$$n_1 = -\frac{n_2\nu_2}{\nu_1}.$$

We then substitute the above expression for a_1 into conditions (1) and solve for n_2,

$$\begin{aligned}\Big(-\frac{n_2\nu_2}{\nu_1}\Big)^2 + n_2^2 &= 1\\ n_2^2\Big(1+\frac{\nu_2^2}{\nu_1^2}\Big) &= 1\\ \frac{1}{\sqrt{1+\big(\frac{\nu_2^2}{\nu_1^2}\big)}} &= n_2.\end{aligned}$$

To construct ν, we recall the unit tangent vector equation

$$\begin{aligned}\nu &= \frac{\frac{\partial}{\partial x}(\nu_1,\nu_2)}{\Big\|\frac{\partial}{\partial x}(\nu_1,\nu_2)\Big\|}\\ \nu &= \frac{\frac{\partial}{\partial x}\big(x,\ g(x,t)\big)}{\Big\|\frac{\partial}{\partial x}\big(x,\ g(x,t)\big)\Big\|}\\ &= \frac{1,\ g_x(x,t)}{\sqrt{1+g_x(x,t)}}.\end{aligned}$$

To construct $\mathbf{n}$,

$$\begin{aligned}\mathbf{n} &= (n_1,n_2)\\ &= \left(-n_2\frac{\nu_2}{\nu_1}, \frac{1}{\sqrt{1+\big(\frac{\nu_2^2}{\nu_1^2}\big)}}\right)\\ &= \frac{1}{\sqrt{1+\big(\frac{\nu_1^2 g_x^2(x,t)}{\nu_1^2}\big)}}\Big(-\frac{\nu_1 g_x(x,t)}{\nu_1}, 1\Big)\\ &= \frac{1}{\sqrt{1+g_x^2(x,t)}}\big(-g_x(x,t),1\big).\end{aligned}$$

APPENDIX B

TRANSFORM METHODS

For convenience, the notation of the Fourier and Laplace transforms defined in (2.0.1) – (2.0.3) is restated:

A Fourier transform, $\widetilde{f}(k)$, of a function $f(x)$, is define by

$$\widetilde{f}(k) = \int_{-\infty}^{\infty} e^{-ikx} f(x) dx,$$

and a Laplace transform, $\Phi(\lambda)$, of a function, $\varphi(t)$, is defined by

$$\Phi(\lambda) = \int_{0}^{\infty} e^{-\lambda t} \varphi(t) dt.$$

Assuming that the stream function and its higher order derivatives tend to 0 as $x \to \pm\infty$, we obtain the following formulae for the Fourier transforms:

$$\int_{-\infty}^{\infty} e^{-ikx} \left(\frac{\partial}{\partial x} \right)^n \psi(x, y, t) dx = (-ik)^n \widetilde{\psi}(k, y, t), \quad n = 0, 1, ...$$

B.1 Fourier transform

B.1.1 Derivation of (2.0.4)

To begin finding the Fourier transform of (1.2.10), we calculate the following Fourier transforms,

- $$\begin{aligned}\int_{-\infty}^{\infty} e^{-ikx}\psi_x(x,y,t)\,dx &= e^{-ikx}\psi(x,y,t)\Big|_{-\infty}^{\infty} + ik\,\widetilde{\psi}(k,y,t)\\ &= ik\,\widetilde{\psi}(k,y,t);\end{aligned}$$

- $$\begin{aligned}\int_{-\infty}^{\infty} e^{-ikx}\psi_{xx}(x,y,t)\,dx &= e^{-ikx}\psi_x(x,y,t)\Big|_{-\infty}^{\infty} + ik\int_{-\infty}^{\infty} e^{-ikx}\psi_x(x,y,t)\,dx\\ &= -k^2\,\widetilde{\psi}(k,y,t);\end{aligned}$$

- $$\begin{aligned}\int_{-\infty}^{\infty} e^{-ikx}\psi_{xxx}(x,y,t)\,x &= e^{-ikx}\psi_x(x,y,t)\Big|_{-\infty}^{\infty} + ik\int_{-\infty}^{\infty} e^{-ikx}\psi_{xx}(x,y,t)\,dx\\ &= ik\,e^{-ikx}\psi_x(x,y,t)\Big|_{-\infty}^{\infty} - k^2\int_{-\infty}^{\infty} e^{-ikx}\psi_x(x,y,t)\,dx\\ &= -ik^3\,\widetilde{\psi}(k,y,t).\end{aligned}$$

Expanding (1.2.10) and calculating the Fourier transform of each term yields,

$$\begin{aligned}&\int_{-\infty}^{\infty} e^{-ikx}\left(\psi_{xxt}(x,y,t) + y\,\psi_{xxx}(x,y,t) + \psi_{yyt}(x,y,t) + y\psi_{yyx}(x,y,t)\right)dx\\ &\qquad = -k^2\,\widetilde{\psi}_t(k,y,t) - ik^3 y\,\widetilde{\psi}(k,y,t) + \widetilde{\psi}_{yyt}(k,y,t) + iky\,\widetilde{\psi}_{yy}(k,y,t).\end{aligned}$$

Therefore we find the following equation of the Fourier transform of (1.2.10),

$$-k^2\,\widetilde{\psi}_t(k,y,t) - ik^3 y\,\widetilde{\psi}(k,y,t) + \widetilde{\psi}_{yyt}(k,y,t) + iky\,\widetilde{\psi}_{yy}(k,y,t) = 0$$

B.1.2 Derivation of (2.0.10)

We apply the Fourier transform to the boundary condition at $y = 0$ (1.2.12). Recall that $g(x,t)$ is an even function and equal to some finite constant $\tau \ll 1$ when $x \in (-R, R)$. First we apply the Fourier transform to both sides of the equation.

- $$\int_{-\infty}^{\infty} e^{-ikx}\, \psi_x(x,0,t)\, dx = \left. e^{-ikx}\, \psi(x,0,t) \right|_{-\infty}^{\infty} + ik \int_{-\infty}^{\infty} e^{-ikx}\, \psi(x,0,t)\, dx$$
$$= ik\widetilde{\psi}(k,0,t)$$

- $$i\omega c \int_{-\infty}^{\infty} e^{-ik\xi}\, g_0(\xi)\, e^{i\omega(\xi - ct)}\, dt = i\omega c \left(\int_{-R-r}^{-R} + \int_{-R}^{R} + \int_{R}^{R+r} \right) e^{-ik\xi}\, g_0(\xi)\, e^{i\omega(\xi-ct)}$$
$$= i\omega c\, e^{-i\omega ct} \left(\int_{-R-r}^{-R} g_0(\xi) e^{i\xi(\omega-k)}\, d\xi + \int_{-R}^{R} g_0(\xi) e^{i\xi(\omega-k)}\, d\xi + \int_{R}^{R+r} g_0(\xi) e^{i\xi(\omega-k)}\, d\xi \right)$$
$$= i\omega c\, e^{-i\omega ct} \left(\int_{R}^{R+r} g_0(-\xi) e^{-i\xi(\omega-k)}\, d\xi + \int_{-R}^{R} \tau\, e^{i\xi(\omega-k)}\, d\xi + \int_{R}^{R+r} g_0(\xi) e^{i\xi(\omega-k)}\, d\xi \right).$$

We must evaluate each integral separately. The first integral we find,

$$\int_{-R}^{R} \tau\, e^{i\xi(\omega-k)}\, d\xi = \tau \int_{-R}^{R} \cos(\xi(\omega-k)) + i\, \sin(\xi(\omega-k))\, d\xi$$
$$= \frac{2\,\tau}{\omega - t} \sin(\xi(\omega-k)) \Big|_0^R$$
$$= \frac{2\,\tau}{\omega - t} \sin(R(\omega-k)).$$

The remaining integrals be summed together using the evenness of $g(x,t)$,

$$\begin{aligned}
&\int_R^{R+r} g_0(-\xi)e^{-i\xi(\omega-k)} + \int_R^{R+r} g_0(\xi)e^{i\xi(\omega-k)}\, d\xi \\
&\qquad = \int_R^{R+r} g_0(-\xi)\Big\{ \cos(\xi(\omega-k)) - i\ \sin(\xi(\omega-k))\Big\} + g_0(\xi)\Big\{ \cos(\xi(\omega-k)) + i\ \sin(\xi(\omega-k))\Big\}\, d\xi \\
&\qquad = 2\int_R^{R+r} g_0(\xi)\cos(\xi(\omega-k))\, d\xi \\
&\qquad = 2\int_R^{R+r} g_0(\xi)\left(\frac{\sin(\xi(\omega-k))}{\omega-k}\right)' d\xi \\
&\qquad = 2\, g_0(\xi)\, \frac{\sin(\xi(\omega-k))}{\omega-k}\Big|_R^{R+r} - 2\int_R^{R+r} g_0'(\xi)\left(\frac{\sin(\xi(\omega-k))}{\omega-k}\right)d\xi \\
&\qquad = -2\tau\, \frac{\sin(R(\omega-k))}{\omega-k} - 2\int_R^{R+r} g_0'(\xi)\left(\frac{\sin(\xi(\omega-k))}{\omega-k}\right)d\xi.
\end{aligned}$$

When summing the afore solved integrals we find,

$$\begin{aligned}
-ik\,\widetilde{\psi}(k,0,t) &= 2i\omega c\, e^{-i\omega ct}\left\{ -\int_R^{R+r} g_0'(\xi)\left(\frac{\sin(\xi(\omega-k))}{\omega-k}\right)d\xi \right\} \\
\widetilde{\psi}(k,0,t) &= -\frac{2\omega c}{k}\, e^{-i\omega ct}\int_R^{R+r} g_0'(\xi)\left(\frac{\sin(\xi(\omega-k))}{\omega-k}\right)d\xi.
\end{aligned}$$

The boundary condition at $y = 0$ is found in Fourier space.

B.2 Laplace transform

B.2.1 Derivation of (2.0.6)

To begin finding the Laplace transform of (2.0.4), we apply the Laplace transform to both sides to (1.2.10),

$$\int_0^\infty e^{-\lambda t}\big(-k^2\,\widetilde{\psi}_t(k,y,t) - ik^3 y\,\widetilde{\psi}(k,y,t) + \widetilde{\psi}_{yyt}(k,y,t) + iky\,\widetilde{\psi}_{yy}(k,y,t) = 0\big)\, dt.$$

Each individual term's Laplace transform is calculated below,

- $$-k^2 \int_0^\infty e^{-\lambda t}\widetilde{\psi}_t(k,y,t)\,dt = -k^2\, e^{-\lambda t}\,\widetilde{\psi}_t(k,y,t)\Big|_0^\infty + k^2\lambda \int_0^\infty e^{-\lambda t}\,\widetilde{\psi}(k,y,t)\,dt$$
$$= k^2\lambda\,\Psi(k,y,\lambda)$$
- $$-ik^3 y \int_0^\infty e^{-\lambda t}\widetilde{\psi}(k,y,t)\,dt = -ik^3\,\Psi(k,y,\lambda)$$
- $$\int_0^\infty \widetilde{\psi}_{yyt}(k,y,t)\,dt = e^{-\lambda t}\,\Psi_{yy}(k,y,t)\Big|_0^\infty + \lambda\int_0^\infty e^{-\lambda t}\widetilde{\psi}_{yy}(k,y,t)\,dt$$
$$= \lambda\,\Psi_{yy}(k,y,\lambda)$$
- $$iky\int_0^\infty \widetilde{\psi}_{yy}(k,y,t) = iky\,\Psi_{yy}(k,y,\lambda)$$

Therefore we find the Laplace transform of (1.2.10) to be,

$$k^2\lambda\,\Psi(k,y,\lambda) + ik^3\,\Psi(k,y,\lambda) + \lambda\,\Psi_{yy}(k,y,\lambda) + iky\,\Psi_{yy}(k,y,\lambda) = \left(\frac{\partial^2}{\partial y^2} - k^2\right)\widetilde{\psi}(k,y,0).$$

This can be simplified further,

$$(\lambda + iky)\left(\frac{\partial^2}{\partial y^2} - k^2\right)\Psi(k,y,\lambda) = \left(\frac{\partial^2}{\partial y^2} - k^2\right)\widetilde{\psi}(k,y,0)$$
$$\left(\frac{\partial^2}{\partial y^2} - k^2\right)\Psi(k,y,\lambda) = \frac{1}{\lambda + iky}\left(\frac{\partial^2}{\partial y^2} - k^2\right)\widetilde{\psi}(k,y,0)$$

B.3 Inverse Laplace transform

B.3.1 Derivation of (2.0.9)

Applying the inverse Laplace transform to (2.0.6) yields,

$$\frac{1}{2\pi i}\int_\gamma \left(\frac{\partial^2}{\partial y^2} - k^2\right)\Psi(k,y,\lambda)\,e^{\lambda t}\,d\lambda = \frac{1}{2\pi i}\int_\gamma \frac{e^{\lambda t}}{\lambda + iky}\left(\frac{\partial^2}{\partial y^2} - k^2\right)\widetilde{\psi}(k,y,0)\,d\lambda,$$

To evaluate the right hand side of the equation, we use the Residue theorem and evaluate along the closed contour in the λ-complex plane (see Fig. 2.1),

$$\begin{aligned}\frac{1}{2\pi i}\int_{\gamma}\frac{e^{\lambda t}}{\lambda+iky}\,d\lambda &= \mathrm{Res}\left(\frac{e^{\lambda t}}{\lambda+iky},\ -iky\right)\\ &= e^{-ikyt}.\end{aligned}$$

Therefore we substitute the afore found into equation (2.0.8) and yield (2.0.9),

$$\left(\frac{\partial^2}{\partial y^2}-k^2\right)\widetilde{\psi}(k,y,t) = e^{-ikyt}\left(\frac{\partial^2}{\partial y^2}-k^2\right)\widetilde{\psi}(k,y,0).$$

APPENDIX C

STATIONARY SOLUTION

For the given system (2.1.6) – (2.1.8),

$$\begin{cases} \left(\dfrac{\partial^2}{\partial^2 y} - k^2\right) Y_0(k,y) = 0, \\ Y_0(k,1) = 0, \\ Y_0(k,0) = -\dfrac{2\omega c}{k} \displaystyle\int_R^{R+r} g_0'(\xi)\, \dfrac{\sin(\xi(k-\omega))}{k-\omega}\, d\xi. \end{cases}$$

that the basis for using eparation of variables is

$$\big\{ \sinh(ky),\ \cosh(ky) \big\},$$

and we rewrite this in the form of the equivalent basis,

$$\big\{ \sinh(ky),\ \sinh(k(1-y)) \big\}.$$

Therefore, solution will be of the form,

$$Y_0(k,y) = A(k)\ \sinh(ky) + B(k)\ \sinh(k(1-y)).$$

From the boundary conditions, and $y = 1$,

$$Y_0(k,1) = A(k)\ \sinh(k) = 0$$

therefore the only solution satisfying the above equation is when $A(k) = 0$.

For the second boundary conditions at $y = 0$,

$$Y_0(k, 0) = \ B(k)\ \sinh(k) = \ -\ \frac{2\omega c}{k} \int_R^{R+r} g_0'(\xi)\ \frac{\sin(\xi(k-\omega))}{k-\omega}\ d\xi$$

therefore we solve for $B(k)$ to be

$$B(k) = -\ \frac{2\omega c}{k\ \sinh(k)} \int_R^{R+r} g_0'(\xi)\ \frac{\sin(\xi(k-\omega))}{k-\omega}\ d\xi.$$

Recalling the form of the solution to $Y_0(k, y)$, the explicit solution to the stationary problem is solved,

$$Y_0(k, y) = -\ \frac{2\omega c\ \sinh(k(1-y))}{k\ \sinh(k)} \int_R^{R+r} g_0'(\xi)\ \frac{\sin(\xi(k-\omega))}{k-\omega}\ d\xi.$$

APPENDIX D

FUNCTION CONDITIONS AND PROPERTIES

D.1 Green's function properties

The below describes the requirements and influence of the boundary conditions and forcing terms in the construction of our Green's function.

Symmetry. The Green's function operates like a Dirac delta function, a fundamental property of it being that

$$\delta(x-y) = \delta(y-x), \quad \text{therefore} \quad G(\eta, y) = G(y, \eta),$$

which falls from *Maxwell's reciprocity*. Maxwell's reciprocity states that the response at x due to a concentrated source at x_0 is the same response at x_0 due to a concentrated source at x, though this is not physically obvious.

Continuity. We allow our function to be discontinuous for the first derivative, but not the second. Thus, we force our function to be continuous. The Green's function behaves like a δ-function; the first derivative of a δ-function is a Heaviside function, and the derivative of the Heaviside function is discontinuous. Physically, a δ-function, with a zero argument given, would result in an infinite source applied at this point, which is not physically possible. Thus, we enforce a continuity condition.

Unit jump of the derivative. If $G(x, x_s)$ has a jump discontinuity at $x = x_s$, then $\frac{\partial G}{\partial x}$ has a

singularity at $x = x_s$. The Green's function is continuous at $x = x_s$ though $\frac{\partial G}{\partial x}$ is not, there exists a unit jump discontinuity obtained by the integration of

$$\mathcal{L}\big(G(x, x_s)\big) = \delta(x - x_s).$$

Boundary conditions. The requirements of homogeneous boundary condition,

$$G(\eta, 0) = G(\eta, 1) = 0$$

s of the Green's function of this research are represented in the figure below.

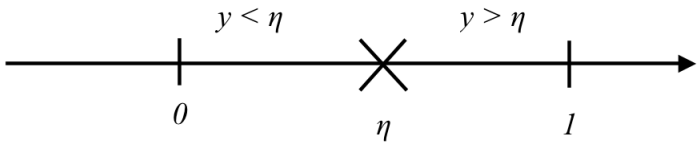

Figure D.1: Conditions of Green's function in domain.

Dirac delta function. We treat the Dirac delta function as an operator with the property that for any continuous function $f(x)$ that

$$f(x) = \int_{-\infty}^{\infty} f(x_i)\, \delta(x - x_s)\, dx_s$$

where

$$1 = \int_{-\infty}^{\infty} \delta(x - x_s)\, dx_s$$

and is like an even function, i.e. $\delta(x - x_s) = \delta(x_s - x)$. Therefore, the Green's function $G(x, x_s)$, is a response at x due to the concentration of the source at x_s.

$$\mathcal{L}\big(G(x, x_s)\big) = \delta(x - x_s).$$

D.2 Assumption of Perturbation of $f(\cdot, y)$

By the assumption of $f(\cdot, y)$

$$\text{supp}\{f(\cdot, y)\} \in (0, r_0), \qquad r_0 > 0, \tag{D.2.1}$$

meaning that $f(\cdot, y) = 0$ for $|x| \geq r_0 > 0$. By definition of the Fourier transform

$$\begin{aligned}\widetilde{f}(k, y) &= \int_{-\infty}^{\infty} e^{-ikx} f(x, y)\, dx \\ &= \int_{-r_0}^{r_0} e^{-ikx} f(x, y)\, dx\end{aligned}$$

where $\widetilde{f}(x, y)$ is come complex valued function for $k \in \mathbb{C}$.

We must check that our function satisfies the Cauchy-Riemann conditions to satisfy the necessary and sufficient condition for a complex function to be complex differentiable (holomorphic). Using the Cauchy-Riemann conditions, given that $\widetilde{f}(\xi, \eta) = u(\xi, \eta) + i\ v(\xi, \eta)$ then

$$\frac{\partial u}{\partial \xi} = \frac{\partial v}{\partial \eta} \qquad \text{and} \qquad \frac{\partial u}{\partial \eta} = -\frac{\partial v}{\partial \xi}$$

must be true. We find each definition of $u(\xi, \eta)$ and $v(\xi, \eta)$ by splitting $\widetilde{f}(\xi, \eta)$ into it's real and imaginary parts,

$$\begin{aligned}u(\xi, \eta) = \mathfrak{R}\ \widetilde{f} &= \mathfrak{R} \int_{-r_0}^{r_0} e^{-i(\xi + i\eta)x}\ f(x, y)\, dx \\ &= \int_{-r_0}^{r_0} e^{\eta x} \cos(\xi x)\ f(x, y)\, dx\end{aligned}$$

$$\begin{aligned}v(\xi, \eta) = \mathfrak{I}\ \widetilde{f} &= \mathfrak{I} \int_{-r_0}^{r_0} e^{-i(\xi + i\eta)x}\ f(x, y)\, dx \\ &= -\int_{-r_0}^{r_0} e^{\eta x} \sin(\xi x)\ f(x, y)\, dx.\end{aligned}$$

To check that the definitions of $u(\xi,\eta)$ and $v(\xi,\eta)$ satisfying the Cauchy-Reimann equations, we take their partial derivatives,

$$\frac{\partial u}{\partial \xi} = -\int_{-r_0}^{r_0} e^{\eta x}\, x\, \sin(\xi x)\, f(x,y)\, dx \qquad \text{and} \qquad \frac{\partial v}{\partial \eta} = -\int_{-r_0}^{r_0} e^{\eta x}\, x\, \sin(\xi x)\, f(x,y)\, dx$$

$$\frac{\partial u}{\partial \eta} = \int_{-r_0}^{r_0} e^{\eta x}\, x\, \cos(\xi x)\, f(x,y)\, dx \qquad \text{and} \qquad \frac{\partial v}{\partial \xi} = -\int_{-r_0}^{r_0} e^{\eta x}\, x\, \cos(\xi x)\, f(x,y)\, dx$$

The Cauchy-Riemann conditions are satisfied, therefore our function $\widetilde{f}(\xi,\eta)$ is holomorphic and as a consequence of being holomorphic, $\widetilde{f}(\xi,\eta)$ is analytic. Holomorphic Fourier transforms of a function, with ξ in the lower half-plane, the modulus $e^{-i\xi x}$ grows exponentially as $x \to \infty$. Holomorphic Fourier transforms of a function, with ξ in the upper half-plane, the modulus $e^{i\xi x}$ grows exponentially as $x \to -\infty$. By the Paley-Wiener theorem a Fourier transform of a function of distribution of compact support on $\mathbb{R}^n$ is an entire function of $\mathbb{C}^n$ and gives estimates on the growth at infinity.